Stability of the IJsselkop bifurcation at design discharge

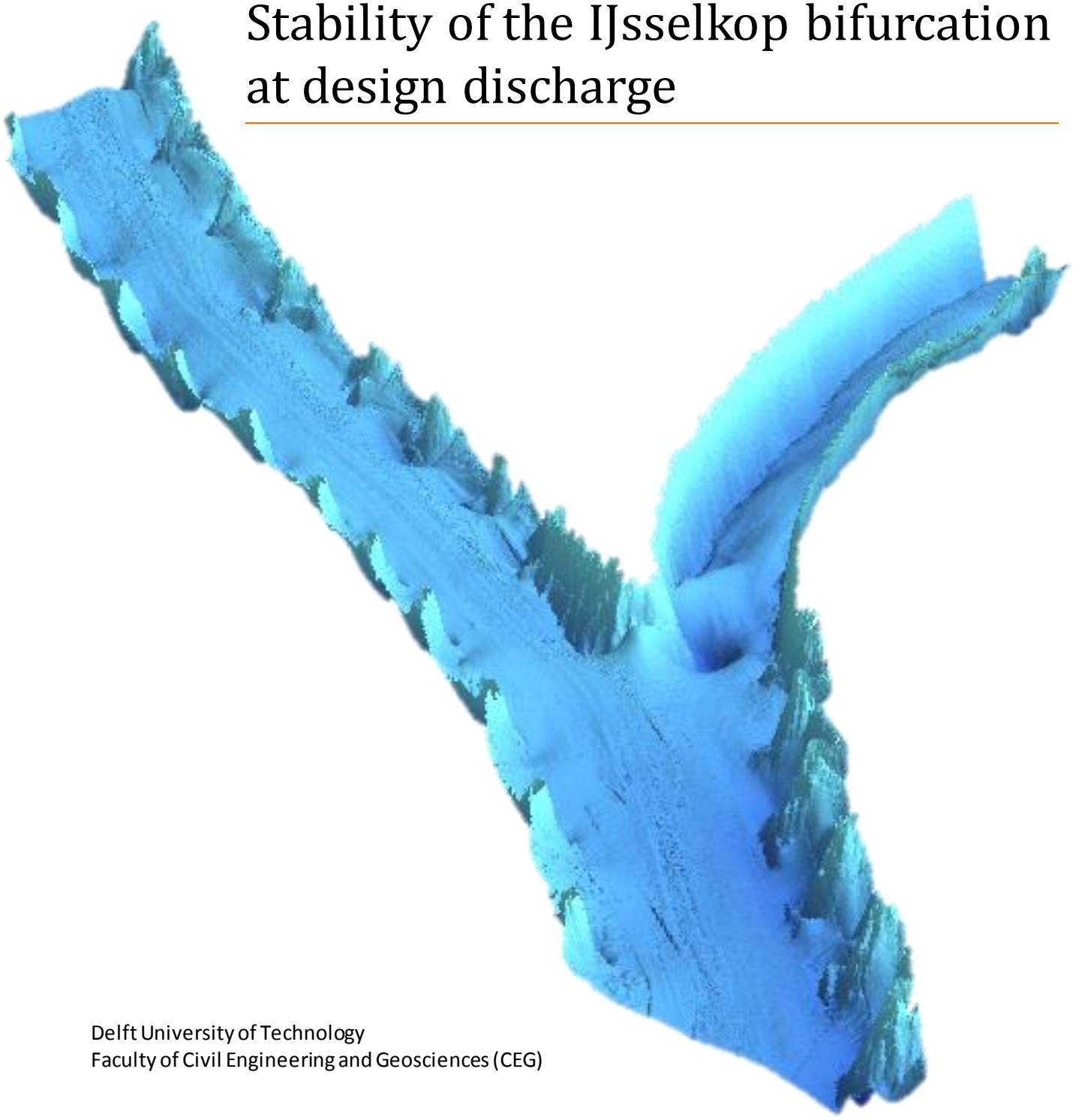

Delft University of Technology
Faculty of Civil Engineering and Geosciences (CEG)

Master of Science thesis

Author
K.H. Vereijken

Stability of the IJsselkop bifurcation at design discharge

Contributors

prof.dr.ir. W.S.J. Uijttewaal (Delft University of Technology)

dr. ir. A. Blom (Delft University of Technology)

dr. ir. E. Mosselman (Delft University of Technology / Deltares)

ir. D. Heineke (Rijkswaterstaat)

MSc thesis K.H. Vereijken

Preface

This master thesis is my graduation research in order to obtain the Master of Science degree at the Delft University of Technology. This is the completion of the master Hydraulic Engineering, specialization River Engineering, at the Faculty of Civil Engineering and Geosciences.

During my internship I discovered the wonderful world of rivers in practice. It was interesting to cope with problems in the Dutch river system. This interest led me to this research subject: the stability of the IJsselkop bifurcation. I was pleased to get the opportunity to perform this research in co-operation with Deltares and Rijkswaterstaat. Contacts with both of the organisations made it easy to collect a lot of data for my research, which enabled me to study this subject from different perspectives. On the other hand, many interesting data and perspectives made it a challenge to stay within the scope of the project.

I would like to thank my entire committee, consisting of prof.dr.ir. W.S.J. Uijttewaal (Delft University of Technology), dr. ir. A. Blom (Delft University of Technology), dr. ir. E. Mosselman (Delft University of Technology / Deltares) and ir. D. Heineke (Rijkswaterstaat), who helped during my thesis with both the content as well as their guidance with the process. Thanks to them I was able to finish my report.

I also would like to thank my colleagues at Deltares for providing data regarding the Delft3D model (Willem Ottevanger) and the drilling and subsoil data (Ane Wiersma). I also extend my thanks to Rijkswaterstaat for providing data of bed topography and discharge measurements. I also would like my colleagues for their support, discussions and small talks during my stay.

Finally I would like to thank my friends and family, who supported me during the highs and lows of this research. Special thanks to Pieter Kerssens and Paul Landa who actively supported me to finalise this report.

Koen Vereijken

Delft, March 2016

Summary

A hydrodynamic study shows high flow velocities at the IJsselkop bifurcation during the design discharge of 16,000 m^3/s. The study, performed in 2005, concludes that these velocities might affect 1) the stability of IJssel river bed and 2) the stability of the grass cover layer of the flood plain at the bifurcation. This report provides a better insight in the behaviour of the river branches at the IJsselkop bifurcation during the design discharge. Furthermore, the likeliness has been studied that these flow velocities influence the stability of both the grass cover layer of the flood plain and the bed of the river IJssel. Additionally, it shows the effect on the discharge distribution at this bifurcation if large scale erosion of the grass cover or IJssel bed occurs. Four research questions are defined to answer this research objective.

1. *What are the characteristics of the IJsselkop area?*
2. *Is the bed layer of the IJssel likely to fail during design discharge conditions?*
3. *Is the grass cover in the floodplain likely to erode during design discharge conditions?*
4. *What are the consequences of erosion of the bed layer of the IJssel and erosion of the floodplain for the discharge distribution?*

The route of the Rhine river towards the sea has changed several times the last few hundred thousand years. It deposited its sediment on various locations with a variation in sediment size, depending on its river type. The top layer of coarse sediment is located close to the surface in the Eastern part of the Netherlands. Additionally, the supply of coarse material results in a coarse top layer of the river bed around the bifurcation at the IJsselkop. The IJssel river bed top layer consists of coarser material than the Lower Rhine bed as a results of the geometry of the rivers. The IJssel bed consists of a coarse layer of approximately 1 m thick on top of a layer with finer sediment. The subsoil of the flood plain consists of 'sandy clay', which has been determined from stratification data. The level of the IJssel bed decreases with 1 – 2 cm/yr between 2002 and 2013, which is in the same order of magnitude as the decrease in water level.

The stability of the IJssel river bed during design discharge has been assessed based on detailed drilling data. Three situations has been analysed for an insight in the behaviour of the river bed. The first situation is initiation of movement based on uniform sediment, which is based on the Shields mobility parameter. The second situation is initiation of movement based on mixed sediment. This is based on the hiding and exposure mechanism, which reduces the stability of the bed material. The third situation includes instantaneous shear stresses that are imposed by the presence of dunes. The analysis showed that a large area of the considered IJssel river bed can be assumed to be unstable during design discharge conditions.

The stability of the flood plain has been assessed with a quantitative and qualitative analysis of the stability of the grass cover. A flow at the flood plain directed from West to East, the lateral discharge, is the result of the water level differences between the two branches just downstream of the IJsselkop bifurcation point, caused by the less gentle bed slope of the IJssel river than that of the Lower Rhine. High flow velocities are present at the entire flood plain, except for the Northwest part. The quality of the flood plain depends on the characteristics of the grass cover and clayey subsoil. The critical flow velocity is 1.3 m/s and 2.0 m/s respectively, based on a `poor' to `normal' grass cover quality and a flow duration of 20 hours for these velocities. The presence of discontinuities in the grass layer can initiate local erosion by the presence of turbulent flow and a weakening of the top layer. The lateral discharge may increase significantly as a result of large scale scour of the flood plain. The influence on the IJssel discharge has been estimated with a rough and conservative approach.

The consequences of a break-up of the top layer in the IJssel river bed are assessed with a numerical model, Delft3D. Three scenarios are assessed: a hydrodynamic computation, morphodynamic computation and imposing an artificial deepening. The discharge of the IJssel varies from 43% to 47% of the Pannerden Canal discharge during the peak discharge. The velocity profile of the Delft3D model shows that the flow velocity in the IJssel is large compared to the flow velocity in the Lower Rhine and Pannerden Canal, which is the result of the small wet cross-section and the relatively steep bed slope of the IJssel. No significant changes are observed of the hydrodynamics when a morphodynamic update is applied. Only a small amount of sedimentation/erosion at the end of the flood wave has been observed. An artificial deepening of the IJssel has been imposed in the third simulation, to simulate the break-up. The deepening does not lead to other significant changes in water levels, flow velocity, discharge and bed level. Based on these computations it has been concluded that in the case of a break-up no large scale changes are expected to occur.

Table of content

List of symbols

Symbol	description	unit
B_i	width of grid cell *i*	[m]
c	weir coefficient	[-]
c_d	discharge coefficient	[-]
C_i	Chézy roughness for location *i*	[$m^{1/2}$/s]
D	grain diameter	[m]
d	water depth	[m]
d_{50}	grain diameter where 50% of the grain mass has a smaller diameter	[m]
d_{90}	grain diameter where 90% of the grain mass has a smaller diameter	[m]
$D_{b,i}$	grain diameter corresponding to the fraction boundary	[m]
D_i	representative grain size of size fraction *i*	[mm]
D_{max}	maximum value of the grain diameter	[m]
D_{min}	minimum value of the grain diameter	[m]
D_{ref}	reference grain size, which is a constant of 1 mm	[mm]
D_{sg}	surface geometric mean diameter	[mm]
F_i	percentage of the grains within fraction *i*	[%]
g	gravitational acceleration (constant of 9.81)	[m/s^2]
H	energy head	[m]
H_0	energy head upstream of the flood plain	[m]
h_1	water level at the flood plain	[m]
$h_{down,IJssel}$	water level at the downstream boundary of the Ijssel	[m]
$h_{down,rhine}$	water level at the downstream boundary of the Rhine	[m]
h_i	water depth for location *i*	[m]
M	grid co-ordinate system in lateral flow direction	[#]
N	grid co-ordinate system in longitudal flow direction	[#]
p	stability value at the river bed	[-]
p_{fp}	stability value at the flood plain	[-]
q	specific discharge	[m^2/s]
Q_{lat}	lateral discharge	[m^3/s]
q_{weir}	specific discharge at the weir	[m^2/s]
Re_*	particle Reynolds number	[-]
S	sediment transport	[m^3/s]
t	time	[s]
U	depth-averaged flow velocity in main direction	[m/s]
u_*	shear velocity	[m/s]

Symbol	description	unit
$\bar{u}_{act}$	acting depth-averaged velocity	[m/s]
u_c	critical flow velocity	[m/s]
$\bar{u}_c$	critical depth-averaged flow velocity	[m/s]
$\bar{u}$	depth-averaged flow velocity	[m/s]
V	depth-averaged flow velocity perpendicular of main direction	[m/s]
z_b	bed level	[m]
α	calibration coefficient for sediment transport	[-]
Δ	relative density of grains under water	[-]
ζ	water level above a reference plane	[m]
θ	Shields mobility parameter	[-]
θ_c	critical mobility parameter	[-]
μ	ripple factor for sediment transport	[-]
ν	viscosity	[m^2/s]
ξ	hiding and exposure multiplication factor	[-]
ρ_g	sediment density (constant of 2650)	[kg/m^3]
ρ_w	water density (constant of 1000)	[kg/m^3]
σ	depth value, 0 at the surface and -1 at bed level	[-]
$\tau^*_{c,i}$	critical shear stress for all sizes D_i	[N/mm^2]
τ^*_{scg}	critical shear stress for D_{sg}	[N/mm^2]
τ_{act}	acting shear stress	[N/m^2]
τ_b	bottom shear stress	[N/m^2]
$\tau_{b,c}$	critical bottom shear stress	[N/m^2]
τ_c	critical shear stress	[N/m^2]
ψ_i	grain size of fraction i on ψ scale	[-]
ψ_s	mean grain size on ψ scale	[-]

Chapter 1 Introduction

1.1 Problem description

The Netherlands has been formed by a complex delta system consisting of several rivers with numerous branches. As a part of this system the river Meuse (originating in France) and the river Rhine (originating in Switzerland) flow into the sea through the Netherlands via numerous branches. The presence of these rivers causes the hinterland to be vulnerable to flooding. The Delta Programme, a Dutch programme for safety against flooding, has set up rules for the permissible failure probabilities of dikes in the Netherlands. Depending on the hinterland and the type of dike each dike has a different permissible failure probability. For river dikes in the eastern parts of the Netherlands this failure probability is 1/1,250 years, while this value for primary flood defences can be up to 1/10,000 years. The discharges corresponding to these return periods are the design discharges.

Over the years, the rivers are regulated to prevent flooding and to improve the navigability of the rivers, which is partly covered by the natural existence of river bifurcations, e.g. the IJsselkop bifurcation (Figure 1-1). The downstream river branches determine the discharge distribution of the flow. The presence of numerous branches, and bifurcations, makes it a complex system to regulate. With the construction of, for example, weirs, the Dutch regulate the discharge distribution during low waters to prevent that the IJssel receives too little discharge (i.e. ships may not be able to pass the river when the amount of discharge is too small, resulting in low water levels).

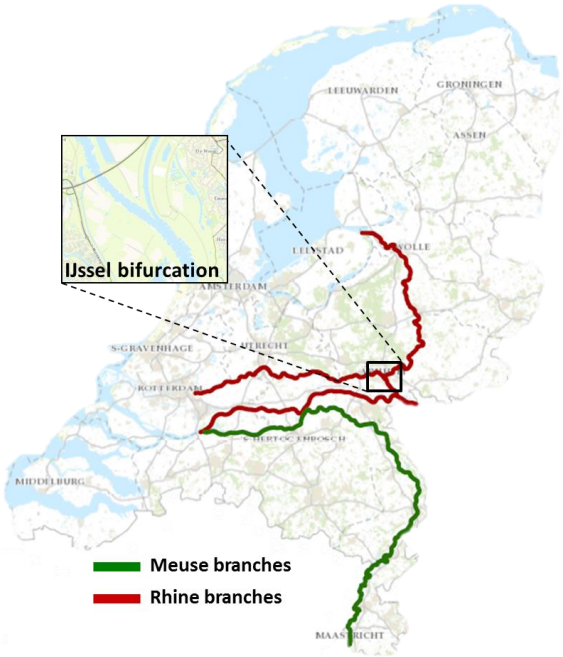

Figure 1-1: Rhine and Meuse branches in the Netherlands

Climate changes cause more frequent and severe rainfalls, an increase of the sea level and a rise in temperature. Because of these developments, the river design discharge (1/1,250 years for the east of the Netherlands) may increase as well. The last floods were in the south-eastern part of the Netherlands during the high water events in 1993 and 1995. Severe discharges like these might occur more frequently in the future. One of the measures that is taken to cope with the higher discharge is the *Room for the River Programme*. The programme is coordinated by the ministry of Infrastructure and Environment. The program has been set-up in order to analyse the developments in these conditions for the rivers and creating a plan to control these changes. The Room for the River Programme has three objectives (Ministerie Verkeer en Waterstaat, 2007):

- By 2015 the Rhine branches need to be able to discharge 16.000 m^3/s without flooding.
- Measures for the increase of safety need to improve the environmental quality as well.
- The extra room these rivers require, remains permanently available.

These plans have resulted in the construction of so called green rivers, which is a side channel parallel to the main river channel that is only activated during peak discharges, which results in a higher

discharge capacity of the river and the lowering of the water level in the main channel during extreme discharge events.

One of these green rivers is the construction of the Hondsbroeksche Pley, close to the IJsselkop bifurcation, which has been constructed to provide that the desired discharge distribution is maintained if high discharge events occur during the Room for the River programme. Delft Hydraulics studied the flow patterns in the area around the bifurcation (Suryadi and Mosselman, 2005), to gain insight in these processes. The study showed that there are indications that extreme discharge events could make the bifurcation unstable. These events might cause changes to the IJsselkop bifurcation (Figure 1-2) geometry in such a way that the river IJssel would receive a larger share of the design flood discharge, resulting in higher water levels and/or velocities in the IJssel than what the downstream dikes are designed for. This topic has been studied in this research. A possible instability of the IJsselkop bifurcation may have several causes. In this research the focus is on the two main concerns:

- The stability of the **armour layer** of the main channel of the IJssel. This is a coarse sediment layer, mainly immobile, at the river bed that may break-up during design floods, what may result in a large amount of erosion of the river bed.
- The **floodplain** between the Dutch Lower-Rhine and the IJssel is covered with grass. When design floods occur, this grass cover may fail, leading to erosion of the flood plain.

Both aspects may affect the water and sediment distribution over the branches downstream.

Figure 1-2: The IJsselkop bifurcation (Google, 2013)

1.2 Research objective

The goal of this research is described into the following research objective:

> *The objective of this research is to asses **(1)** the likeliness of the armour layer or grass cover to break-up and **(2)** the consequences of the break-up to the discharge distribution over the downstream branches of the IJsselkop bifurcation and the consequences of the scour holes, due to the break-up, to the local stability.*

1.3 Research questions

In order to answer the research objective, the following research questions are formulated. The steps necessary to find answers for these questions, the methodology, are elaborated in §1.4.

1. *What are the characteristics of the IJsselkop area?*
2. *Is the bed layer of the IJssel likely to fail during design discharge conditions?*
3. *Is the grass cover likely to erode during the design discharge conditions?*
4. *What are the consequences of erosion of the bed layer of the IJssel and erosion of the floodplain for the discharge distribution?*

1.4 Methodology

The research questions from §1.3 are covered by defining the methodology for each question.

1. What are the characteristics of the IJsselkop area?

In order to understand how extreme floods affect the IJsselkop area, it is important to get an understanding of the characteristics of this area. This research question covers the analyses of the (history) background, the bed and substrate properties, drillings and eventually the water depth and discharge measurements of the last century.

2. Is the bed layer of the IJssel likely to fail during design conditions?

Whether or not the armour layer of the IJssel river bed breaks up, and the possible failure location, are studied by performing analytical calculations regarding the stability of the grains on the river bed for uniform sediment, mixed sediment and the effect of dunes on the actual shear stresses.

3. Is the grass cover likely to erode during the design discharge conditions?

Initial flow computations in WAQUA[1], performed by Delft Hydraulics (Suryadi and Mosselman, 2005) showed high velocities at the floodplain. The stability of this floodplain has been studied with both analytical calculations regarding the stability of the grass cover at the design flood and observations from a site visit.

4. What are the consequences of erosion of the bed layer of the IJssel and erosion of the floodplain for the discharge distribution?

The hydrodynamic and morphodynamic conditions and the consequences of possible break-up are studied with computations by using a numerical model, Delft3D. This research question covers the analysis of computations of 1) the hydrodynamics only 2) morphodynamic update applied and 3) an artificially imposed break-up of the armour layer, and the influence of each added property by compare them with each other. A qualitative analysis has been performed for the influence of the break-up of the grass cover of the flood plain.

1.5 Report outline

Each research question is discussed in a chapter. Chapter 2 gives a description of the IJsselkop area. Chapter 3 covers the stability of the IJssel river bed and Chapter 4 treats the stability of the grass cover. The set-up of the computer model is discussed in Chapter 5 and the model results are presented in Chapter 6. Discussions are presented in Chapter 7 and the conclusion in Chapter 8. The last chapter, Chapter 9, describes the recommendations for further research.

[1] A 2 dimensional computer model for hydrodynamic simulations

Chapter 2 IJsselkop description

2.1 Introduction

This chapter provides an answer to the research question: *What are the characteristics of the IJsselkop area?* This question is answered by an analysis of the long and short term historic development of the substrate and river system, the stratification of the substrate, the bed topography development and the development of the hydrodynamics around the IJsselkop. Each of these subjects is covered in a section.

Definitions

There are two main river branches in the Netherlands that flow into the sea. The Rhine (discharging water from glaciers and rainfall) originates in Switzerland and crosses the German-Dutch border at Lobith. The Meuse (rain-fed) originates in France and crosses the Belgium-Dutch border at Eijsden. Both rivers discharge through several branches (in)directly into the sea, as presented in Figure 2-1. More details on the active and abandoned river sections of the Rhine branch are presented in Figure 2-1b. In the remainder of this report the mentioned Rhine branches are described by the names as defined in Figure 2-1c, in which the bifurcations are the boundaries for each section.

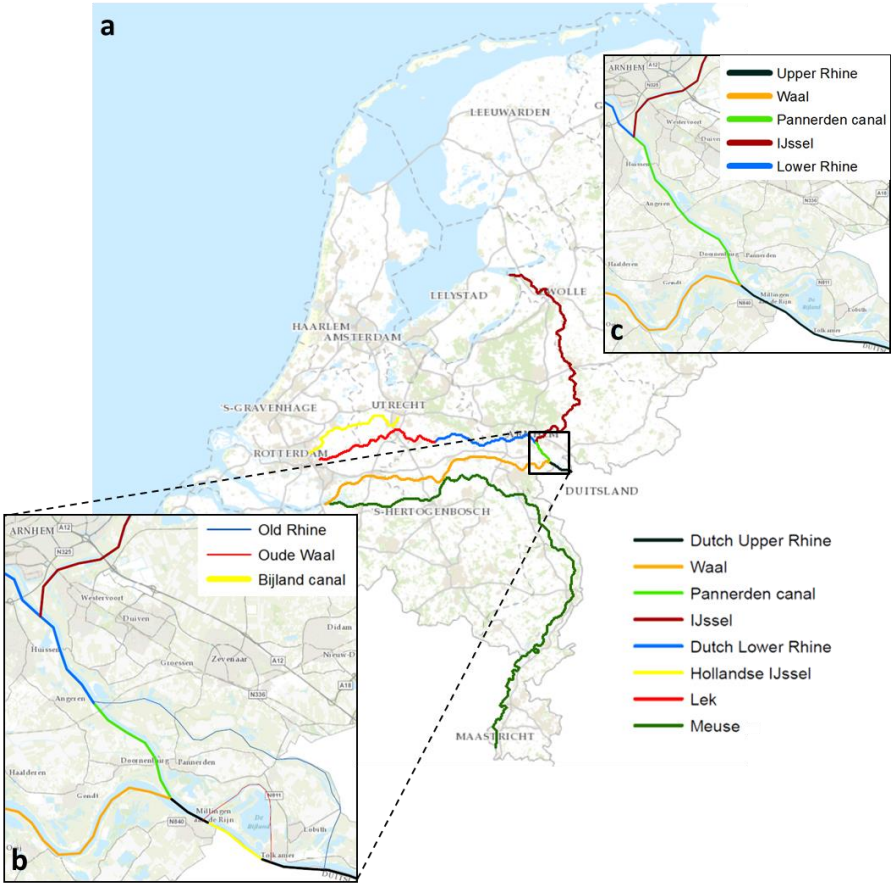

Figure 2-1: Overview of the names and location of (a) the main waterways in the Netherlands (b) close-up around the IJsselkop and (c) the simplified names for further use

2.2 Historic developments

Long term developments

The river development of the Dutch delta started when the glaciers made their way southwards in the Saalian stage (about 200,000 years ago). It forced the (braiding) river Rhine to change its route from northward direction to go westwards. These glaciers left sandy moraines in the mid-east of the Netherlands (e.g. the *Veluwe*). Palaeographic research (Cohen et al., 2009) showed that (inter)glacial eras caused large scale avulsions and different types of sediment deposition in the Netherlands. In the inter-glacial period after the Saalian glacial stage (90,000 – 70,000 years ago) and after the last glacial era (which ended about 9,000 years ago), the Rhine discharged its water in west- and northward direction into the North Sea. In the last glacial era (70,000 – 9,000 years ago) the Rhine was forced to discharge all water to the west because of the glacier boundary in the North. This research (Cohen et al., 2009) showed the link between the river branches and sediment deposition over these years. Large amounts of sand and gravel were deposited in the eastern part of the Netherlands (formation of *Kreftenheye*) during this period because of the longer distance to the sea, which influences the streamwise sorting[2]. The Rhine was back then a braiding river that deposited mostly gravel and sand. After this glacial era less coarse sediment was deposited, varying from gravel to clay (formation of *Echteld*). Clay settled at the natural flood plains ('*komgrond*'), while gravel and sand settled in the main channel. Because of the continuous avulsions, the soil became heterogeneous with a wide range of sediment.

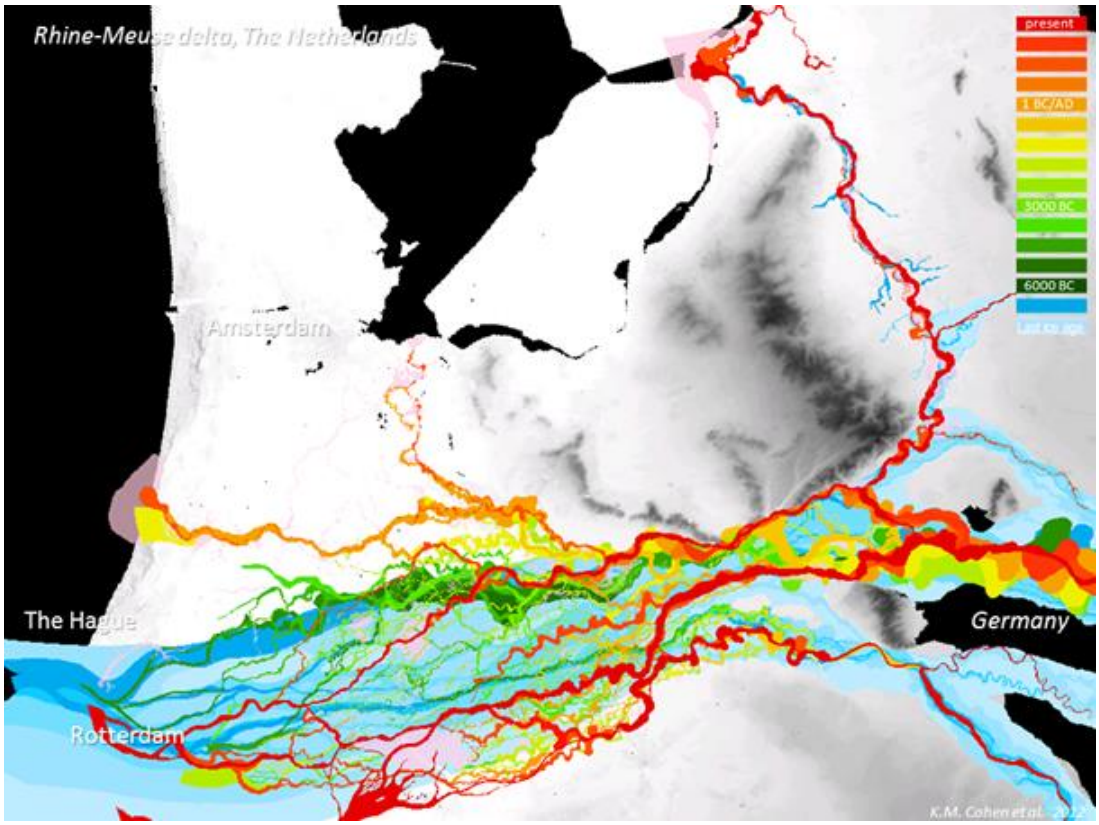

Figure 2-2: Avulsions of the Rhine-Meuse delta in the last 10.000 years (Cohen and Stouthamer, 2012)

[2] A typical river profile has a decrease of bed slope in downstream direction, which is accompanied by a decrease in bed shear stress so that coarse grains are likely to settle in the upstream part and fines in the downstream part. Wearing by interaction between grains is also of influence for downstream fining (FRINGS, R. M. 2008. Downstream fining in large sand-bed rivers. *Earth-Science Reviews,* 87**,** 39-60.). Some of these abrasion processes result in sand and gravel (e.g. splitting, chipping) while others results in silty or clay (e.g. crushing, cracking or grinding).

The last 10,000 years the IJssel valley was abandoned for a long period, but flooded again a few thousand years ago, which led to re-activation of the gullies in the valley. The flooding was caused by the landward increase of the Rhine delta. The Rhine-Waal apex shifted upstream, in combination with an increase of the concentration of silt, which was caused by the increased agriculture in Germany. Palaeographic research (Cohen and Stouthamer, 2012) shows the avulsions of the Dutch rivers in the last 10,000 years, as presented in Figure 2-2.

Short term developments

The Rhine's river mouth shifted from Katwijk to Rotterdam (the *Nieuwe Waterweg*) in the early Roman age because of several flooding events. The first deliberate human intervention dates back to the Roman age, when the Romans wanted to make the Lower Rhine more navigable by constructing a dam in the Upper Rhine to divert more water into the Lower Rhine. Later on, channels (e.g. Pannerden Canal) were constructed in order to connect several river branches [3]. During the Middle Ages the human population increased and man moved towards the rivers and a lot of peat and clay was mined along the river, resulting in lower lying areas. To prevent the villages from flooding, because of the subsided land, dikes were constructed. Due to the absence of flood plains and the quality of the dikes, several dike breaches occurred, resulting in avulsions. One of those floods is the *St.-Elizabethflood*, which eventually led to a shift in landward direction of the river mouth of the Waal (van Heezik, 2007). The Waal got more discharge, because of the reduction in river length and thus a reduction of the resistance, while the Dutch Lower Rhine and the IJssel received less. This could eventually lead to a completely abandoned Lower Rhine (and IJssel) if no interventions were done. The discharge reduction was initially not visible for the IJssel river, because of the ongoing water supply from other branches, such as Oude IJssel or Berkel, that originates from the German Rhine (van Heezik, 2007).

The Lower Rhine and the IJssel had a strategic function as well, since these rivers kept the enemy at a distance if enough water was available. The *Pannerden Canal* was built in 1707 (van de Ven, 1976), because of the effects of the redistribution, and connected the Waal and the Rhine (the Old Rhine in Figure 2-1). The channel attracted more water than expected, because of unexpected bank and bed erosion, which led to an undesirable low discharge towards the Waal. The stabilization (e.g. bank protection) of the Pannerden Canal profile was the beginning of the control of the discharge distributions in the upstream regions in the Netherlands (van de Ven, 1976). For the next step, it was agreed (mid-18th century) to standardize the distribution of the branches; the Waal would receive 2/3rd of the upstream discharge and the Pannerden Canal 1/3rd. Downstream of the Pannerden Canal the Dutch Lower Rhine would get 2/3th and the IJssel 1/3th of the Pannerden Canal discharge. Measures were performed for the realisation of this standard, as for example the relocation of the IJsselkop bifurcation (Figure 2-3). Regardless of these actions, dike failure, in the 18th century, near Bijland almost caused a large scale avulsion in the Upper Rhine. The Bijland channel (Figure 2-1) was constructed (1773) to prevent the Waal and Pannerden Canal to dry out (van de Ven, 1976). Increase in navigability of the river became more important, which resulted in the construction of dams and groynes and the cut-off of several meanders in the Rhine branches. The regulation of the water level in the Lower Rhine and IJssel branch

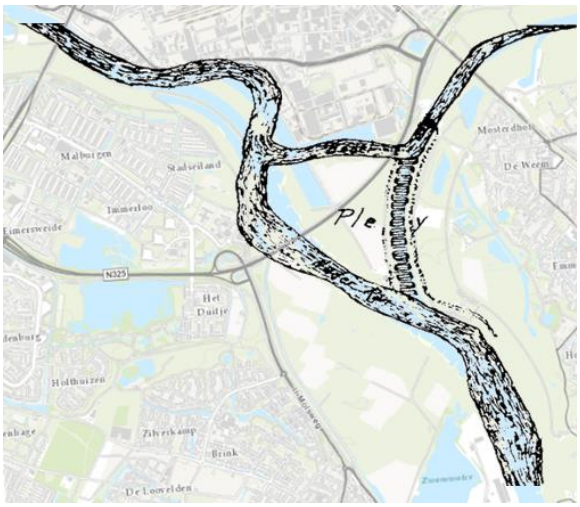

Figure 2-3: Digging through the Pley in 1774 with guide walls (Dutch: leidammen) on a background of the present situation (van Keulen, 2014)

[3] For a long time it was believed that the river IJssel originated from one of these channels; the *Drususgracht*. Cohen (2009) showed, however, that IJssel originates from flooding events from the river Rhine.

was eventually improved by constructing weirs (finished in 1970) in the Lower Rhine (Rijkswaterstaat, 2014b).

2.3 Stratification of the substrate

Drillings of the substrate provide insight in the characteristics of the river bed and the flood plain in the area of interest. GeoTOP [4] data (TNO, 2011) give information about the lithostratigraphic classifications (e.g. peat, coarse sand, gravel) of the substrate in grids with a size of 100 m x 100 m and a layer thickness of 0.5 m.

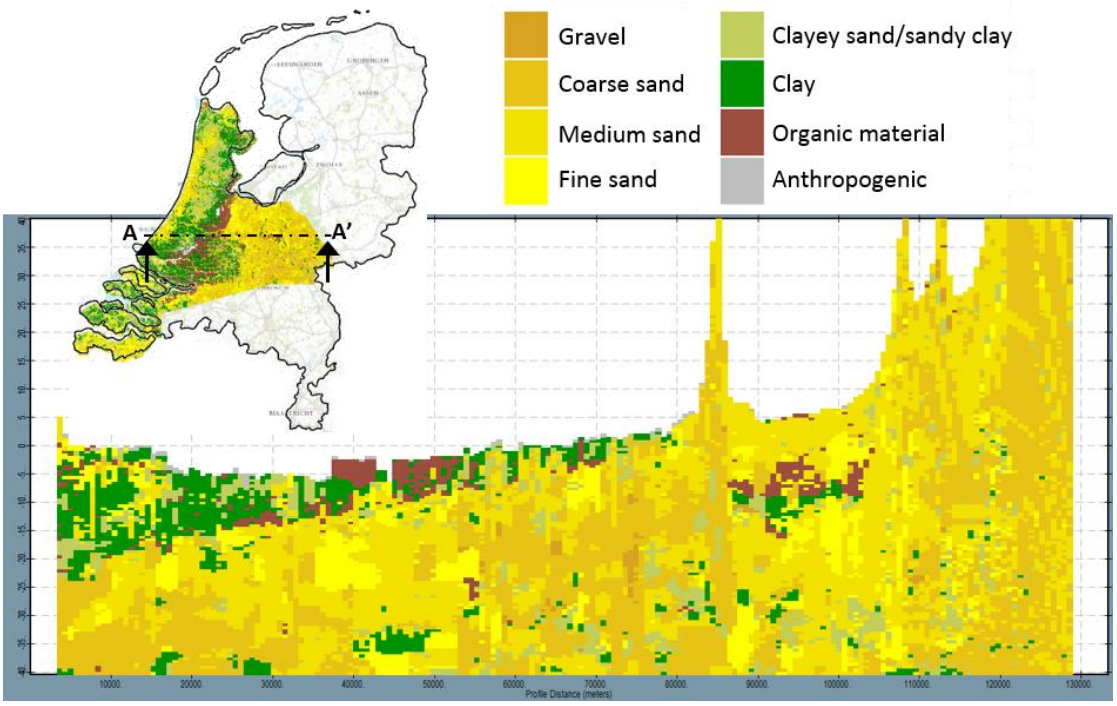

Figure 2-4: Representation by iMOD of a cross-sectional area (A-A') of the litho-classification of the Netherlands (TNO, 2011)

Formations are defined by grouping of the lithostratigraphic classifications, like the Formation of Kreftenheye for areas with coarse sediment. The area of the available stratification data is shown in Figure 2-4. The sand fractions are divided into grades: 'fine sand' (fraction grain size: 63-150 µm), 'medium sand' (150-300 µm) and the 'coarse sand' (300-1000 µm). The data is visualised using the software model iMOD[5]. Figure 2-4 shows that in the western part of the Netherlands large amounts of clayey material are present just below the surface, and along the coast up to -20 m +NAP[6] to -30 m +NAP. The left yellow peak and the right yellow peaks present the *Utrechtse Heuvelrug* and the *Hoge Veluwe* respectively. The upper and lower boundary of the Formation of Kreftenheye are defined by the data from Figure 2-4. This data shows, in combination with the bed topography data, that the top of this formation is located just below surface level, which indicates that coarse material can be expected at bed level of the river, originating from this layer. It must be noted that these data only provides an indication of the characteristics of the substrate.

[4] GeoTOP provides a three-dimensional insight in the geological development of The Netherlands and gives information of the substrate up to a depth of 50 metres below surface

[5] *iMOD* is software, developed by Deltares, and is used to read the borehole data. Several images in this report regarding the sub soil classification are rendered with this software

[6] NAP = Normaal Amsterdams Peil, also Amsterdam Ordnance datum, which is a vertical datum with its zero value at mean sea level

Stratification of the flood plain

The lithology classes are mapped in Figure 2-5 up to a depth of -6.0 m +NAP. The data are represented by grid cells of 100 x 100 m with a thickness of 0.50 m. Therefore, it does not exactly follow the surface profile, but it gives a good indication of the lithology.

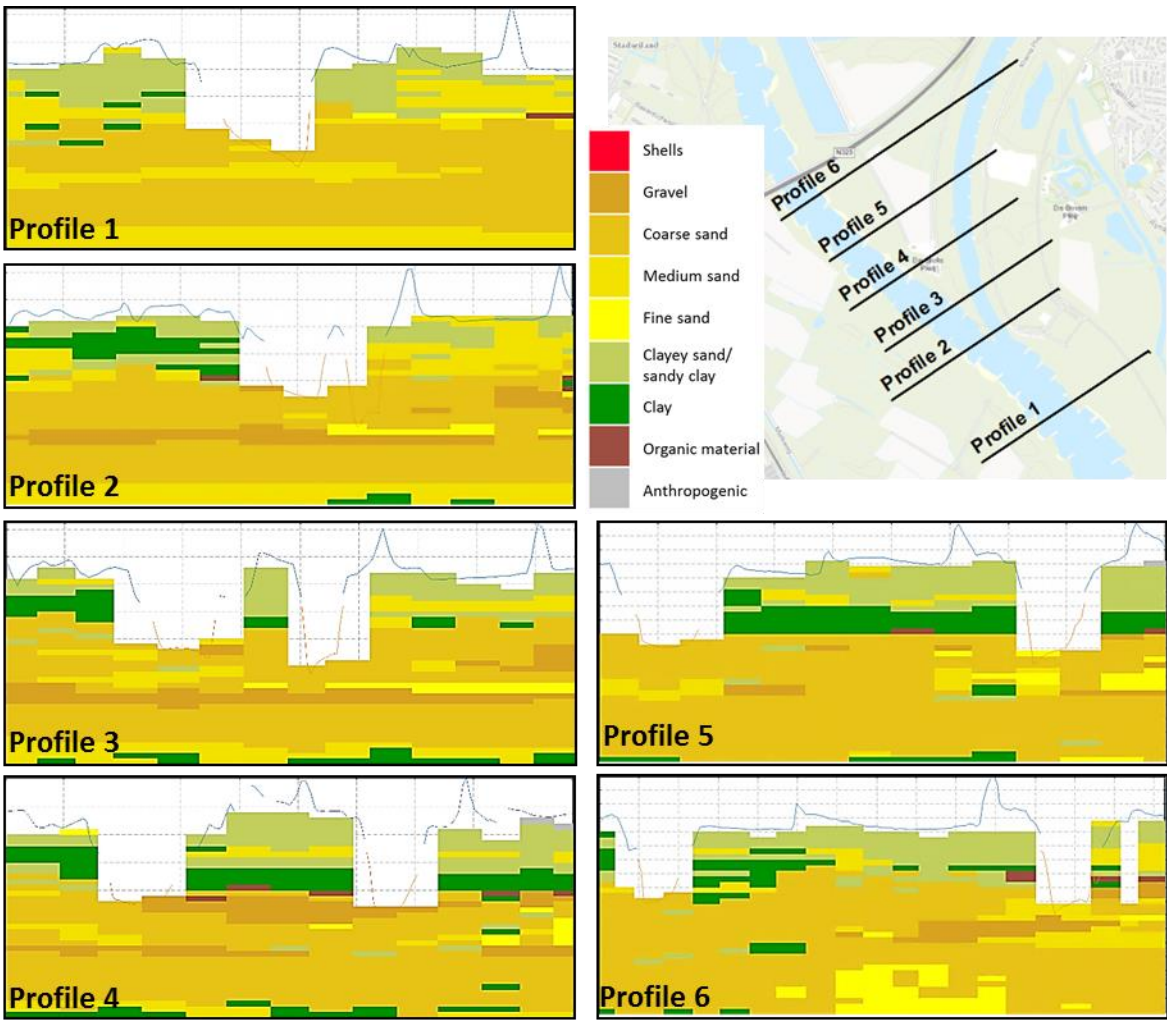

Figure 2-5: Cross-sections of the lithology at the IJsselkop flood plain with the bed topography profiles (red lines) and the surface profiles (blue lines) (TNO, 2011)

The figure shows the presence of fine sediment in the flood plains upstream of the bifurcation (profile 1 and profile 2) and at the V-shaped flood plain between both branches (profiles 3 to 6) with a thickness of up to 2.5 m, which agrees with the expectation that fine sediment often settles at flood plains after high water conditions. The fine sediment layer is on top of a coarse sand layer that is likely to originate from the Formation of Kreftenheye and is also located below the main channel and varies from 'medium sand' to 'gravel'. A field visit showed that vegetation is present across the flood plain on top of a fine sandy environment, which is locally exposed due to damages. An analysis of the substrate, surface characteristics and stability of the flood plain is performed in Chapter 4.

Stratification of the main channel

The data from Figure 2-5 showed that a coarse layer is present in the substrate below the main channel. Detailed bed characteristics are obtained by using interpolated data of drillings that have been carried out by TNO (TNO, 2003) in cooperation with the University of Utrecht along the Rhine branches. The drillings have been performed up to a depth of 6 m below bed level. The data are interpolated and converted to a grid with cells of 25 m x 25 m. These data points only provide information about the bed characteristics of the main channel and are used for the analytical calculations of the bed stability

in Chapter 3. The drilling samples are cut into vertical segments of 20 cm. Figure 2-6 shows an example of the data resulting from a drilling. The grains are categorized according to the logarithmic Wentworth classification as shown in Table 2-1.

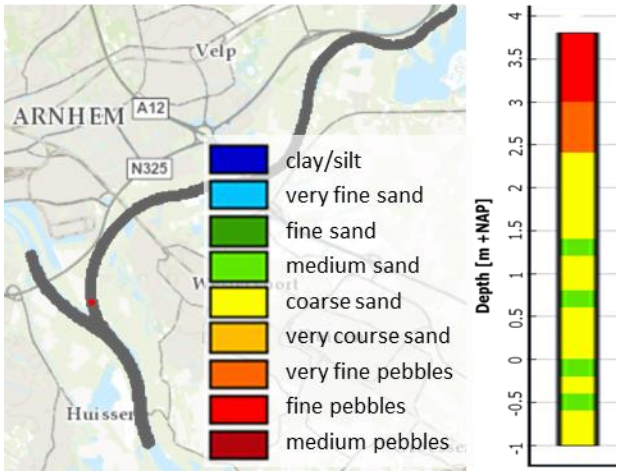

Figure 2-6: Example of a borehole (on the right) at the location of the red dot

Table 2-1: Wentworth classification for sediment

Classification	Min value [mm]	Max value [mm]
Clay/silt	0.001	0.062
very fine sand	0.062	0.125
fine sand	0.125	0.250
medium sand	0.250	0.500
coarse sand	0.5	1.0
very course sand	1.0	2.0
very fine pebbles	2.0	4.0
fine pebbles	4.0	8.0
medium pebbles	8.0	16.0

A coarse layer of pebbles (orange-red) is present on top of a finer layer with sand (yellow), which illustrates the presence of a coarse top layer. Figure 2-7 shows a 2D-map of the grain size (d_{50}) of the top layer of the bed material. The top layer in the IJssel branch is almost completely covered with grains up to 8 mm, while the overall diameter in the Lower Rhine does not exceed 4 mm, which is the result of lateral sediment sorting in river bends[7] and influence of the primary flow on the bed sediment composition.

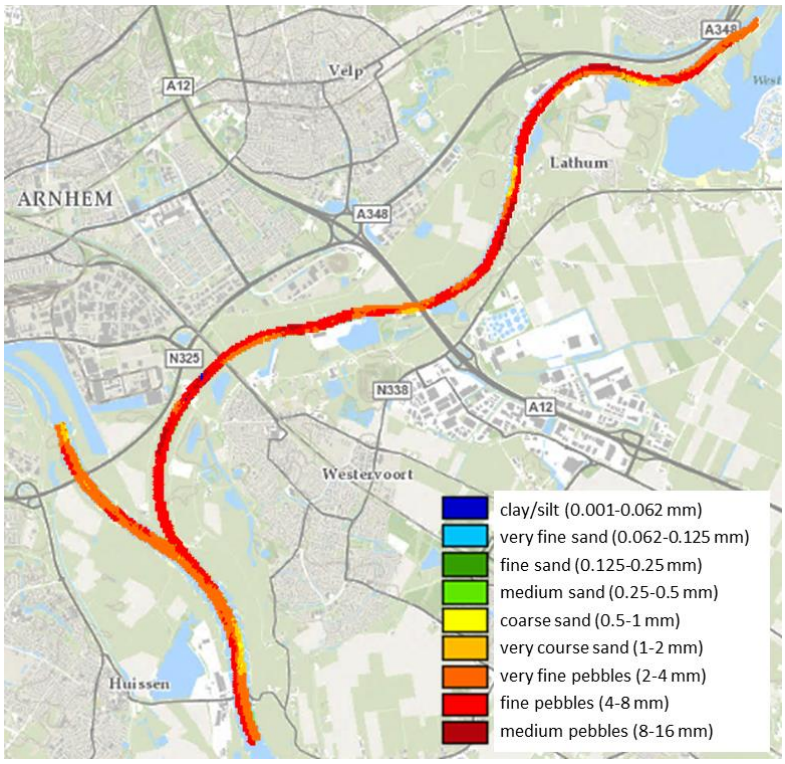

Figure 2-7: Grain diameter d_{50} of the top layer

[7] Secondary flow, as a result of a pressure gradient, results in erosion in the outer bend and sedimentation in the inner bend with a lateral sorting of fine sediment in the inner bend and coarse sediment in the outer bend

A long-section along the IJssel river (Figure 2-8) shows a coarse top layer with varying thickness of 0.5-1.5 m with a d_{50} up to 8 mm. Underneath the top layer a sandy environment is present with a d_{50} up to 1 mm. This layer structure can be applied for locations more downstream in the IJssel branch as well (up to the boundary of available data). Some core samples are less visible than others in Figure 2-8. The presented core samples in the figure are located at the red cross-sectional line in the lower right corner.

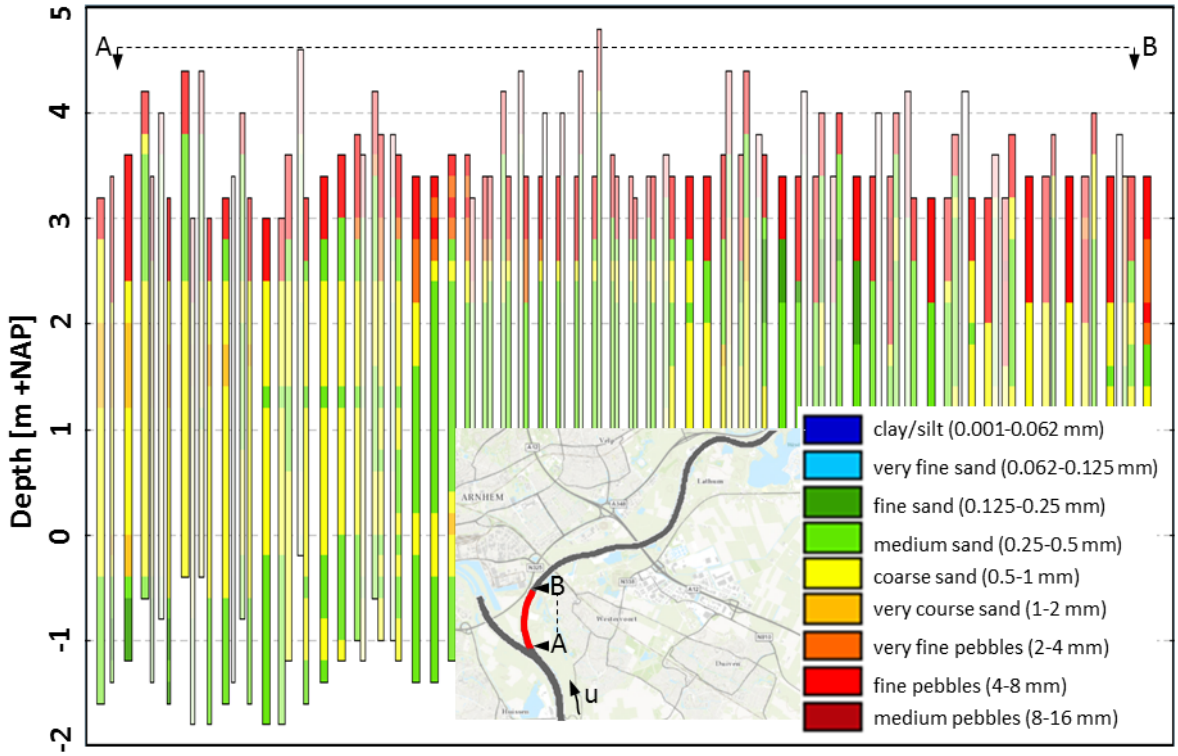

Figure 2-8: Representation of a long-section of the cores along the IJssel river axis on the red line. The most left core equals the most upstream location. All core samples in a buffer zone of 20 m on both sides of the line are shown as well, becoming vaguer when the distance to the actual line increases

Cross-sections over the river (see Figure 2-9) show core samples below the river bed for each profile. The layer structure with a coarse top layer and a layer with fine sand below is visible in this figure as well as the lateral distribution of the grains. The latter is visible in profile 2, where the IJssel (outer bend) has coarser sediment than the Lower Rhine (inner bend). Some discrepancies between the top of the core and the river bed (the blue lines) are caused by the fact that these drillings have been carried out some ten years earlier than the measurements of the bed topography profiles. From bed level downward there is a layer with a d_{50} of about 6-7 mm with a thickness of 0.20-0.40 m on top of a layer with a thickness of 0.40 m with a d_{50} of 4-5 mm. Below this layer less coarse sediment is present with a d_{50} up to 1 mm. Overall it can be concluded that there is a coarse top layer of about 0.7 to 1.0 m.

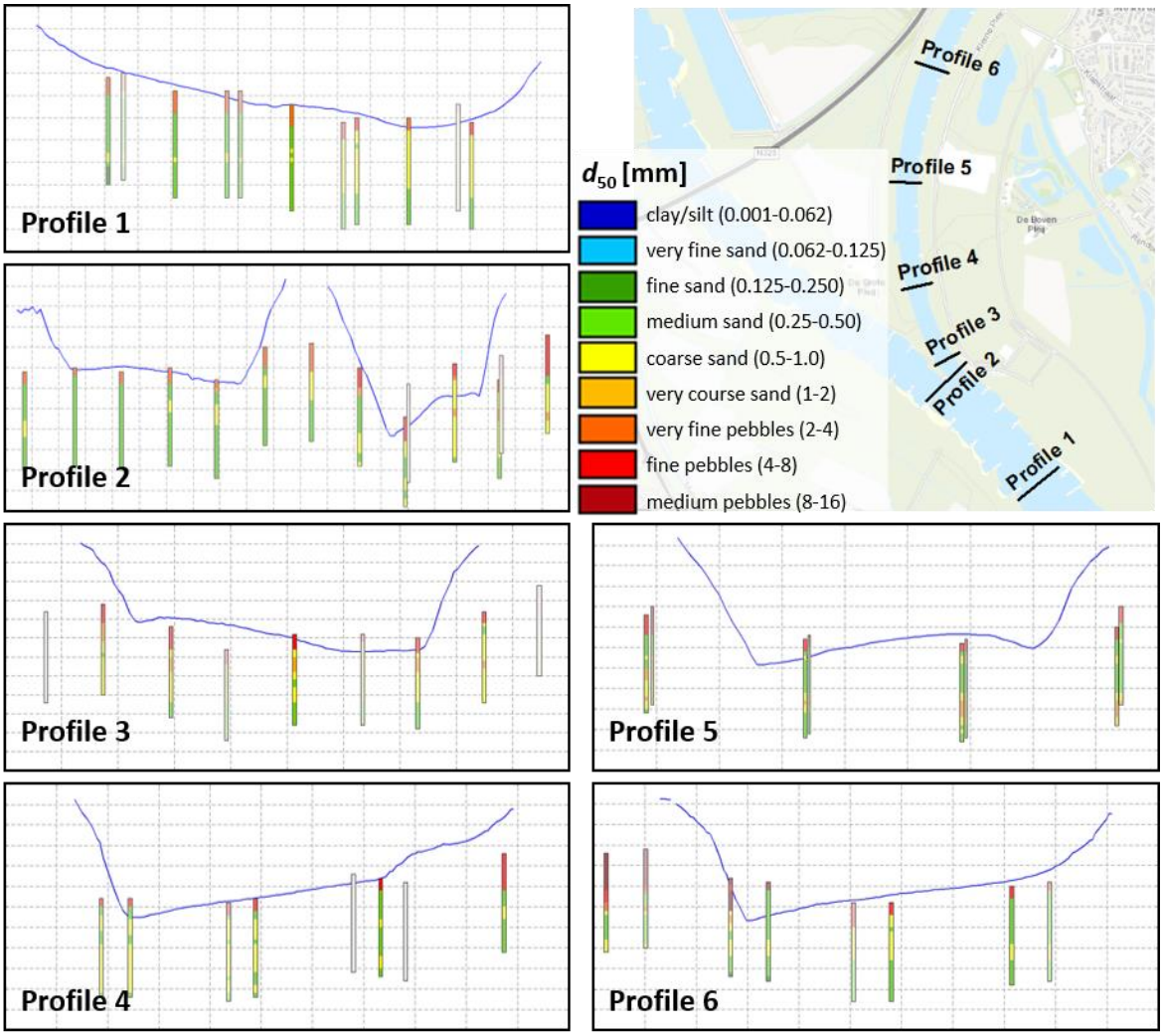

Figure 2-9: Cross-section river bed with the cores. The distance between the vertical grid lines is 10 m and the distance between the horizontal grid lines 1 m

2.4 Bed topography

To get insight in possible erosion and sedimentation patterns, bed level data of Rijkswaterstaat from 2002 to 2013 have been analyzed. The annual measurements are performed with a vessel using multi-beam altimetry and were performed under average conditions, a discharge at Lobith between 1000 and 3000 m^3/s. More background about these measurements is presented in Appendix A.

Short term bed topography developments

Yearly bed level measurements (Rijkswaterstaat Oost-Nederland, 2014b), from 2002 to 2013, show the short term developments of the bed level around the IJsselkop. An example of the bed topography is shown in Figure 2-10. The outer bends are deeper, due to the secondary flow. Furthermore, a deeper bed downstream of the groynes and shallower parts upstream of the groynes can be observed. The bed levels in the branches show an overall lower bed level in the IJssel branch compared to the Lower Rhine branch. This observation supports the observation that the IJssel bed slope is steeper than the Lower Rhine bed slope.

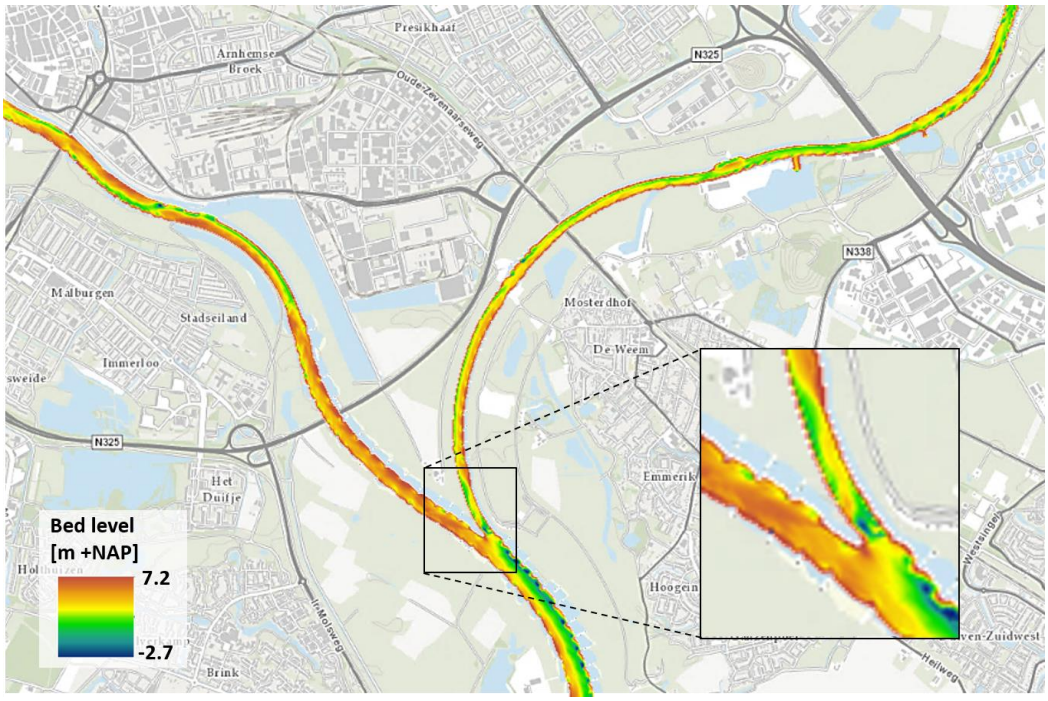

Figure 2-10: Interpolated bed topography of measured data in 2013 of the main channel at the IJsselkop

Figure 2-11: Bed level difference between 2013 and 2002

A comparison between the first and last data of the yearly measurements shows a general decrease in bed level (Figure 2-11). Some differences in bed level may be influenced by different circumstances during the measurements, e.g. a dune can cause a local bed level difference of a few decimetres.

The magnitude of sedimentation and erosion differs from location to location. In the Lower Rhine branch a lot of erosion has occurred just downstream of the bifurcation, whereas sedimentation has taken place more downstream. A large erosion peak (up to 3 m) is visible in the IJssel branch close to the bifurcation. This phenomenon, a deep erosion pit, is discussed in more detail in the next paragraph. Furthermore, a pattern of alternate sedimentation and erosion areas along the IJssel river are present according to Figure 2-11.

Bed level development

The bed level difference (with 2002 as reference value) for fixed locations (kilometre markers) is plotted in time in Figure 2-12. The missing kilometre markers between km891 and km896 result from cut-offs in the seventies, when the river became shorter, but the kilometre markers weren't changed.

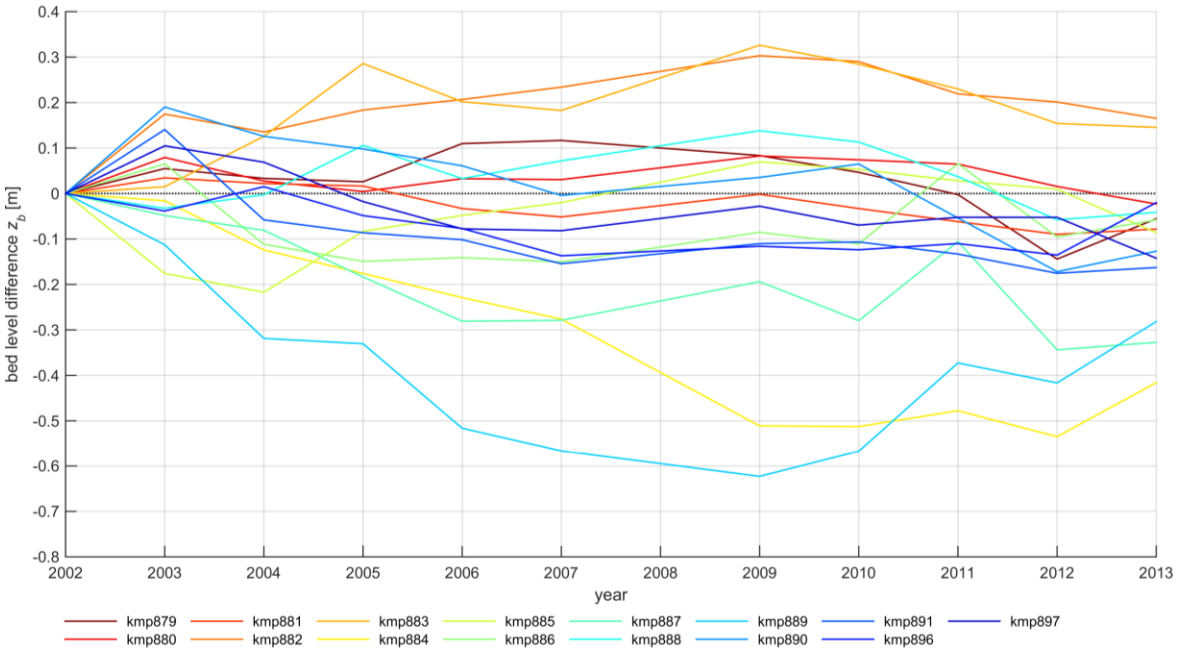

Figure 2-12: Calculated bed level development between 2002 and 2013

At each kilometre marker an average depth value is calculated from the depth points within a rectangle domain of 30 m width and 100 m long. The centre of this rectangle is the intersection between the river axis and kilometre marker. A domain averaged bed level value is chosen above one bed level value in order to prevent that local bed forms cause unrealistic bed elevation values. The bed level at km 881 is low compared to the locations more up- and downstream, which may be caused by the presence of a bridge just upstream. According to the data in Figure 2-12, the trend in bed level evolution is an average decrease with a magnitude of about 1-2 cm/year.

Scour hole

A scour hole is observed in the IJssel branch close to the bifurcation (see Figure 2-10). The measured development of this erosion pit is shown in Figure 2-13. Due to the limited sediment supply the erosion pit will not be filled as would be expected from an alluvial river. Also the local turbulent processes, caused by both the bifurcation and the pit itself, prevent the pit to be filled with sediment. The hole is mostly filled with coarse material, according to the data of the drillings (TNO, 2003), which is only supplied during higher discharges.

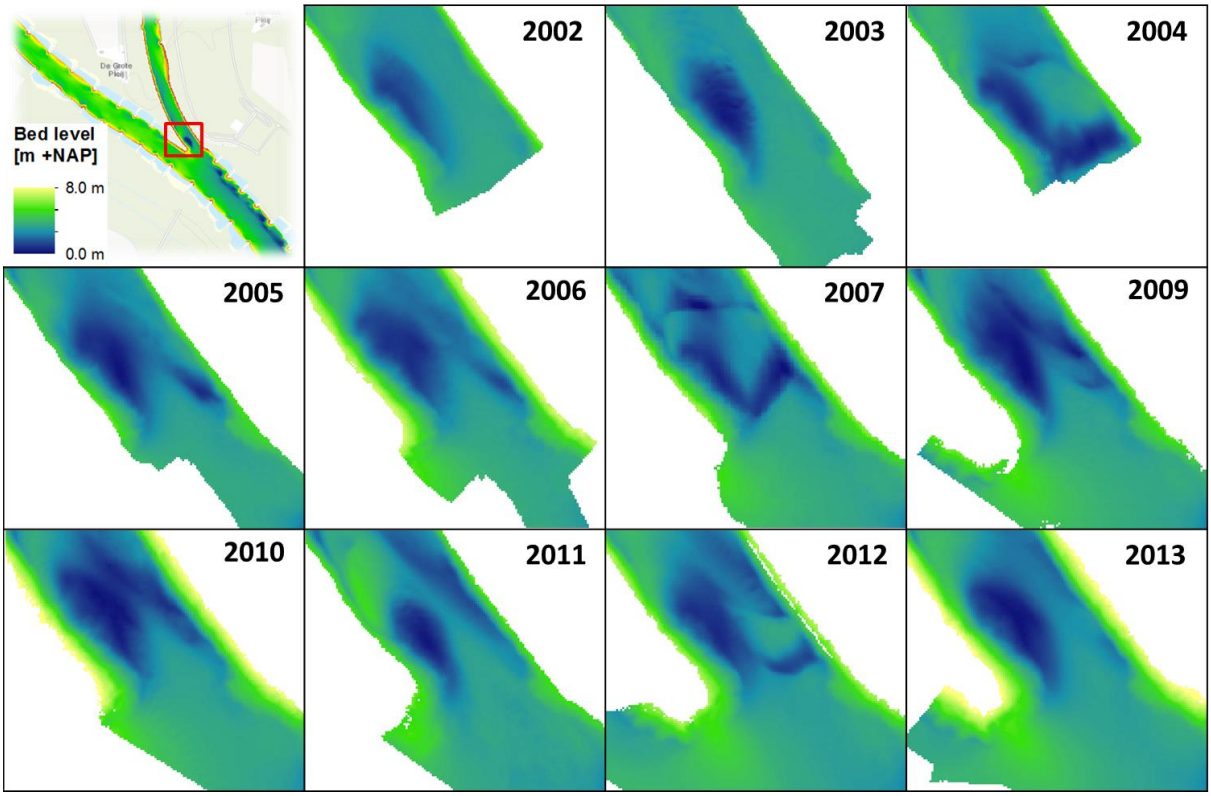

Figure 2-13: Measured data (Rijkswaterstaat Oost-Nederland, 2014b) on bed elevation of the erosion pit between 2002 and 2013

Strange transitions, with a deeper part in lateral direction, between 2003-2004, 2006-2007 and 2011-2012, may be caused by ships that ran aground at the bifurcation during low water. These holes have been filled up in time, while the initial pit (from 2002) remains present. The reason for the presence of this hole may be the flow pattern in that area. Due to the geometry (i.e. steeper bed slope) of the IJssel, more water is attracted to this branch. The corresponding acceleration of the water that flows into the IJssel may maintain this scour hole.

2.5 Hydrodynamics

Introduction

Daily discharge and water level data (Rijkswaterstaat Oost-Nederland, 2014a) gives insight in the hydrodynamic developments during the last decades. The data have been gathered from 1901 to 2013 at the monitoring location of Lobith and from 1962 to 2013 at the monitoring location of the IJsselkop. The daily water level values were measured at 08:00AM up to 1989 and since 1989 these values are the daily average. The discharge calculation is performed by using a *Q-h* relation until mid-2003 and since then by using a *Q-f* relation, which was introduced when more knowledge was gathered about involved parameters[8]. More background about the data measurements is presented in Appendix A.

Historical discharge developments

The daily discharges at Lobith, from 1901 to 2013, are presented in Figure 2-14. The average Lobith discharge during this period is approximately 2,200 m^3/s, with several discharge peaks above 10,000 m^3/s. The highest peaks are highlighted in the figure, including the most recent one in 1995 which caused floodings in the South-East of the Netherlands. This peak value was close to the maximum known peak at Lobith, which dates from January 1926 with 12,225 m^3/s.

[8] The *f* in the name refers to 'function', which implies that several parameters are included in this relation

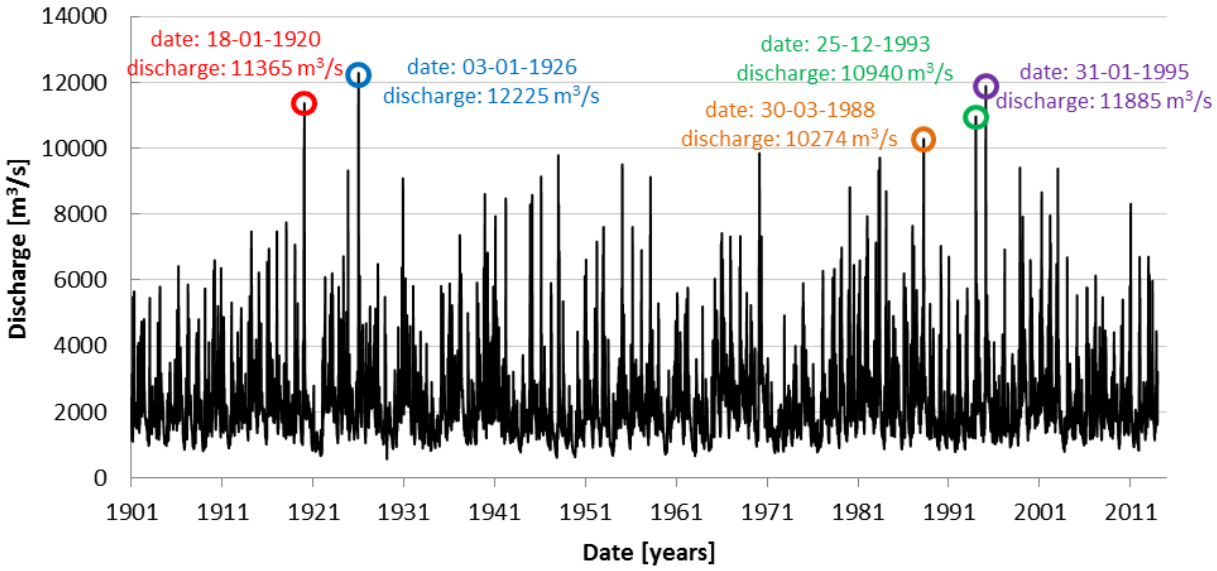

Figure 2-14: Measured daily discharge at Lobith (1901-2013)

The amount of discharge at Lobith that is distributed towards the IJssel is presented in Figure 2-15. The daily discharge distribution between 1961 – 2013 showed each year the same pattern, so that this graph shows the average daily distribution over these years. The figure shows that the desired IJssel discharge distribution of 1/9th of the Lobith discharge is not met. The first part of the year shows a distribution of about 1/7th (15%), while the second part of the year even 1/6th of the discharge at Lobith is distributed towards the IJssel. Peaks of above 20% (1/5th) have been occurred as well.

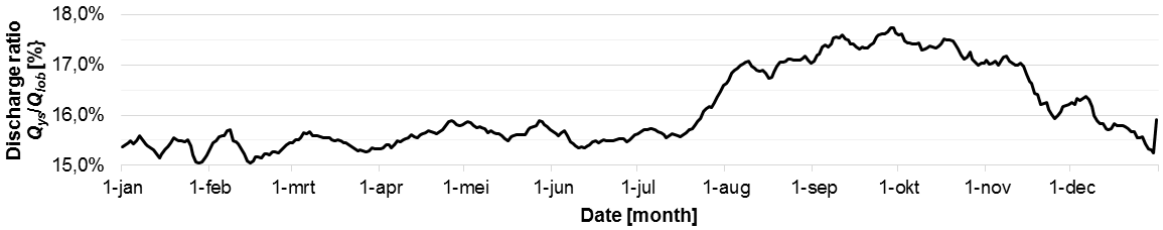

Figure 2-15: Daily IJssel discharge in terms of the Lobith discharge averaged over 1961-2013

Trend of the discharge

No significant changes are observed in the discharge development over the last century. The average discharge has been more or less constant over this period and the probability of occurrence is also more or less the same for each decade. From the few discharge peaks above 10,000 m^3/s it cannot be concluded if extreme discharges occur more often, due to the small probability of occurrence. Because of more severe weather conditions, it is expected though that these will occur more often in the future.

Historical water level developments

The daily water levels from 1901 to 2013 (see Figure 2-16) show a slight decrease in average water level over time. Moreover, the peaks are less extreme compared to the discharge data, which is caused by the non-linear relation between the discharge and water level ($Q \sim h^{3/2}$).

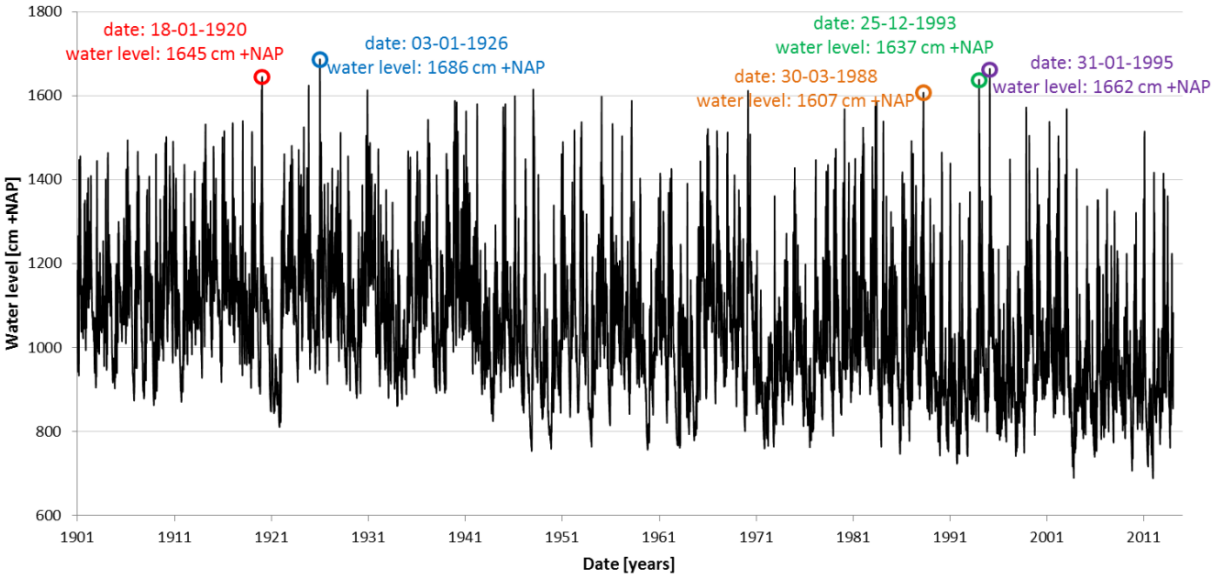

Figure 2-16: Measured daily water levels at Lobith (1901 - 2013)

Analysis of the hydrodynamic developments

More knowledge about the hydrodynamic developments is gathered when the measured discharge and water levels at the IJsselkop are plotted against each other (see Figure 2-17). This relation is known as the *Q-h* relation, the Dutch term for the discharge rating curve. Insight in the development is provided by dividing the data into decades.

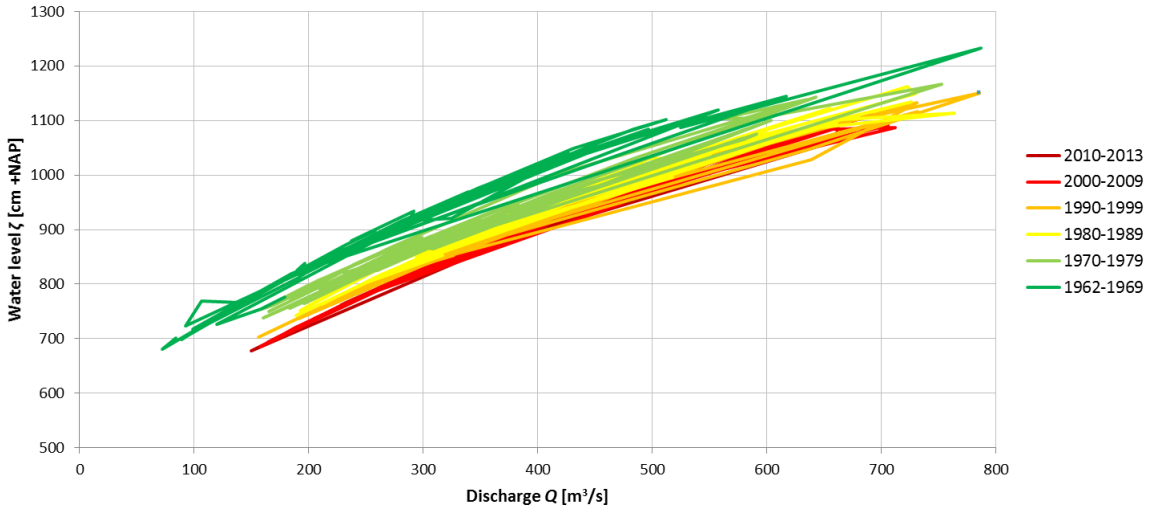

Figure 2-17: *Q-h* relation at the IJsselkop

The first thing to note in the figure is the minimum discharge of about 160 m^3/s since the seventies, which is the result of the construction of weirs in the Lower Rhine. The weir at Driel guarantees a minimum amount of discharge for the IJssel with 3 regimes as shown in Table 2-2.

Table 2-2: The Driel weir positions (Rijkswaterstaat, 2011)

Discharge *Q* at Lobith [m^3/s]	Function of weir
Q < 1300	Minimal 25 m^3/s is provided for the Lower Rhine. The remaining part of the discharge goes to the IJssel
1300 < Q < 2400	The weirs are opened with a variable height so that 285 m^3/s flows into the IJssel. The discharge towards the Lower Rhine increases with increasing discharge at Lobith
Q > 2400	Weirs are completely open. The discharge distribution is no longer affected by the weirs

Another aspect to notice is the small curve at about 400 m^3/s in Figure 2-17, which is the visualization of the 'activation' of the flood plain as from reaching a certain water level. From that point on, the flowing area increases and the water level is rising slower for increasing discharge. At last, a decrease of the *Q-h* curve over the decades is observed, which indicates that for a given discharge the water levels have decreased in the last decades. The water level has decreased by more than one metre since 1960, which agrees with the conclusion from the data in Figure 2-16.

Apart from the eroding main channel, it is possible that the whole area is exposed to subsidence of the subsoil, but it not likely to occur due to the presence of relative coarse material in the substrate. Other aspects that are of influence are the river normalizations, bend cut-offs and subsidence of the Ruhr area. The constructed dams in the German Rhine (Rhein) reduces the supply of sediment in the future, though it is not known what the exact consequences are. The influence of these aspects is not investigated in this research.

2.6 Conclusion

The conclusions of this chapter answers the research question: *What are the characteristics of the IJsselkop area?*

A coarse sediment layer is present just below the surface and at the top of the river bed around the IJsselkop area, which originates from the formation of Kreftenheye. This is a coarse sediment layer that is deposited between glacial eras tens of thousands of years ago. Drillings show that the first metre below bed level consists of coarse material, up to a grain size (d_{50}) of 8 mm, on top of a significant less coarse sediment layer with a d_{50} up to 2 mm. The flood plain has a top layer of sandy/clayey sediment, which is covered with vegetation.

The bed level decrease in the period 2002 to 2013 is about 1-2 cm/year, which is equal to the average decrease in water level over the last 50 years at the IJsselkop. The subsidence may be caused by the deficit in sediment supply and the fact that bend cut-offs have been constructed in the IJssel. The analysis of a scour hole development in the IJssel branch close to the bifurcation over the last 11 years, showed that the hole is maintained by turbulent processes around the bifurcation and the fact that flow accelerates into the Ijssel. Bed topography data from before 2002, which was not available for this research, might show more information about origin of the scour hole and the processes around the bifurcation. Some temporary scour holes at the bifurcation, which existed over the years, were caused by ships that ran aground during low water levels.

The IJssel discharge hasn't been below 160 m^3/s since the construction of a weir in the Lower Rhine in the seventies, which provides a minimum IJssel discharge.

Chapter 3 Stability of the armour layer

3.1 Introduction

This chapter shows the answer to the question: *Is the bed layer of the IJssel likely to fail during design discharge conditions?* This question is answered by a stability analysis of the IJssel river bed. This is done by making analytical calculations of the particle mobility during high discharge conditions. Failure of the river bed takes place when a large amount of erosion of this bed layer is expected. The calculations are performed for three different cases. The particle mobility of the IJssel river bed is determined for 1) a bed with uniform sediment 2) a bed with mixed sediment and 3) the effect of dunes on the shear stresses, so an insight is gathered into the behaviour of the river bed.

There are three types of transport; *Bed load transport, suspended load transport* and *wash load*. This research focusses on the grains that move initially as bed load transport.

River bed material

The river bed consist of a coarse layer with a grain size (d_{50}) of 2-11 mm with a thickness of approximately 1 m on top of a finer substrate with a grain size up to 2 mm (Section 2.3). For every 25 m of the river bed a grain size distribution is available (TNO, 2003). Figure 3-1 shows the grain size distribution for several locations.

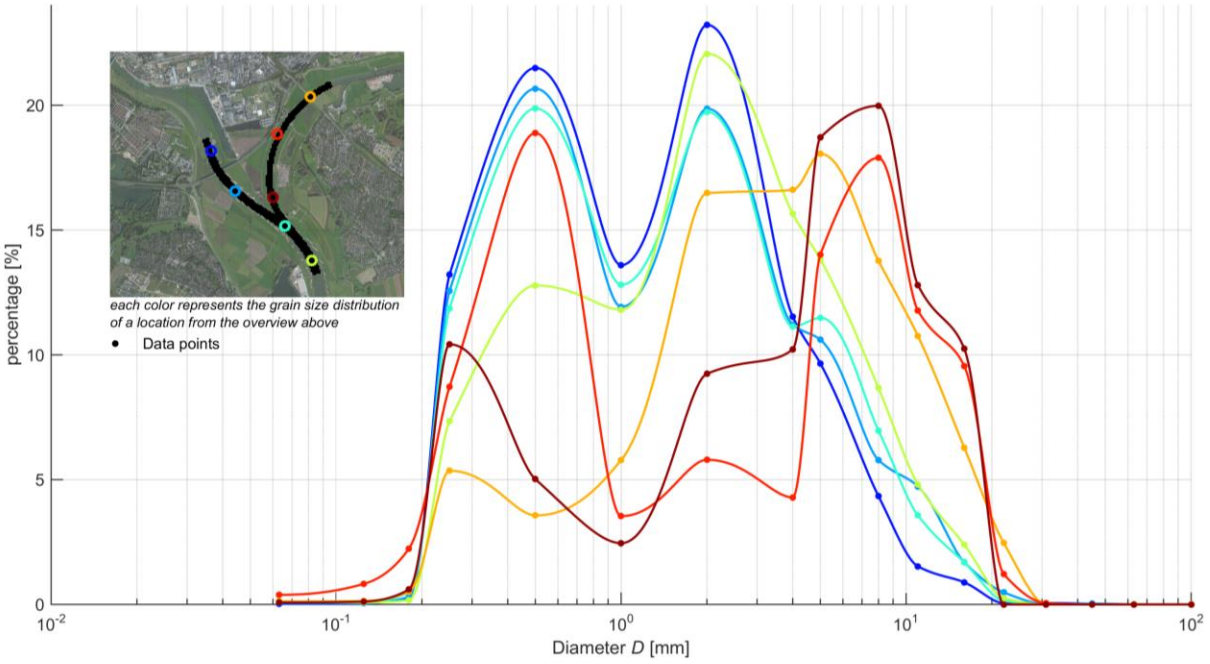

Figure 3-1: Grain size distribution (TNO, 2003) of the top layer at several locations. Each colour represents a location (top left)

A relatively large amount of gravel is present in the top bed layer of the IJssel branch, while the Pannerden Canal and the Lower Rhine branch bed materials is dominated by sand. A large amount of fine sand is present in the three branches as well.

Coarse top layer

The coarse top layer originates partly from the development of the formation of Kreftenheye (see §2.3), but may also be the result of armouring; the coarsening of a sediment mixture. A distinction is made between *static armouring* and *dynamic armouring*. Static armouring is the process that, under no circumstances transport takes place in the coarse bed layer. This layer is likely to be present in gravel rivers where the supply of gravel is cut off due to dams or gravel extraction. A dynamic armour layer is a coarse bed layer that becomes occasionally into transport, and is usually applicable for rivers with a supply of coarse sediment. A static armour layer gets coarser in time, while a dynamic armour layer shows a spatial variation which changes during every high water. Turbulent flow is able to activate finer sediment in the mixture, which leaves the coarser grains (*winnowing*). Winnowing causes the coarsening of the bed and lowering of the coarse layer, which continues until the layer reaches a level from where it becomes immobile (Blom et al., 2003). The IJssel river bed has a dynamic armour layer, since it is occasionally into movement.

Critical parameters regarding the bed stability

Calculations regarding particle stability starts with assigning the strength part (the resistance of the grain particle) and force part (the drag force by the flow). The strength is represented by a critical shear stress $\tau_{b,c}$ or flow velocity u_c, while the force is represented by the acting shear stress τ_b or depth-averaged velocity $\bar{u}$. When the resulting shear stress around the particle becomes higher than its critical value, it starts to move. More information about the particle motion and its governing equations is presented in Section 3.2. Results from a WAQUA simulation of a flood wave with a peak discharge of about 16.000 m^3/s at Lobith (Suryadi and Mosselman, 2005), are used as input for the calculation of the force acting on the grains ($\bar{u}$).

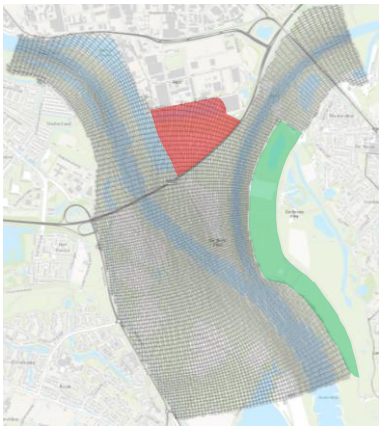

Figure 3-2: WAQUA-grid of selected area (Suryadi and Mosselman, 2005)

For grid points in a specified domain (Figure 3-2) the maximum flow velocity (magnitude and direction) and the maximum water level (Figure 3-3) are determined during the peak discharge. The present situation differs slightly from the one used in the computations by Suryadi and Mosselman because of the developments in the last decade. For example, the polder north of the road (the red area in Figure 3-2) is closed off and the Hondsbroeksche Pley, a flood channel with regulating structure, has been constructed (the green part in Figure 3-2). These developments influence the flow conditions and water levels and are not included in the WAQUA computations. The outcome of this analysis is expected to be conservative regarding the situation[9].

Figure 3-3 shows the water level and flow velocities, which result from the WAQUA computations during the peak discharge of 16,000 m^3/s. The IJssel branch attracts a large amount of discharge, which is shown by the strong gradient in water level (decrease) and flow velocity (increase) just downstream of the bifurcation in the IJssel branch. The flow velocity in the upstream part of the IJssel is high, which is caused by the presence of a steep slope and the small stream width. In WAQUA a curvilinear coordinate system is used in which the cells are numbered in the directions *M* (lateral from the river axis) and *N* (longitudinal from the river axis). This grid is converted into the same coordinate system as for the available grain data (Cartesian), by using GIS-software (ArcGIS), with each data point 25 m located from each other. The resulting water level and velocity profiles are used as input for the acting force in the stability analysis.

[9] The flood channel increases the width of the flow, which decreases the velocity in the main channel.

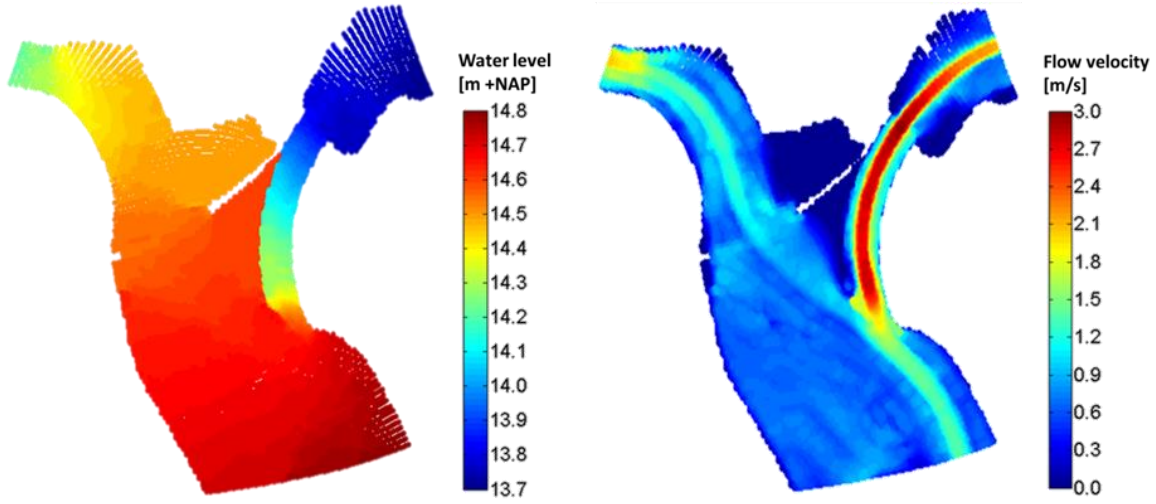

Figure 3-3: Computed water level (left) and flow velocity (right) during design conditions. Data is obtained from WAQUA computations (Suryadi and Mosselman, 2005)

3.2 Initiation of movement based on uniform sediment

The stability of the river bed is first assessed under the assumption that a uniform grain size is present at the river bed. The assessment of the stability of grains at the river bed is performed by studying the (critical) Shields mobility parameter (Shields, 1936).

Critical shields value

The Shields mobility parameter θ indicates the mobility of sediment:

$$\theta = \frac{\tau_b}{\left(\rho_g - \rho_w\right) g D_{50}} = \frac{u_*^2}{\Delta g D_{50}} \tag{3.1}$$

where:

D_{50} = grain diameter [m]
g = gravitational acceleration [m/s^2]
u_* = shear velocity [m/s]
Δ = relative density [-]
ρ_g = density of sediment, constant of 2650 kg/m^3 [kg/m^3]
ρ_w = density of water, constant of 1000 kg/m^3 [kg/m^3]

For values below a critical value θ_c no transport of sediment occurs. The mobility parameter depends on grain properties and the flow pattern near the bottom. The near-bottom flow pattern is defined by the particle Reynolds number Re_*:

$$\mathrm{Re}_* = \frac{u_* D}{\nu} \tag{3.2}$$

Based on experiments, Shields (1936) determined the critical value of the mobility parameter θ_c, as a function of Re_* (Jansen et al., 1979). The critical Shields value can be assumed constant since these grains have a large Reynolds number, $Re_* \geq 500$. For further usage, the Shields mobility parameter is here assumed to be $\theta_c = 0.055$ (Schiereck, 2000), since it is presumed that the critical condition is present when continuous movement of the grains occurs.

Stability calculation

The calculation of the critical mobility parameter, Equation (3.1), is reworked into an equation in terms of the depth averaged velocity $\bar{u}$ and Chézy coefficient C:

$$\theta_c = \frac{\bar{u}_c^{\,2}}{C^2 \Delta d_{50}} \tag{3.3}$$

The Chézy coefficient C_i is a logarithmic function of the water depth h and the 90% passing value of the sieve curve d_{90}.

$$C = 18 \log\left(\frac{12h}{d_{90}}\right) \tag{3.4}$$

The water level is based on the results of WAQUA (Figure 3-3) and the 90% diameter is calculated from the grain size data (TNO, 2003). From Equation (3.3) and (3.4) the critical depth averaged velocity is calculated. By combining both equations, the depth-averaged critical velocity for each location i, $\bar{u}_{c,i}$ becomes:

$$\bar{u}_{c,i} = 18 \log\left(\frac{12h_i}{d_{90,i}}\right) \sqrt{\theta_c \Delta d_{50,i}} \tag{3.5}$$

The critical bed shear stress $\tau_{c,i}$ for each location is calculated using Equation (3.6):

$$\tau_{c,i} = \frac{\rho_w g}{C_i^{\,2}} \bar{u}_{c,i}^{\,2} \tag{3.6}$$

where $\bar{u}_{c,i}$ is computed from Equation (3.5). Both the critical shear stress and the critical velocity based on the d_{50} of the top layer are presented in Figure 3-4. The critical values in both branches are larger in the outer bends. The lateral sediment distribution in river bends cause the fines to be diverted to the inner bend, and the larger grains to be diverted to the outer bend. An area with a relatively low critical flow velocity is located between the two red areas in the bend in the IJssel branch.

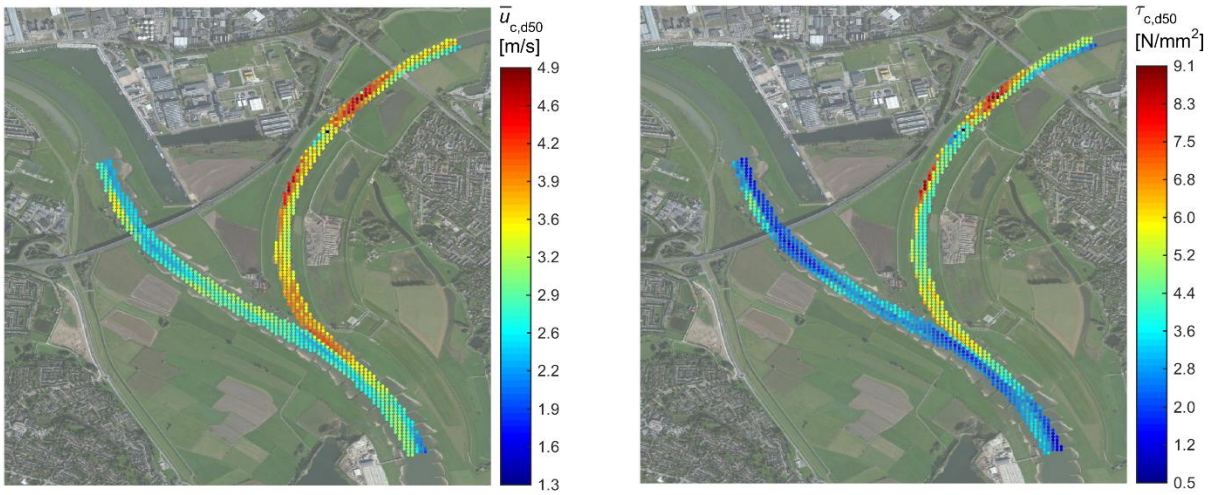

Figure 3-4: Overview of the critical depth-averaged velocities (left) and the critical shear stresses (right) based on the d_{50} of the top layer according to Shields

Bed stability based on uniform sediment

The stability of the river bed is determined by calculating the ratio between the depth-averaged acting velocity $\bar{u}$ (data from Figure 3-3) and depth-averaged critical velocity $\bar{u}_c$ (data from Figure 3-4):

$$p = \frac{\bar{u}}{\bar{u}_c} \tag{3.7}$$

When the stability value p exceeds 1, it means that the acting velocity is larger than the critical velocity and therefore the sediment is mobile. The ratio p is shown in Figure 3-5.

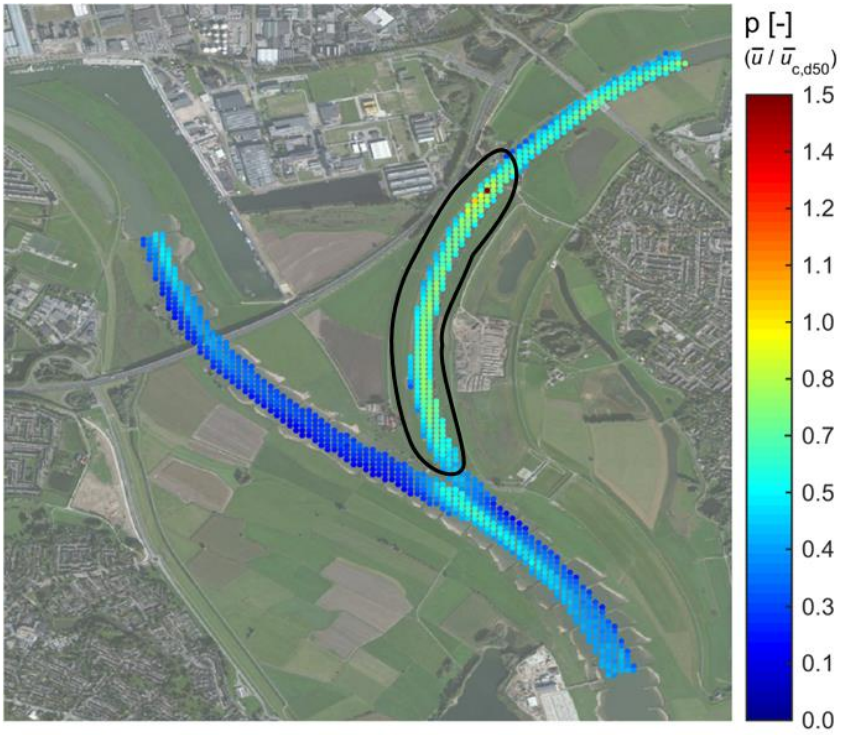

Figure 3-5: Stability value *p* for the river bed based on uniform sediment

Variation in bed stability is visible in both the lateral flow direction and the main flow direction. Overall, the stability in the inner bend is less than the outer bend and the IJssel is less stable than the Lower Rhine. The bed can be indicated as stable, because the overall values do not exceed 1 according to the stability calculation based n uniform sediment. However, lower values for p are marked as critical, because of the inaccuracy in the parameters. Critical values above the lower stability boundary value of p = 0.7 are presented in the encircled black area in Figure 3-5.

3.3 Initiation of movement based on mixed sediment

Since the river bed consists of widely mixed sediment instead of uniform sediment, the influence of the mixture is investigated. The influence of the mixture is described by using the hiding and exposure principle.

Method

The Shields value in Equation (3.3) is only applicable when there is a clear sorting of the sediment, like unimodal or bimodal (Figure 3-6a and b).

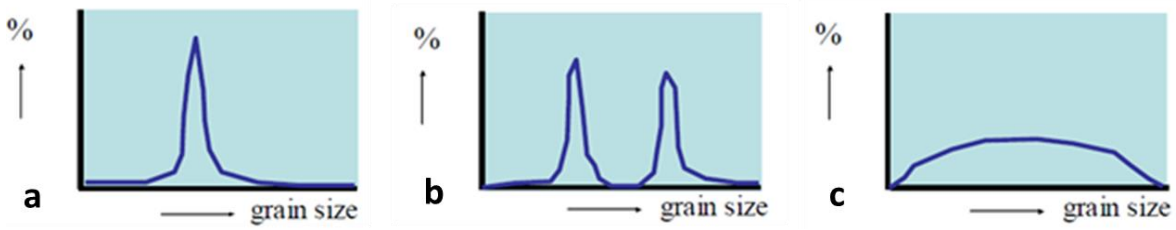

Figure 3-6: distinction between a (a) unimodal, (b) bimodal and (c) badly sorted unimodal mixture

The theory of Shields is insufficient for a well graded grain distribution. The stability of a grain depends on the grain sizes it is surrounded by. With a large variation in grain sizes, the smaller grains can shelter between the larger grains. Due to this shelter, these small grains are not likely to be entrained with a velocity as expected from Shields. The other way around, the larger grains are exposed more, which enables the flow to entrain these grains at a lower velocity than expected from Shields. (Egiazaroff, 1965) termed this process the *hiding and exposure mechanism*. A correction factor is introduced for each grain fraction, in which a distinction is made between the fractions that are larger and smaller than the surface geometric mean diameter D_{sg} (Ashida and Michiue, 1972). The factor ξ is the ratio between the critical shear stress according to Shields (τ^*_{scg}) and the shear stress that includes the hiding and exposure principle ($\tau^*_{c,i}$) it is defined as (Parker, 2004):

$$\xi_i = \frac{\tau^*_{c,i}}{\tau^*_{scg}} = \begin{cases} 0.843\left(\dfrac{D_i}{D_{sg}}\right)^{-1} & \text{for } \dfrac{D_i}{D_{sg}} \le 0.4 \\ \left[\dfrac{\log(19)}{\log\left(19\dfrac{D_i}{D_{sg}}\right)}\right]^2 & \text{for } \dfrac{D_i}{D_{sg}} > 0.4 \end{cases} \tag{3.8}$$

where:

$$D_{sg} = 2^{\psi_s} \tag{3.9}$$

$$\psi_s = \sum_{i=1}^{N} \psi_i F_i \tag{3.10}$$

$$\psi_i = \log_2\left(\frac{D_i}{D_{ref}}\right) \tag{3.11}$$

$$D_i = \sqrt{D_{b(i)} D_{b(i+1)}} \tag{3.12}$$

$$F_i = F_{b(i+1)} - F_{b(i)} \tag{3.13}$$

in which:

D_i = representative grain size of size fraction i [mm]
D_{sg} = surface geometric mean diameter [mm]
D_{ref} = reference grain size, which is a constant of 1 mm [mm]

$\tau^*_{c,i}$ = critical shear stress for all sizes D_i [N/mm^2]
τ^*_{scg} = critical shear stress for the mean size D_{sg} [N/mm^2]
ψ_s = mean grain size on ψ scale [-]
ψ_i = grain size of fraction i on ψ scale [-]
F_i = percentage of the grains within fraction i [%]

The subscript b represents the fraction boundary value. The cumulative grain size distribution curve is distributed in five parts of equal grain size interval on log scale, so that the indicator i has a range of 1 to 5. Each boundary is named D_{b1} up to D_{b6}. These values are found by first determining the log values of D_{max} and D_{min}. The value of each of these fractions is calculated according to Equation (3.14):

$$D_{b,i} = \log^{-1}\left[\log(D_{min}) + \frac{i}{5}\log(D_{max}) - \log(D_{min})\right] \tag{3.14}$$

The area between boundary 1 and 2 is the first fraction, the area between boundary 2 and 3 is the second fraction etc. An example is given in Figure 3-7.

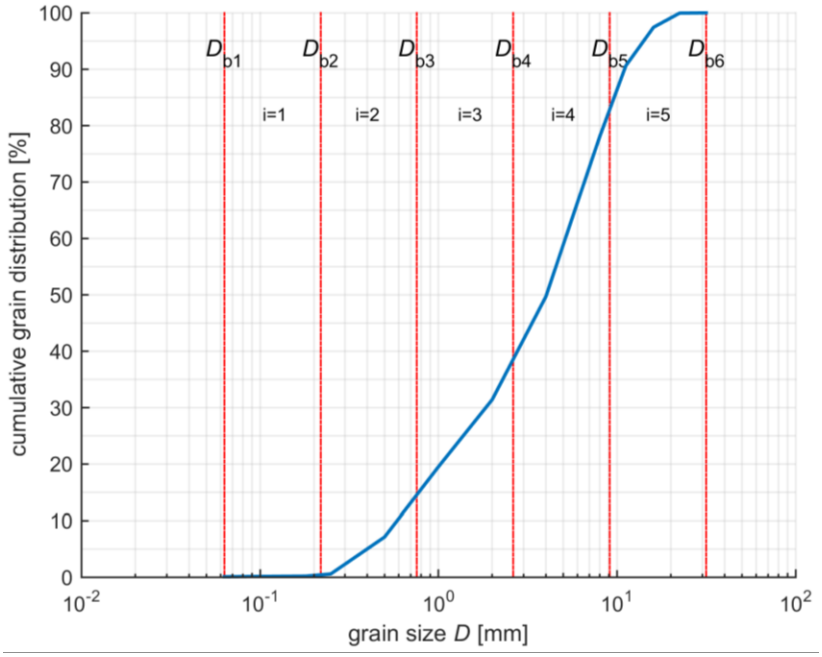

Figure 3-7: cumulative grain size distribution, divided in fractions

Hiding and exposure factor τ_{ci}^*/τ_{scg}^*

The hiding and exposure factor is calculated by using Equation (3.8). This factor differs for each location and each fraction. Table 3-1 gives an indication of the correction factor ξ by showing the median of the upper layer of all locations for each fraction i. The smaller grain fractions become more stable (hiding) and the larger fractions less stable (exposure).

Table 3-1: median values of the correction factor per fraction

Fraction i	Median of ξ_i
1	20.7239
2	5.8351
3	1.7149
4	0.7109
5	0.3840

Comparison of the shear stresses between corrected and original Shields values

For assessing the grain stability according to Shields including the hiding and exposure multiplication factor ξ_i, the critical shear stresses are calculated using Equation (3.15):

$$\tau_{c,i} = \xi_i \theta_c \rho_w g \Delta D_i \tag{3.15}$$

Figure 3-8 shows for a random location how the larger grains become less stable and fines become more stable.

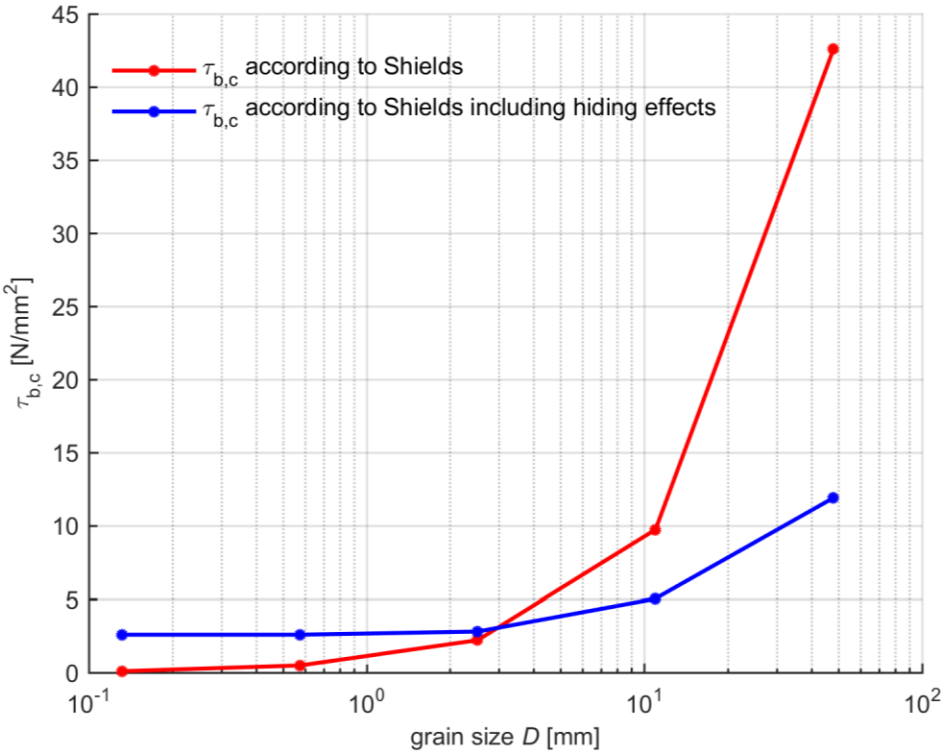

Figure 3-8: Comparison of the critical shear stress of a random location according to Shields and Shields including the hiding and exposure mechanism (according to Equation 3.10)

Failure of fraction 5 indicates that almost all grains are already washed away and the bed is unstable. Failure of fraction 3 causes erosion of these and smaller grains, but it is assumed that the non-eroding amount of fraction 4 (and 5) keeps the layer more or less stable. It is determined that failure of fraction 4 may cause break-up of the river bed, since it is a coarse fraction with a high percentage of occurrence (≈ 40%, see example in Figure 3-7). Figure 3-9 shows the reduction of the critical shear stress when the hiding and exposure mechanism is taken into account. The figure shows a comparison for the critical shear stress value with and without taking into account the hiding and exposure mechanism of fraction 4.

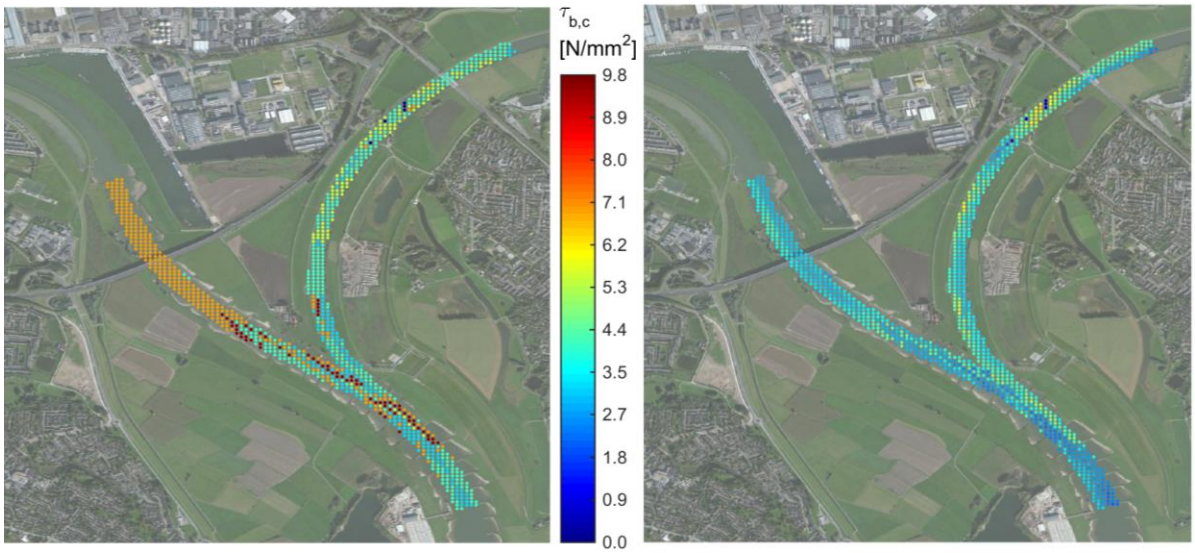

Figure 3-9: Comparison of the critical shear stresses of fraction 4 for Shields (left) and the hiding and exposure mechanism (right)

Stability value *p* for mixed sediment

The stability values are again determined using Equation (3.7). The stability of the larger grain diameters becomes more critical, while the stability for the smaller fractions increases. The results are presented in Figure 3-10.

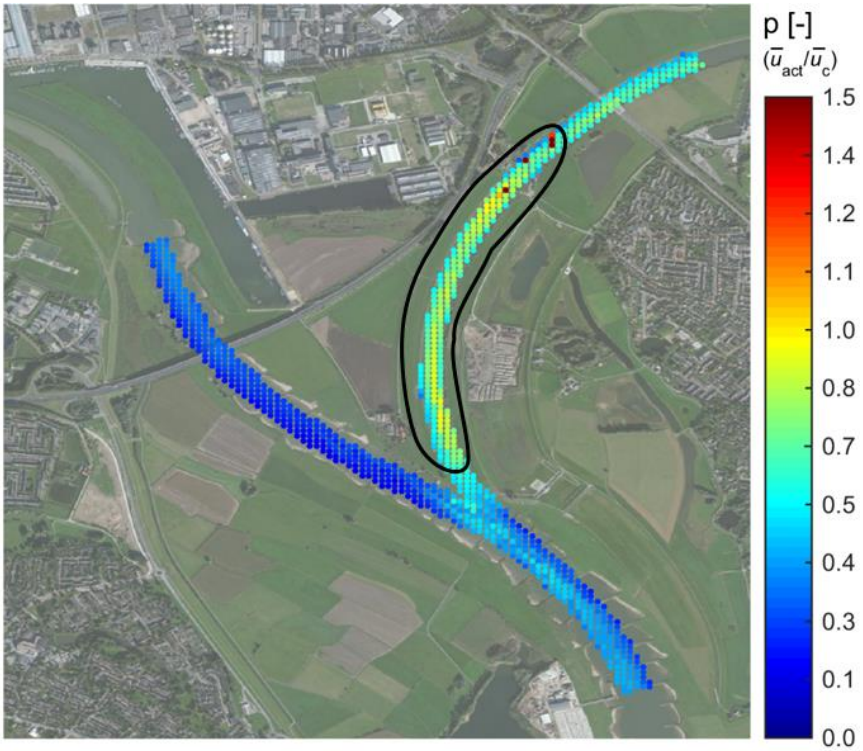

Figure 3-10: Calculated *p* value, stability for mixed sediment, for fraction i = 4

The bed stability decreased compared to the scenario based on uniform sediment (lower left plot in Figure 3-10). Again, the most critical values are located in the encircled area, the same area as for the scenario with Shields only (uniform sediment). The influence of the hiding and exposure factor is visible in the presence of a significant decrease in bed stability for locations with large grain sizes, which has especially changed for the IJssel branch. The differences between the stability based on

uniform sediment (Shields without the hiding and exposure mechanism) or based on mixed sediment (hiding and exposure mechanism included) are less significant for the Lower Rhine or Pannerden Canal.

3.4 Effect of dunes on the actual shear stresses

Bed forms affect the bed stability. First of all, the presence of dunes induces vertical sorting of sediment with fine sediment on top of coarser sediment. Coarse grains roll down the lee face of the dune and settle at the trough, while finer sediment experience more friction and settles along this lee face (Blom et al., 2003), see Figure 3-11. Most of the sediment in the mixture goes into transport when a high shear stress is present, provided that it is above a certain threshold value. For lower shear stress not all grains go into transport. This forms an *immobile layer* below the active layer, which is shown in experiments (Blom et al., 2003). This results in migrating sand dunes on top of an immobile coarse layer. Figure 3-12 shows the results of a sediment sorting experiment with a sand-gravel mixture (Kleinhans et al., 2000).

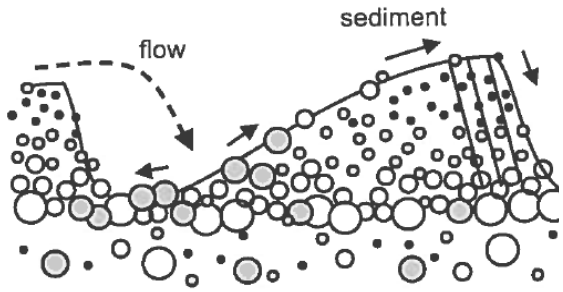

Figure 3-11: Schematization of downward coarsening because of dune formation (Blom et al., 2003)

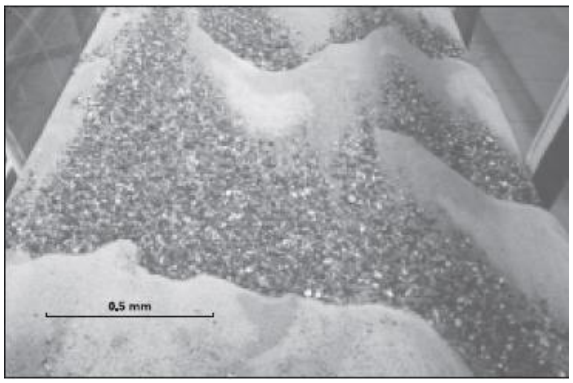

Figure 3-12: Result of experiments with gravel-sand mixture. Sandy bed form on top of a gravel layer (Kleinhans et al., 2000)

Secondly, dunes can affect the depth-averaged flow velocity. For a constant value of the specific discharge q, the depth-averaged flow velocity is higher at the crest of the dune compared to the trough of the dune, according to Equation (3.16):

$$u_2 = u_1 \frac{h_1}{h_2} \tag{3.16}$$

with indices 1 and 2 for the location at the trough and the crest of the dune respectively. The corresponding depth-averaged flow velocity at the crest is larger than assumed according to section 3.1 and 3.2, which may give a rough estimation of the influence of dunes. Additionally the overall bed shear stress increases when bed forms are present (Jansen et al., 1979), the turbulent flow around the dune causes local fluctuations in bed shear stress. The upstream slope of a dune is gentle, while the downstream slope has a rather large gradient. The abrupt flow expansion causes the flow to separate. As a result, the water just downstream the dune has a small mean flow velocity, but has a large turbulence. The vertical separation between the flow and this turbulent area is the *shear layer*. Further downstream the flow attaches to the bed again, at the so called '*re-attachment point*'. The high instantaneous shear stresses at this point may cause failure of the armour layer. Little is known about this process and is thus not treated in detail in this research This phenomena can be important when interpreting the results.

In order to take this instantaneous shear stress into account, a multiplication factor is introduced that increases the acting shear stress on the river bed. Large-eddy simulations (LES) (Yue et al., 2006) show predictions for the flow around dunes. In order to obtain a multiplication factor of the local velocity,

the LES results from Figure 3-13 are used. z_b is the vertical distance from the bed, h the dune height, x the downstream distance from the dune crest and $\langle u' \rangle_{\mathrm{rms}}/U_0$ the velocity ratio of interest. Figure 3-13 shows that the highest value of this velocity ratio is present at a distance of approximately 4 times the dune height, with a maximum turbulence intensity of 0.2 of the free surface velocity. Therefore, the acting velocity $\bar{u}$ is multiplied by 1.20 to take into account the influence of turbulence behind dunes on the stability of the IJssel bed.

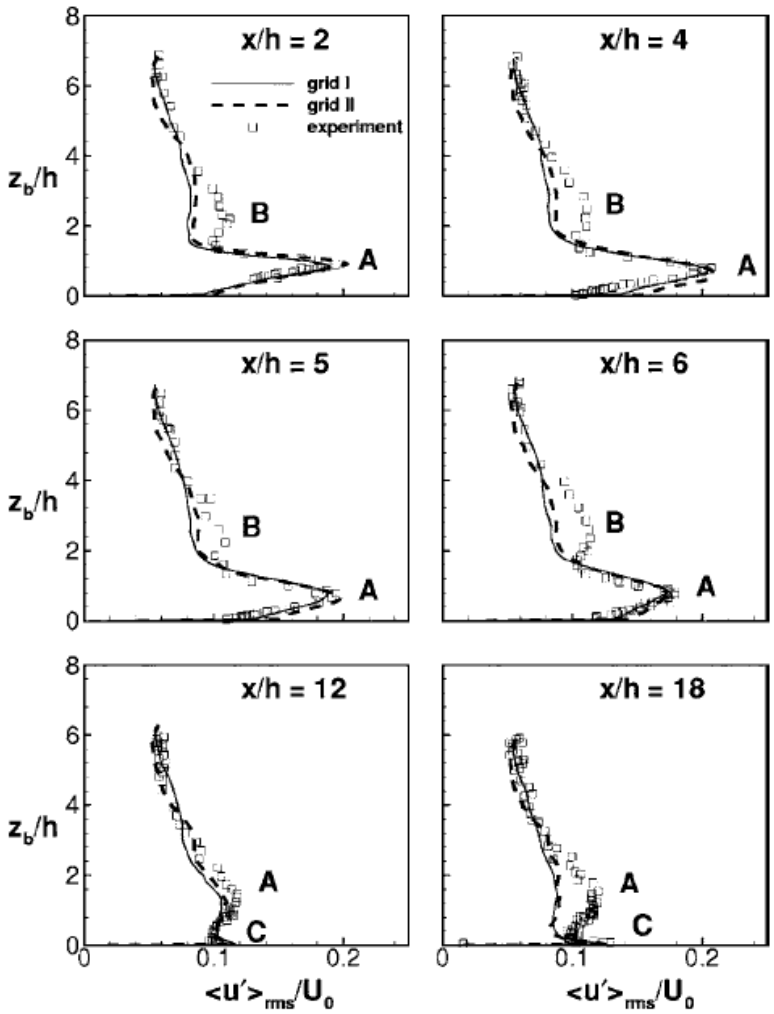

Figure 3-13: Comparison of streamwise component of RMS velocity (Yue et al., 2006)

Bed stability based on dune presence

The *p*-values for the stability analysis taking into account the effects of dunes are presented in Figure 3-14. The plot shows the bed stability values for fraction 4 with the hiding and exposure principle included. As expected, an overall decrease of the bed stability is present. A remarkable large area has high *p*-values (the black encircled area in Figure 3-14). This implies that for the design event of Q_{lob} = 16,000 m^3/s, a large area with a likely instability of the bed is present. Values get as high as p = 1.5.

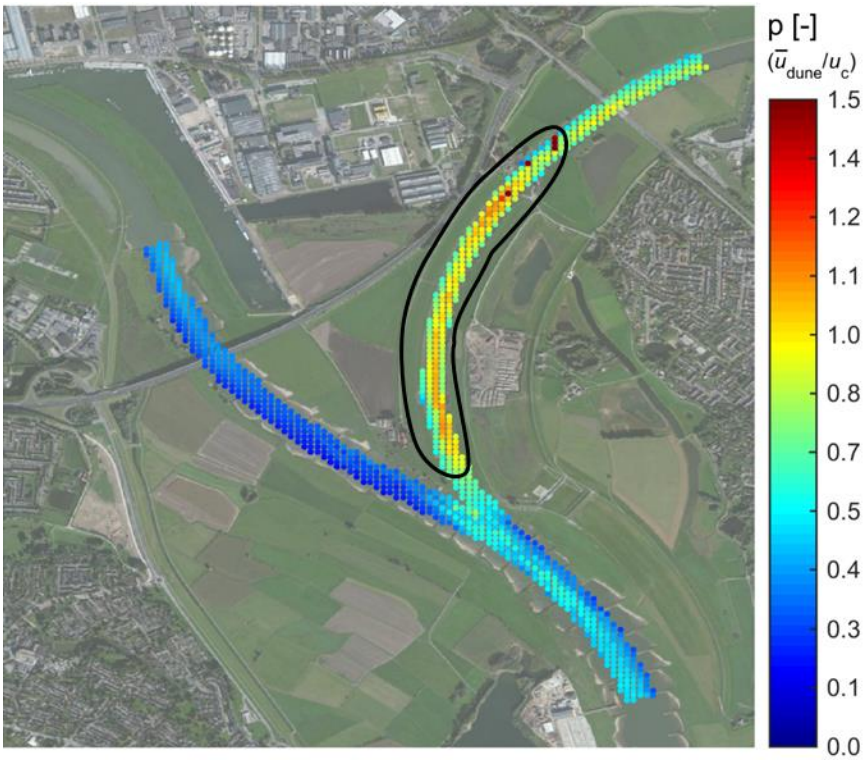

Figure 3-14: Calculated *p* value, stability for mixed sediment, for fraction i = 4 and the dune multiplication factor

3.5 Conclusion

The analysis in this chapter provides an answer to the research question: *Is the bed layer of the IJssel likely to fail during design discharge conditions?*

During the design conditions it is likely that large scale erosion occurs. The analysis shows that the widely graded coarse top layer causes a high probability of erosion. This probability increases if dunes are present.

An analysis of the upper 20 cm of the bed layer showed a mixture of gravel and sand in the IJssel branch, while the Pannerden Canal (less coarse sand and gravel) and Lower Rhine (fine sand) consist of mainly finer material. Stability of this sediment is assessed by calculating the ratio between acting and critical velocities, the stability value: $p = \bar{u}/u_c$. The first stability analysis is performed based on uniform sediment (based on the d_{50} of the mixture). This analysis shows a large critical area in the IJssel branch where the actual velocity is close to the critical velocity. The stability value is less in the Pannerden and Rhine branch due to the significant lower acting velocity compared to the IJssel branch.

The areas with large grain sizes become less stable and fines become more stable when accounting for mixed sediment, compared to the scenario based on uniform sediment (Shields only). A hiding and exposure factor is determined for several grain size ranges, by dividing the cumulative density function into several parts. It is assumed that erosion of the fraction with the highest amount of sediment (the second highest fraction) is the critical fraction for instability of the top layer. Comparison of the uniform and mixed sediment analyses shows that the IJssel branch becomes less stable at the better part of the calculated domain with 25% when the hiding and exposure effects are included, while the stability in the Lower Rhine remains more or less the same and the Pannerden Canal has a small increase in bed stability. The dune influence causes an increase of about 20% of the acting velocity compared to the analysis with mixed sediment only. These instantaneous velocities are located in the turbulent region downstream of the dunes.

Chapter 4 Stability of the grass cover

4.1 Introduction

This chapter provides an answer to: *Is the grass cover in the floodplain likely to erode during design discharge conditions and what are the consequences for the discharge distribution?* The IJsselkop bifurcation divides the discharge from the Pannerden Canal into the Lower Rhine and the IJssel. During summer discharge conditions the distribution is determined by the geometry of the main channel. The IJssel branch attracts more water, because of the steeper bed slope. This results in a strong flow towards the IJssel around the bifurcation, which happens during the average discharge conditions. During periods with large discharges the flood plains become active, resulting in a larger cross-section discharging the water. The flood plain, part of the bifurcation geometry, influences the water and sediment distribution. The velocity profile during the design peak discharge and dike crest heights are sketched in Figure 4-1. The blue area indicates low flow velocity. The dike with its crest level at 15m +NAP separates the flow from the IJssel branch (right side). More southwards lateral flow occurs (see hatched area in Figure 4.1) from the Lower Rhine to the IJssel. This lateral flow may cause erosion of the grass cover, which may result in an undesirable water redistribution. This chapter discusses if the flood plain is likely to erode by means of a quantitative analysis (grass cover and subsoil stability) and a qualitative analysis (appearance of the flood plain). This chapter ends with an analysis of the consequences of flood plain erosion for the discharge distribution, which is a part of the 4th research question.

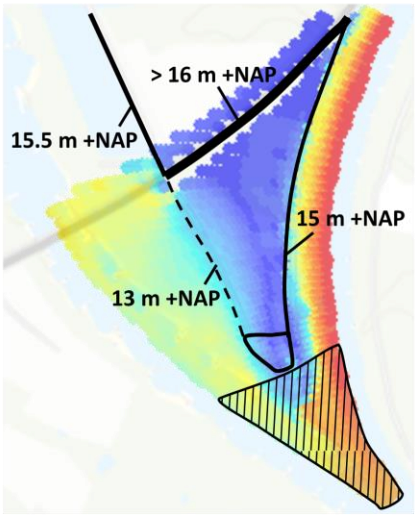

Figure 4-1: Computed velocity profile with dike heights

4.2 Quantitative analysis

The stability of the flood plain depends on both the acting flow velocity and the critical flow velocity. The acting flow velocity at the flood plain are obtained from WAQUA calculations (Suryadi and Mosselman, 2005) and are presented in Figure 4-2.

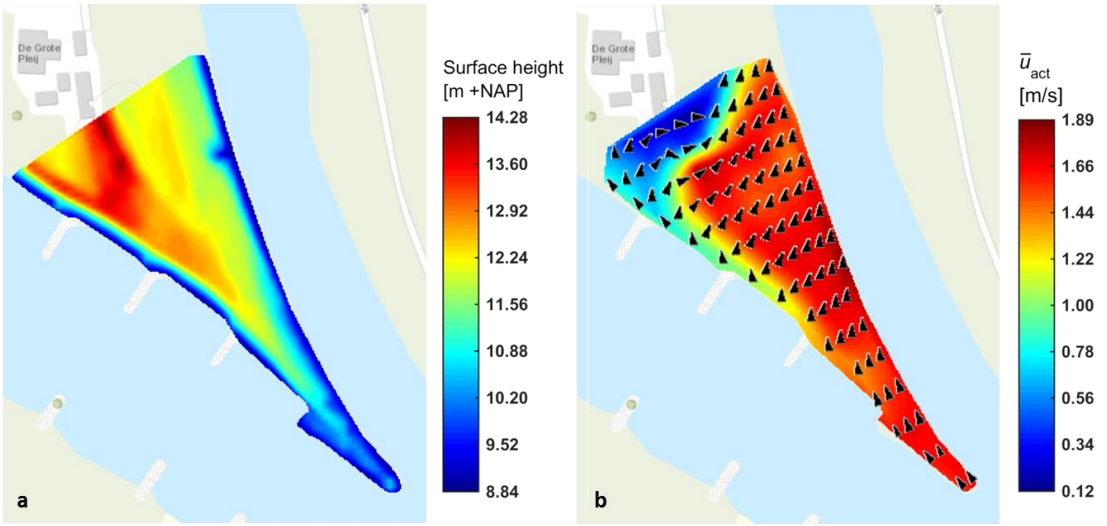

Figure 4-2: Actual hydrodynamic conditions for a design flood at the flood plain with a) the surface level and b) the flow velocity and direction.

Low velocities are present at the Northwest boundary. High velocities are present at the Eastern river bank, directed in the main flow direction of the IJssel, and at the middle of the flood plain, directed towards the IJssel. The maximum velocity (up to 1.89 m/s) is located at the protected bank of the IJssel branch. The maximum velocity in the middle of the flood plain is 1.84 m/s, just south of the shallowest part where the lowest velocities are present. High flow velocities (up to 1.89 m/s) occur at the entire flood plain. However, at the North-western part of the flood plain occur significantly lower velocities, which is caused by the relatively high bed surface.

The strength of the grass cover depends on both the type and state of the vegetation as well as the soil directly below the surface. The ecotope[10] at this floodplain is determined as '*production grassland*' (Rijkswaterstaat, 2014a).

Grass cover quality

The main purpose of assembling grass cover on a flood plain is to increase the strength of the subsoil against erosion. Three flow regimes are distinguished for the flow over grass cover vegetation. The first type is if the flow depth is less than the length of the grass leaves, only small de flection of the grass occurs. Secondly, when the water level rises up to the length of the grass leaves, deflection and oscillation of these grass leaves occur. The third regime still has an increase in water level, when the force becomes generally high enough to lay down the grass vegetation. Grass covers have several erosion mechanisms, see Figure 4-3. Depending on the flow velocity, the flow is able to erode leaves, causing erosion around the roots and the transport of weakly rooted grasses (Figure 4-3a - c). Inequalities and/or potential weaknesses may induce erosion of an entire root mat by 'roll up' of the soil, shallow slip of the soil or the uplift of the grass mat be cause of seepage flow (Figure 4-3d - f).

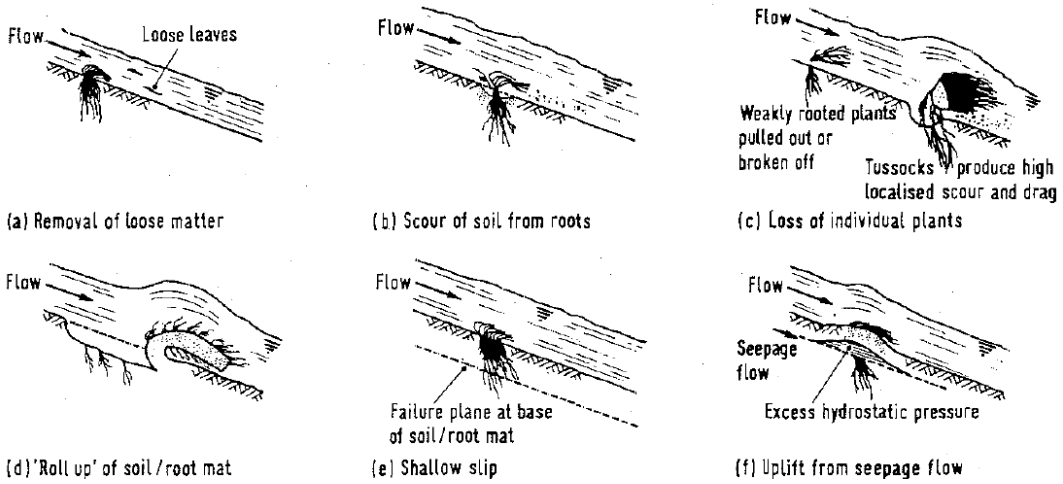

Figure 4-3: Erosion mechanisms for plain grass waterways (Hewlett et al., 1987)

A good grass cover can withstand flow velocities up to 2 m/s for more than 10 h, for several hours it is able to withstand flow velocities up to 3-4 m/s and for short periods flow velocities up to 5 m/s (TAW, 1985). In spite of these criteria it is common that the initiation of scour is determined by local imperfections of the surface and the grass cover. The erosion resistance of the flood plain depends on both the hydraulic characteristics of the flood plain (friction and geometry) and the characteristics of the vegetation (length/stiffness of the grass, surface area of grass leaves, strength and density of the roots and the area covered by the grass). These parameters are all season dependent. A stable grass cover requires the grass to grow all year long and only a few to die during winter. The grass length should not be less than 5-8 cm during winter to provide enough coverage of the subsoil and to be resistant against draught and frost (TAW, 1985). The limiting flow velocity, and therefore the actual erosion process and extent, depend on both the flow duration and grass cover quality (Figure 4-4).

[10] A mapping and classification system of the landscape

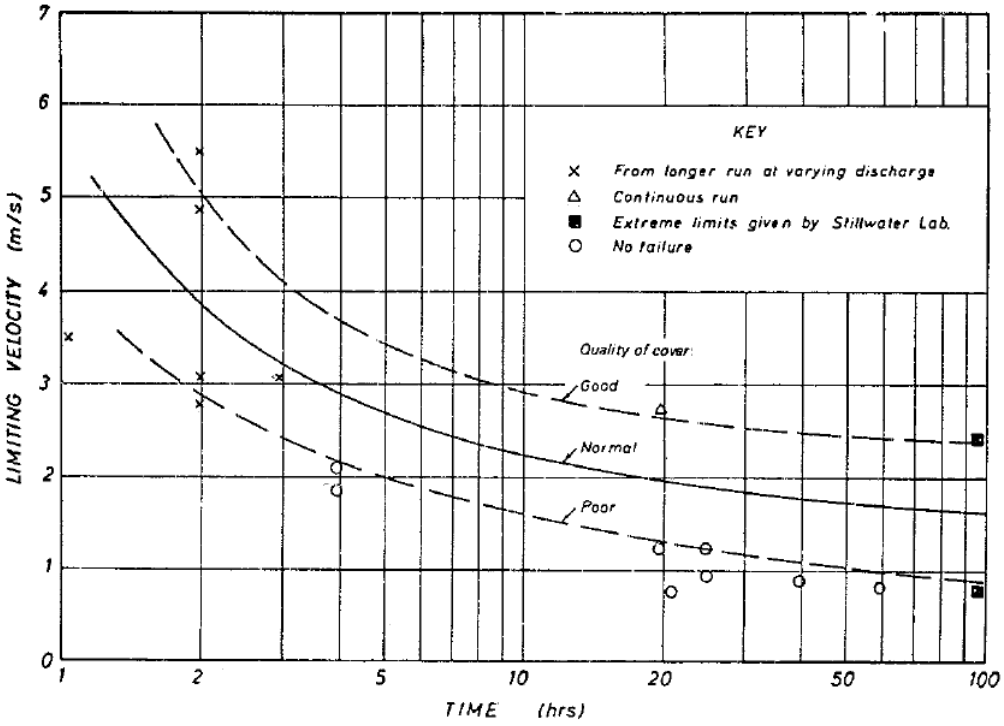

Figure 4-4: Recommended limiting values for erosion resistance of grass (Hewlett et al., 1987)

To determine a threshold velocity the quality of the grass cover needs to be assessed. The grass cover quality is expressed in three categories: good, average (normal) and poor. The quality is partly determined by the type of maintenance of the vegetation and is classified in four categories (A, B, C and D), see Table 4-1.

Table 4-1: Properties of maintenance types of grassland (Ministerie Verkeer en Waterstaat, 2007)

Cat.	Maintenance type	Grass mat characteristics		Resulting grass cover quality
		Cover	Root system	
A	haying without fertilizing	> 70%	many thin and thick roots of 0-0.15 m	Good
B	grazing. Fertilizing max 70 kg N/ha or 7-8x mow without fertilizing	> 85%	many thin roots of 0-0.08 m	Normal
C	grazing. Fertilizing more than 70 kg N/ha	> 85%	few thin roots of 0-0.05 m	Poor
D	Haying with fertilizing	< 60%	several thick roots of 0-0.15 m	Poor

The management type for the IJsselkop flood plain is category A. Additionally the type of vegetation is also important to determine a threshold value for the velocity. A distinction can be made between two grassland types for category A maintenance (Table 4-2). The actual quality depends on the root density of the grass.

Table 4-2: Grassland types in relation to the management (Ministerie Verkeer en Waterstaat, 2007)

Vegetation type	Coverage	Root density	Grass cover quality
Meadow. variety of grasses, not fertilized, periodically grazed by cattle	< 70%	good	Poor
	> 70%	good	Good
Hayfield. Prolonged haying	< 70%	good	Poor
	> 70%	good	Good

The root properties such as actual root density and root length gives additional information about the grass quality. The grass quality is assessed as `poor' for the flood plain, since nothing is known in detail about these properties. This belongs to the management type category A and a grass coverage lower than 70%. This is a conservative assumption. For more accurate results, it is recommend to gather more background information about the vegetation of this specific flood plain.

Erosion resistance of soil underneath the grass cover

The subsoil underneath vegetation also contributes to the erosion resistance. Clay may, for example, resist velocities up to 6 m/s, while a sandy subsoil may erode from velocities at 3 m/s (TAW, 1985). The subsoil is categorized in three types (Ministerie Verkeer en Waterstaat, 2007), which is shown in Table 4-3. The category depends on the yield strength W_l [%], the plasticity index I_P [%] and the sand percentage Z_k [%]. No measurements are done for determination of the soil type, but it is expected that strongly sandy clay is underneath the grass cover (Section 2.3). Therefore, the clay is expected to be 'Normal'. These classifications require a situation with a grass cover layer without imperfections. During a flood, however, waves and obstacles may cause local scour on this horizontal grass cover and subsoil, which may reduce the resistant against erosion.

Table 4-3: Categories of clay at subsoil below grass cover (TAW, 1996)

Category	criteria	
Good erosion resistant clay	W_l	> 45
	I_p	> 0.73*(W_l – 20)
	Z_k	< 40
Normal erosion resistant clay	W_l	< 45
	I_p	> 18
	Z_k	< 40
Poor erosion resistant clay	W_l	< 0.73*(W_l – 20)
	I_p	< 18
	Z_k	> 40

Critical velocity of the cover

The flood plain quality is categorized between 'poor' and 'normal', because of the assumption that the coverage is lower than 70%. The critical velocity is extracted from Figure 4-4. When assuming a duration of approximately 20 hours[11], the critical velocity is 1.3 m/s for a 'poor' grass quality and 2.0 m/s for a 'normal' grass quality. The ratio between the acting velocity (Figure 4-2) and the critical velocity can now be determined. This ratio is defined by:

$$p_{fp} = \frac{\overline{u}_{act}}{u_c} \tag{4.1}$$

When the ratio p_{fp} exceeds 1, the acting velocity becomes higher than the critical velocity, which results in erosion. Figure 4-5 shows this ratio for both critical velocities. It must be noted that 1) the average flow velocity is lower at most locations, as already discussed and 2) the actual flow velocity close to the bed (which is relevant for the bed stability) is lower than the depth-averaged flow velocity.

[11] 20 hours is the duration of the peak discharge, as defined in the numerical model

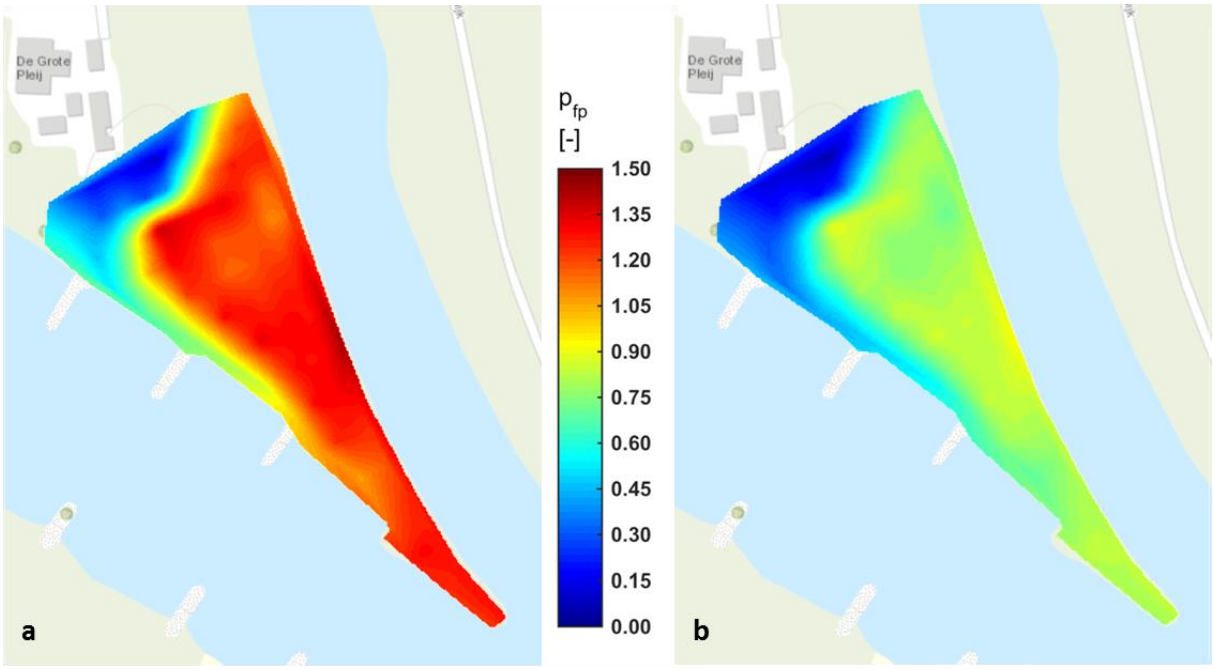

Figure 4-5: Unity check distribution over the flood plain for a uniform critical velocity of a) 1.3 m/s and b) 2.0 m/s

The stability comparison is performed for the velocity. It is therefore clear that the high velocity areas are more likely to erode. A 'poor' grass cover leads to a critical stability value *p* for almost the entire flood plain, while a 'normal' grass cover leads to values with a maximum of 0.9. The grass cover may not be assumed stable for the latter scenario because of the uncertainties, e.g. the presence of imperfections as shown in Figure 4-7.

4.3 Qualitative analysis

The condition of the flood plain is important for the failure probability of the grass cover. Grass cover failure may be caused by local instability. One of those local instabilities is failure of the bank protection along the main channel. When the rip-rap is not placed correctly, or individual stones are moved, the total protection may fail at high flow velocities, resulting in erosion of the flood plain. An example for moved rip-rap is the protrusion of an individual stone (Figure 4-7b), which is probably caused by historic flow events. Another local instability is the presence of local scour holes, which may be caused by historic flow events as well. Several of these holes are present at this flood plain (Figure 4-7d), which causes sediment to be washed out more easily. The presence of objects on the flood plain may cause local weakening as well. The presence of the trees/bushes at the flood plain are shown in Figure 4-6. It shows that one bush or tree grows at the high velocity locations in the middle of the flood plain (shown in Figure 4-7a) and several bushes are located along the banks of the IJssel branch. No scour is expected at the trees and bushes in areas with low flow velocity. Objects in general may cause turbulence, and therefore a higher risk of erosion at that location. Examples of objects at the IJsselkop flood plain are fences, a stock of rubble and the already mentioned trees and bushes, which in addition to the increase in turbulence level may cause tearing of the grass cover layer. Figure 4-7 shows these obstacles at the IJsselkop flood plain.

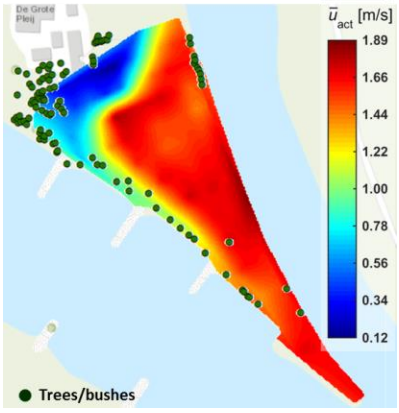

Figure 4-6: Presence of bushes/trees at the floodplain with the 2d-velocity profile according to Suryadi & Mosselman

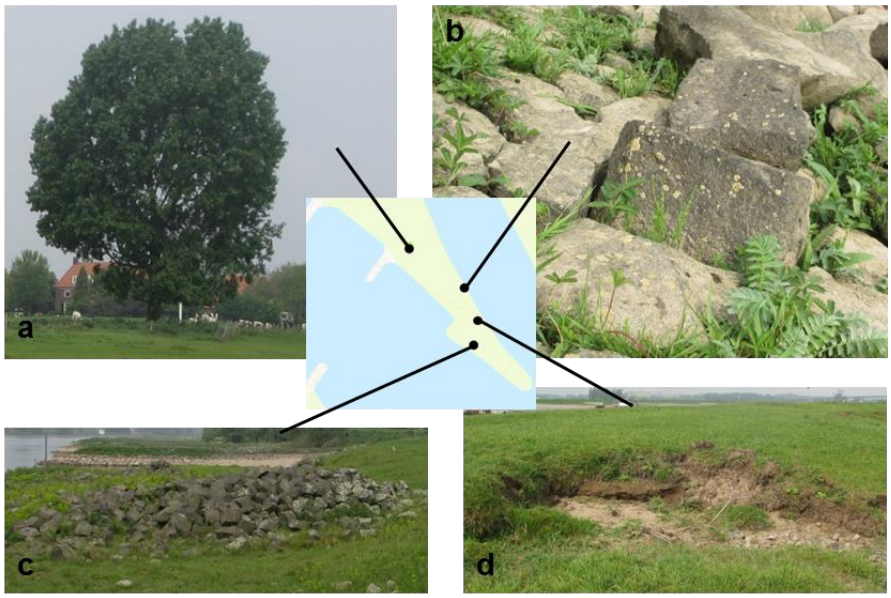

Figure 4-7: Presences of imperfections, which may cause local washout with a) a tree b) protrusion by riprap c) stock of riprap d) scour and exposure of the subsoil

4.4 Consequences of a flood plain failure

An initial analysis of the flood plain showed that large scale erosion is not likely, provided that damages are not present when the design flood wave occurs. If this does happen though, it may have consequences for the discharge distribution at the IJsselkop bifurcation. The likeliness and order of magnitude of the redistribution is studied in this section by means of a schematization of the situation. There are, globally, two flow patterns around the flood plain. The first one is the main flow that flows in the main flow direction over the flood plain, while the second pattern is lateral directed from the Lower Rhine to the IJssel. The latter flow pattern is assessed in this section.

Schematization

The influence of the discharge on flood plain erosion (i.e. lowering of the flood plain surface level) has been schematized by an ongoing channel (the Lower Rhine) with an extra branch (flow from Lower Rhine to the IJssel) in which the flood plain functions as a weir (Figure 4-8). The question therefore become: *what happens to the discharge flow in the side branch when the weir is lowered?* The flow Q_{side} into this side channel is imposed by the water level difference between both sides of the flood plain. The downstream water level is above the flood plain surface for the lateral flow conditions, so conditions regarding submerged-flow have to be applied. The water level on top of the upstream side of the flood plain is smaller than half the flood plain width ($H < ½ L$) which makes it a broad-crested weir. With H as the energy head above the weir crest and c as weir coefficient, the amount of discharge over the weir equals:

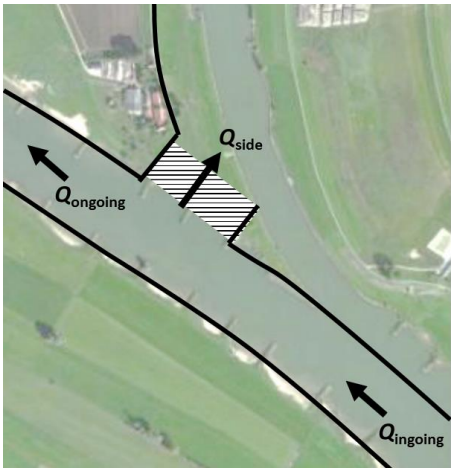

Figure 4-8: weir schematization of flood plain

$$q_{weir} = cH^{1.5} \tag{4.2}$$

in which the weir coefficient is a function of the gravitational constant g and the discharge coefficient c_d:

$$c = c_d \frac{2}{3}\sqrt{\frac{2}{3}g} = 1.71 c_d \tag{4.3}$$

The value of the discharge coefficient depends on the curve of the flow above the crest. For broad-crested weirs this value is $c_d = 1.0$, so that the weir coefficient becomes $c = 1.71$ and Equation (4.2) can be rewritten as:

$$q_{weir} = 1.71 H^{1.5} \tag{4.4}$$

According to this formula, the amount of discharge that flows from the Lower Rhine towards the IJssel only depends on the energy head at the upstream side of the flood plain. The Boussinesq relation, which describes discharge induced by water level differences (Ankum, 2002), in terms of the upstream energy head H_0 and the weir water level h_1 equals:

$$q_b = h_1\sqrt{2g(H_0 - h_1)} \tag{4.5}$$

It has been found that the maximum discharge occurs when the water level at the weir is a 2/3th of the energy head upstream. Using this ratio in Equation (4.5) results in Equation (4.4). Figure 4-9 shows a cross-sectional profile of the flood plain during the peak discharge, with its corresponding mean values for the schematization presented in Table 4-4.

Table 4-4: Average values at floodplain during peak discharge

	water level *h* [m +NAP]	water depth *d* [m]	bed level *z* [m +NAP]
Lower Rhine (lr)	14.69	10.63	4.06
Flood plain (fp)	14.51	3.43	11.08
IJssel (ys)	14.48	11.51	2.96

The difference between the water level h_{lr} and bed level z_{fp} is the upstream energy level $H = 3.61$ m. When using Equation (4.4), the specific discharge over the weir becomes $q_{weir} = 11.69$ m^2/s for the present situation. The curve from Figure 4-10 becomes less steep when the initial energy head is larger, and steeper when the initial energy head is smaller. When the flood plain erodes about 1 m, the specific discharge increases with 50%, while an erosion of 2 m causes an increase of 100% (see Figure 4-10). It is thus expected that if such an amount of erosion occurs, the change in discharge is not negligible and needs to be taken into account.

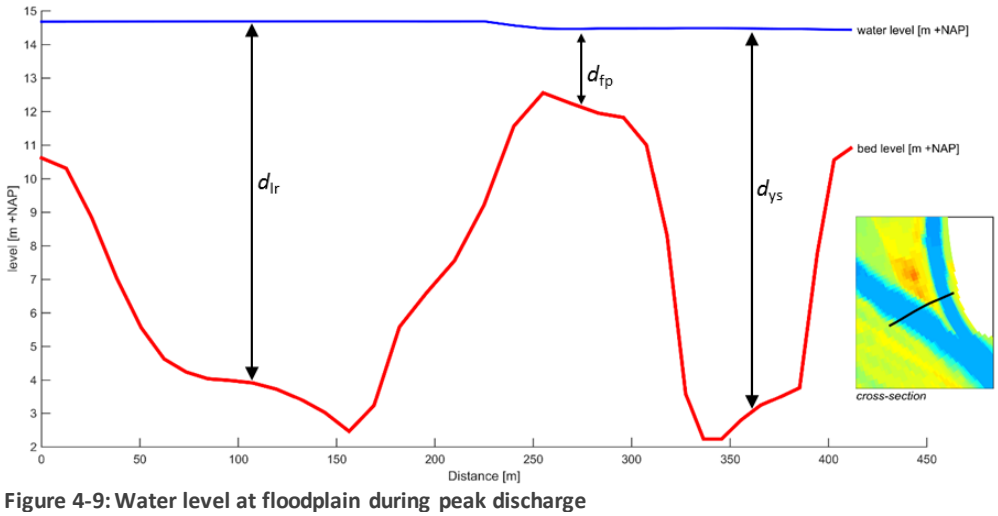

Figure 4-9: Water level at floodplain during peak discharge

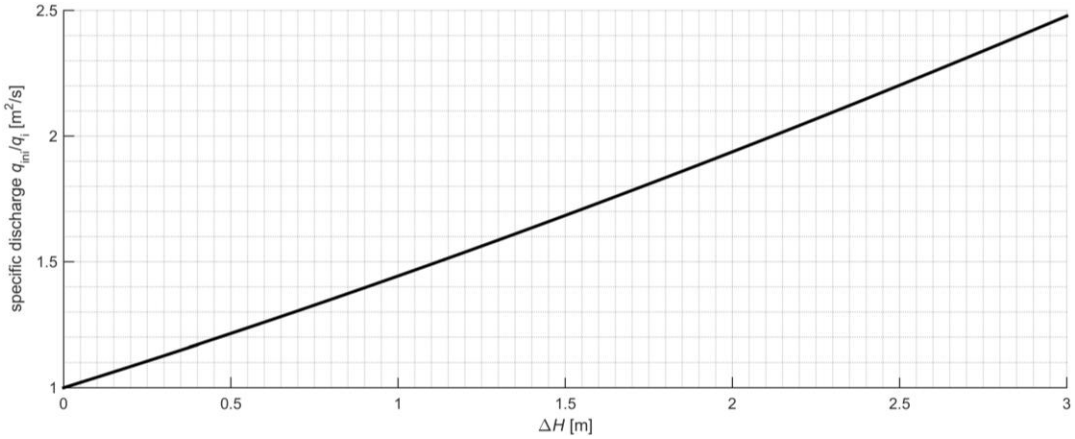

Figure 4-10: Change in specific discharge for varying erosion rates (with H_{ini} = 3.61m)

It is not known, however, what the absolute amount of discharge is for the present situation. An estimation has been done with the data gathered from the WAQUA computations (Suryadi and Mosselman, 2005).

The velocity direction has been used for the determination of the cross-sectional area in which the flow is directed from the Lower Rhine to the IJssel. The velocity magnitude and direction are presented in Figure 4-11. The cross-section has been arbitrarily determined, with taken into account that the velocity direction needs to be as much as possible in lateral direction. A depth averaged velocity magnitude $\bar{u}$ and water depth h has been determined for each data point, with the specific discharge as a result: $q = \bar{u}h$. The absolute discharge has been calculated by multiplying the width of the grid cell B_i with the specific discharge q. The discharge at the cross-section, which flows from the Lower Rhine towards the IJssel during the peak discharge, becomes:

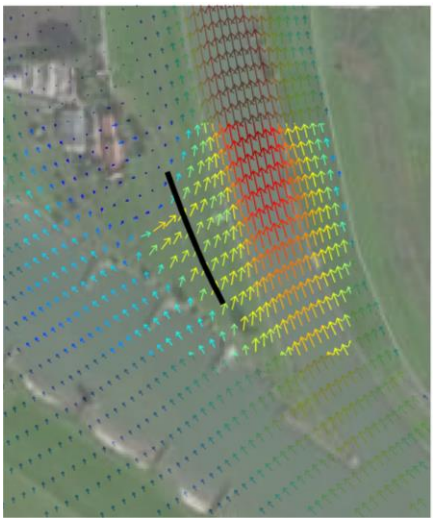

Figure 4-11: cross-section profile for defining lateral discharge during peak discharge, with the velocity directions according to Suryadi & Mosselman

$$Q_{lat} = \sum B_i \bar{u}_i h_i = 536 \text{ m}^3/\text{s} \tag{4.6}$$

The total IJssel discharge is about 2750 m^3/s during the peak, which makes the lateral discharge accountable for 20%. It must be noted, however, this calculation has been performed under the assumption that the flow is directed perpendicular to the grid cell boundary, which is not completely true as can be seen in Figure 4-11. The actual lateral discharge is therefore lower than defined in Equation (4.6). Flood plain erosion of 1 m causes an increase of the IJssel discharge of 9%, while the increase is 19% when an erosion of 2 m takes place. It is expected though, that these percentages are lower due to the overestimation in lateral discharge. For 100 m^3/s difference in the lateral discharge, the change in IJssel discharge changes with 1.82% per metre of erosion.

4.5 Conclusions

The analysis in this chapter provides an answer to: *Is the grass cover in the floodplain likely to erode during design discharge conditions and what are the consequences for the discharge distribution?*

It is most likely that the velocities up to 1.89 m/s do cause extensive erosion on the flood plan , if the current damages are present when the design discharge occur. If the grass cover is in good condition it should be able to withstand the flow velocities (> 2 m/s) during the design flood event. The grass cover has to be determined as 'poor' due to the presences of imperfections, which may cause large scale scour.

Turbulence due to local disturbances, such as scour holes, large vegetation and rip-rap at the river bank, may cause instantaneous forces on the grass cover, which may induce erosion. Good maintenance is therefore advised for the following objects:

- *The bank protection:* The rocks of the bank protection need to be checked for displacement in order to prevent failure;
- *Grass coverage:* Exposure of the subsoil may cause erosion in an earlier state in the flooding process;
- *Presence of objects:* Objects that are not meant to be at the flood plain should be removed.

For the present situation it is concluded that the presence of erosion holes, trees and unstable lying rip-rap may cause undesirable scour during a 1/1,250 year flooding event. Resolving these matters reduces the possibility of large scale scour.

Because of the rippled/dune flood plain surface, the actual velocity close to the surface differs from the depth-averaged velocity as used for this analysis. The actual velocity is the depth-averaged velocity multiplied by the ratio between the depth-averaged water depth and the actual water depth. Turbulence regions, e.g. the downstream side of a dune, may result in large instantaneous bed shear stresses that induces erosion. The rippled surface, presence of objects and presence of damages may induce erosion during the design discharge. The exact influence of these aspects is currently unknown.

An analysis of possible consequences of the flood plain failure to the discharge distribution showed that the discharge over the flood plain increases significantly, provided that erosion occur. An erosion depth of 1 m of the flood plain causes a change of 50% in the lateral discharge and 2 m erosion causes an increase in lateral discharge of 100%. It is estimated that approximately 20% of the total IJssel discharge originates from the flow over the flood plain. An erosion of 1 m causes a total increase of 9% in IJssel discharge, while 2 m erosion causes an increase of 19% of the total IJssel discharge. When the flowing width through each cell is more accurate calculated, i.e. taken the flow angle in account, the calculated discharge reduces significantly. However, an increase in discharge in the IJssel branch leads to more degradation and eventually more discharge that is discharged to the IJssel.

Chapter 5 Model set-up

5.1 Model introduction

The hydrodynamic and morphodynamic developments during a design flood wave are assessed to get insight in the behaviour of the IJsselkop bifurcation, which has been performed by using a numerical model. For this study the numerical model Delft3D has been used as it is able to appropriately simulate the developments to be expected. Moreover, there is already an existing Delft3D model for the Rhine branches available, which has been used as base for this study. This chapter provides information about the set-up of the Delft3D model, which for the better part based upon the existing model. Some parameters have been adjusted by means of this study.

Delft3D performs computations, by several modules, for purposes as flows, waves, sediment transport, ecology and water quality. Each of these modules can interact with each other. Computations can be performed for 1D, 2D and 3D scenarios. The governing equations that are solved by Delft3D are described in Appendix B. For this research, 2D-flow and morphodynamic computations are performed. Therefore only the FLOW module has been used and only those processes are described further in this chapter.

5.2 Model grid

The computational grid consists of a curvilinear co-ordinate system, with ξ and η as co-ordinates. Each grid cell contains its predetermined properties and computed values. The water levels are computed in the middle of the grid, while the velocities are defined at the borders and the depth points at the corners of the grid (Figure 5-1).

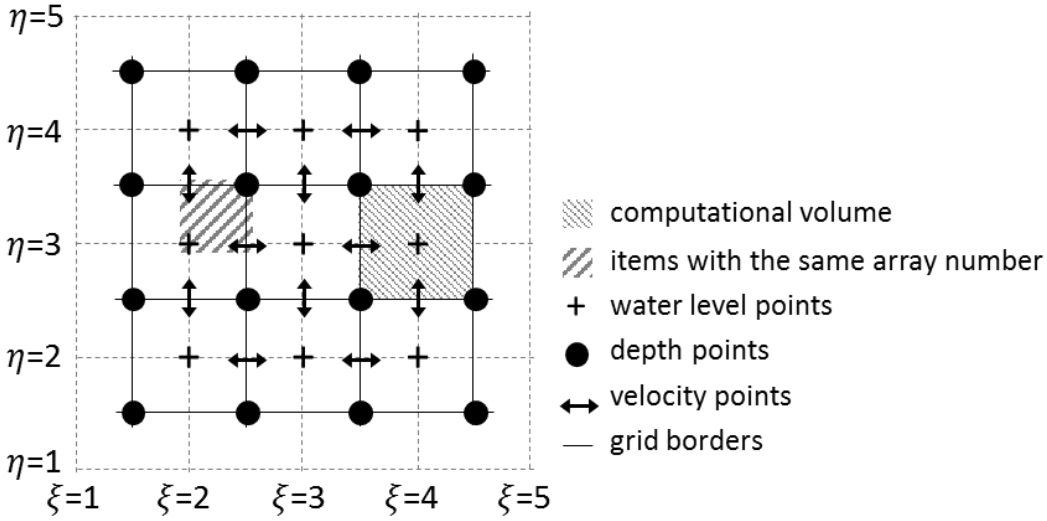

Figure 5-1: Location of properties in the grid for a curvilinear co-ordinate system

An additional border is automatically added around the constructed grid, the *staggered grid* (dashed lines in Figure 5-1), which makes it possible that e.g. water levels are imposed at the boundary of a grid. The borders of this staggered grid are defined as the grid enclosure.

The curvilinear system makes it possible that the grid boundaries matches as well as possible with the actual river banks and flow directions, so that no large inadequacies are expected (i.e. a rectangular grid approaches the shape of the banks less adequate).

Applied grid

The grid used for this study has been gathered from an overall model that covers the entire Rhine delta. Three domains of the overall model, all linked to the IJsselkop bifurcation, are used for this research (Figure 5-2). A dense structure of the grid is present at the main channel, since developments on a smaller scale than at the floodplain are expected. The presence of the boundary lines are explained later on.

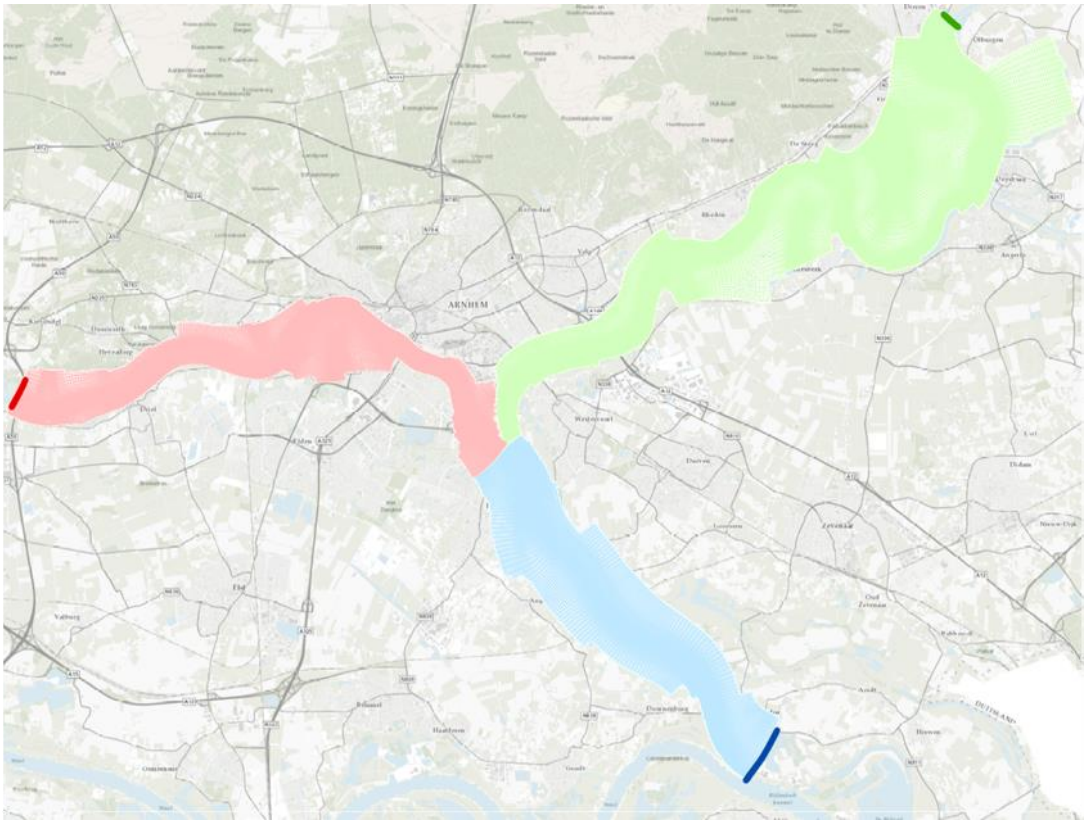

Figure 5-2: Computational grid as input in Delft3D. The upstream grid in blue is the Pannerden Canal, the downstream grid in red is the Lower Rhine and the downstream grid in green is the IJssel. The bold lines represent boundaries.

Since these domains are initially 'decomposed' domains, these are manually coupled. This is imposed by linking the grid cells from one domain to the other, by specifying the grid cell numbers [M,N].

Grids are validated by several criteria, e.g. the orthogonality criterion (cosine of the grid cell < 0.02-0.04), the aspect-ratio (M-size/N-size in the range of [1 2]) or the ratio of adjacent grid cells (length ratio in M and N-direction between the grid cells ≤ 1.2). These criteria reduces the errors by the computations.

5.3 Bed topography

The bed topography of the model has been set by imposing a value for each grid cell node (see Figure 5-1). The height-value in the centre of the cell has been defined by the minimum height value of the four surrounding cell corners. The bed topography of 2013 that has been obtained for this study (Section 2.4) is converted into the grid for this Delft3D model and used as input.

5.4 Hydrodynamic boundary conditions

The grid cell borders that are not connected to other cells and where no boundary conditions are imposed, are closed boundaries by default. The model in this research has no imposed boundary conditions at the left and right side of the through flowing area. The downstream and upstream

boundaries are imposed with a condition. These conditions are discussed in this paragraph. The location of these boundaries are shown in Figure 5-2, as the coloured lines.

Upstream boundary

The discharge has been imposed at the upstream boundary (i.e. the first cell rows of the Pannerden Canal domain). In this research the subject of interest is the influence of a flood wave on the hydro- and morphodynamic conditions, so that a uniform and steady discharge as boundary condition is not representative for this flood wave. A time-varying discharge, that follows the properties of the design flood wave, will therefore be imposed. The upstream discharge time-series (for Lobith) has been derived from the hydrograph of a 16,000 m^3/s flood wave (Ministerie Verkeer en Waterstaat, 2007) and shown in Table 5-1. Since former computations have been performed up to 8592 m^3/s at Lobith, it is possible to use those results as starting point for this research. The corresponding discharge into the Pannerden Canal has been derived from the discharge distribution data (Ministerie Verkeer en Waterstaat, 2007). The background and derivation of the data are presented in Appendix C.

Table 5-1: Derived time-series discharge input at the upstream boundary

Duration [hours]	Lobith [m^3/s]	Pannerden [m^3/s]
25	8592	2754
25	10617	3455
25	13187	4482
10	14997	5360
5	15591	5709
20	16000	5942
5	15645	5723
10	15106	5429
25	13581	4661
50	10617	3455
25	8592	2754

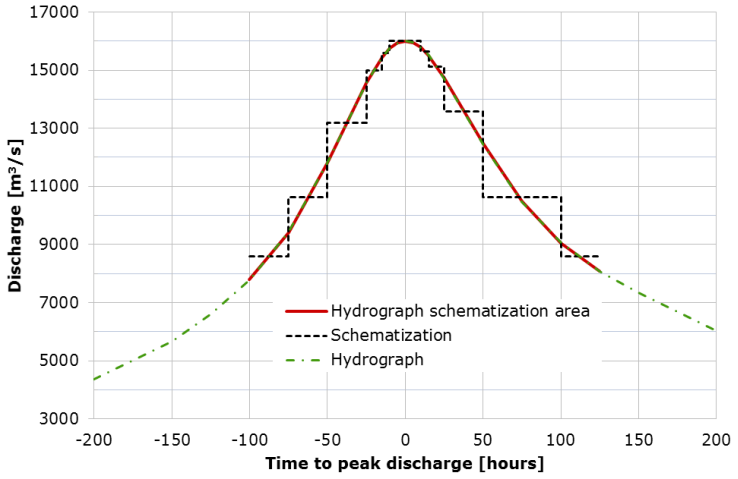

Imposing a total discharge may cause errors in the discharge distribution over the width of the through flowing area (i.e. sedimentation/erosion may cause the grid cell to attract more/less water). Therefore a discharge per cell has been imposed. The distribution of the discharge per cell in the Pannerden Canal Q_{pk2} is presented in Figure 5-3 below. The derivation of the total discharge to the discharge per cell is presented in Appendix C.3.

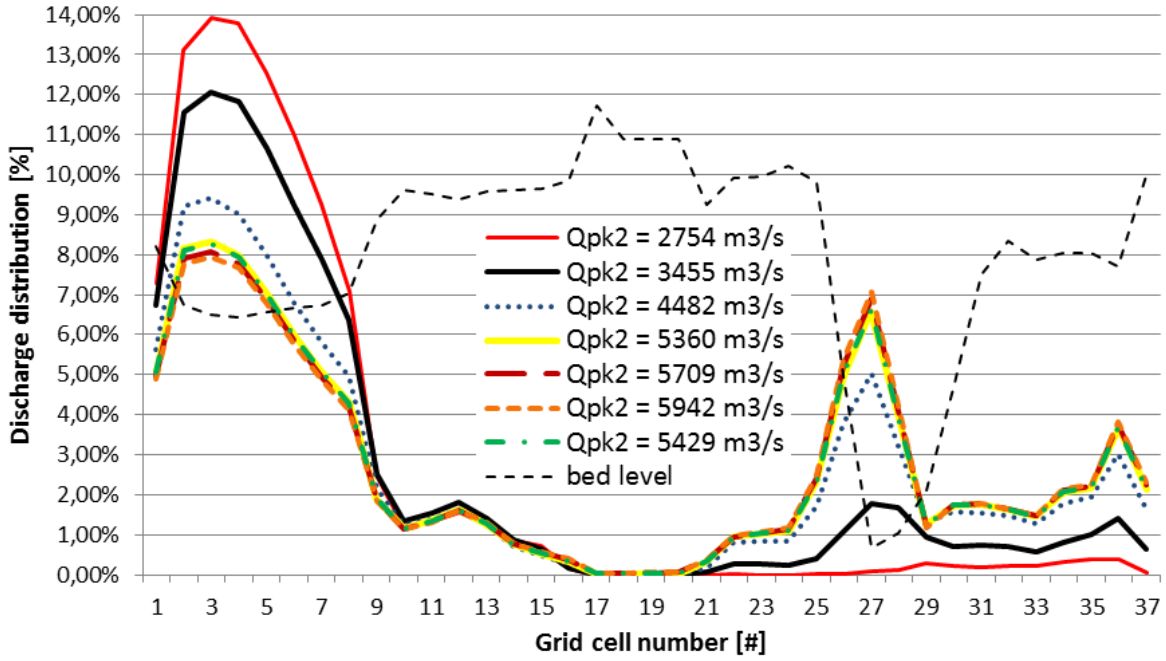

Figure 5-3: Discharge distribution for the input discharges at the upstream boundary in the Pannerden Canal. The bed level contours shows the main channel on the left side of the graph and a basin at the deeper part on the right.

Downstream boundary

A water level boundary is imposed at the downstream locations of the Lower Rhine and the IJssel. Because of the time-series discharge, the water level boundary is in a time-series format as well (i.e. $Q \sim h$). These water level values are not known be forehand. Water level measurements are performed on a regular base, but not at the area of interest. Next to that, no measurements are performed with the severe discharge conditions that are imposed. The imposed water levels are the result of the interpolation of the data from available WAQUA computations. The water levels for both downstream branches are presented in Table 5-2.

Table 5-2: Derived downstream water level boundary values

Duration [hours]	Q_{lob} [m³/s]	$h_{down,rhine}$ [m +NAP]	$h_{down,ijssel}$ [m +NAP]
25	8592	10,56	9,26
25	10617	11,24	9,76
25	13187	11,70	10,24
10	14997	12,03	10,56
5	15591	12,14	10,67
20	16000	12,22	10,74
5	15645	12,14	10,67
10	15106	12,05	10,58
25	13581	11,77	10,31
50	10617	11,24	9,76
25	8592	10,56	9,26

The downstream boundaries for the IJssel branch and Lower Rhine branch are located 25 km and 15 km respectively from the IJsselkop bifurcation. The computed water level at these boundaries may differ from the imposed water level, which results in a backwater curve that influences the water level (and the discharge distribution) at the bifurcation. The extent of influence depends on the actual difference between the imposed water level and the computed water level. A difference of 20 cm, for example, may result in a water level difference of a few centimeters at the bifurcation. The extent of influence of the imposed water level is not discussed in more detail in this report.

5.5 Initial conditions

The initial conditions, i.e. the conditions that are imposed to the model at the start of the computation, are the values of the highest discharge that has been applied for the computation where the model is previously used for. This maximum discharge was 8,592 m^3/s at Lobith. These files for the initial conditions contain the necessary data of each grid cell at a discharge of 8,592 m^3/s and are used as starting point for the computations in this research.

5.6 Morphodynamic conditions

Sediment characteristics

Sediment characteristics are imposed at the river bed to analyse the erosion/sedimentation patterns. The sediment has been subdivided into ten different fractions, with minimum and maximum diameters as described in Table 5-3. The sediment density is set to 2650 m^3/s and the dry bed density is set to 1600 m^3/s.

Table 5-3: Sediment fractions input in Delft3D-model

Name	D_{min} [m]	D_{max} [m]
Sediment1	0.000063	0.00025
Sediment2	0.00025	0.0005
Sediment3	0.0005	0.001
Sediment4	0.001	0.002
Sediment5	0.002	0.0028
Sediment6	0.0028	0.004
Sediment7	0.004	0.008
Sediment8	0.008	0.016
Sediment9	0.016	0.032
Sediment10	0.032	0.064

The presence of each fraction depends on its location. Therefore, an additional file is created with the *space-varying initial amount of sediment mass* (in kg/m^2) per grid cell for each fraction. The total amount of sediment per cell is set in such a way that there is no supply deficit during the flood wave. The sediment input is initially a well-mixed graded bed, which implies that all the fractions are nicely mixed. In Appendix C.4 some of the fractions are all separately visualised in space.

Morphology characteristics

The *morphology characteristics* describes the computational parameters for the sediment computation, in which values like the morphological time scale and multiplication factors are determined.

A bed stratigraphy module is applied in order to specify the amount and size of the eroded/deposited sediment as well as possible. This module introduces layers in the bed, which is a transport layer of a maximum thickness of 1.0 m above (a maximum of) two underlayers with both a maximum thickness of 0.5 m and a base layer at the bottom. The underlayers provide that the sediment that is deposited most recently, erodes first. After the initial conditions, a change of conditions causes adjustments in the layers. In case of sedimentation, the sediment is added to the top layer (transport layer) when this layer is less than its maximum thickness (1.0 m). When this layer reach its maximum, the sediment is 'moved' to an underlayer. When this underlayer reaches its maximum thickness (0.5m), the sediment is 'moved' to a second underlayer (maximum number of underlayers is set to two). When still deposition takes place and both transport layer and underlayers reach their maximum thickness, the sediment is 'moved' to the base layer. The process is the other way around in case of erosion. The sediment is removed from the transport layer. This transport layer is replenished up to 1.0 m thickness with the available sediment in the underlayers. When no more sediment is available, the transport

layer thickness reduces. From an arbitrarily determined threshold thickness (0.7 m), the sediment capacity is reduced.

The morphological time factor is set to 1, since the relevant development is the consequence of the flood wave on the river bed.

Sediment transport equation

The sediment transport formula that has been applied is defined by:

$$S = \alpha D_{50} \sqrt{\Delta g D_{50}} \theta^b (\mu\theta - \xi\theta_{cr})^c \tag{4.7}$$

where ξ is the factor due to hiding and exposure and the mobility parameter θ, with q as specific discharge, as:

$$\theta = \left(\frac{u}{C}\right)^2 \frac{1}{\Delta D_{50}} \tag{4.8}$$

The coefficients are valued according to Table 5-4, which has been gathered from the existing Rhine branch model.

Table 5-4: User defined sediment parameter values

Parameter	symbol	value	unit
Calibration coefficient	α	5	-
Power	b	0.0	-
Power	c	1.5	-
Ripple factor	μ	0.7	-
Critical mobility factor	θ_{cr}	0.025	-

The hiding and exposure ξ effect is included in the computation by using the Ashida & Michiue formula:

$$\xi = \begin{cases} 0.8429 \dfrac{D_m}{D_i} & \text{if } \dfrac{D_i}{D_m} < 0.38889 \\ \left(\dfrac{^{10}\log 19}{^{10}\log 19 + {}^{10}\log\left(D_i/D_m\right)} \right)^2 & \text{otherwise} \end{cases} \tag{4.9}$$

With D_m as the arithmetic mean diameter and D_i as the diameter of the sediment fraction. For more background on the hiding and exposure is referred to Section 3.3. For further details about the transport equation are found in the Delft3D manual (Deltares, 2014).

5.7 Secondary flow

Due to the presence of bends, secondary flow is an important process that needs to be taken into account. The spiral motion is a three-dimensional process and is included in 3D-computations, by the presence of vertical layers. By introducing the influence of this helical flow, an extra parameter is added to the momentum equation and will be solved as an advection-diffusion equation. An extra factor is introduced, that gives an indication of the magnitude of the secondary flow, which is known as the spiral motion intensity *I*:

$$I = \int_{-1}^{0} \left| v(\sigma) \right| d\sigma \tag{4.10}$$

where σ represents the depth, 0 at the surface and -1 at bed level, and $v(\sigma)$ as the velocity distribution over the vertical. Next to that, a parameter β_c is introduced that indicates the influence of the spiral motion in the depth-averaged model. In this model the value is set to $\beta_c = 0.5$.

5.8 Additional parameters

Additional parameters, both physical and numerical, are defined in order to fulfil the computations. These are shown in Table 5-5.

Table 5-5: User defined additional parameter values

Parameter	symbol	value	unit
Physical parameters			
Gravity	*g*	9.81	[m/s^2]
Water density	ρ_w	1000	[kg/m^3]
Bed roughness		0.255	
Horizontal eddy viscosity		0.5	[m^2/s]
Horizontal eddy diffusivity		0.5	[m^2/s]
Numerical parameters			
Threshold depth		0.1	[m]
Marginal depth		-999	[m]
Smoothing time		0	[min]

Next to these pre-defined parameters, extra parameters and files are introduced into the model: *data weir files* defines the weir locations in the Lower Rhine branch (these are, however, not active for the flood wave discharges) and *trachytope files* define the bed roughness for each grid cell. The complete input values and files are shown in Appendix D.

Chapter 6 Delft3D – results

6.1 Introduction

This chapter provides an answer to the question: *What are the consequences of erosion of the bed layer of the IJssel for the discharge distribution?* This is provided by means of an assessment of the hydrodynamic and morphodynamic effects of failure of the armour layer using numerical Delft3D computations (for which the set-up is elaborated in Chapter 5). Failure of the armour layer is incorporated in the calculations by including an artificial deepening. The results of these computations (#3) are compared with two reference scenarios (#1 and #2):

1. Only hydrodynamics applied
2. Morphodynamic update is applied
3. Morphodynamic update with artificial deepening

A design flood wave of 16,000 m^3/s at Lobith has been simulated in the models. Each scenario is covered in a section. The analyses include the developments of the bed level, flow velocity, water level and discharges and are analysed in time and space.

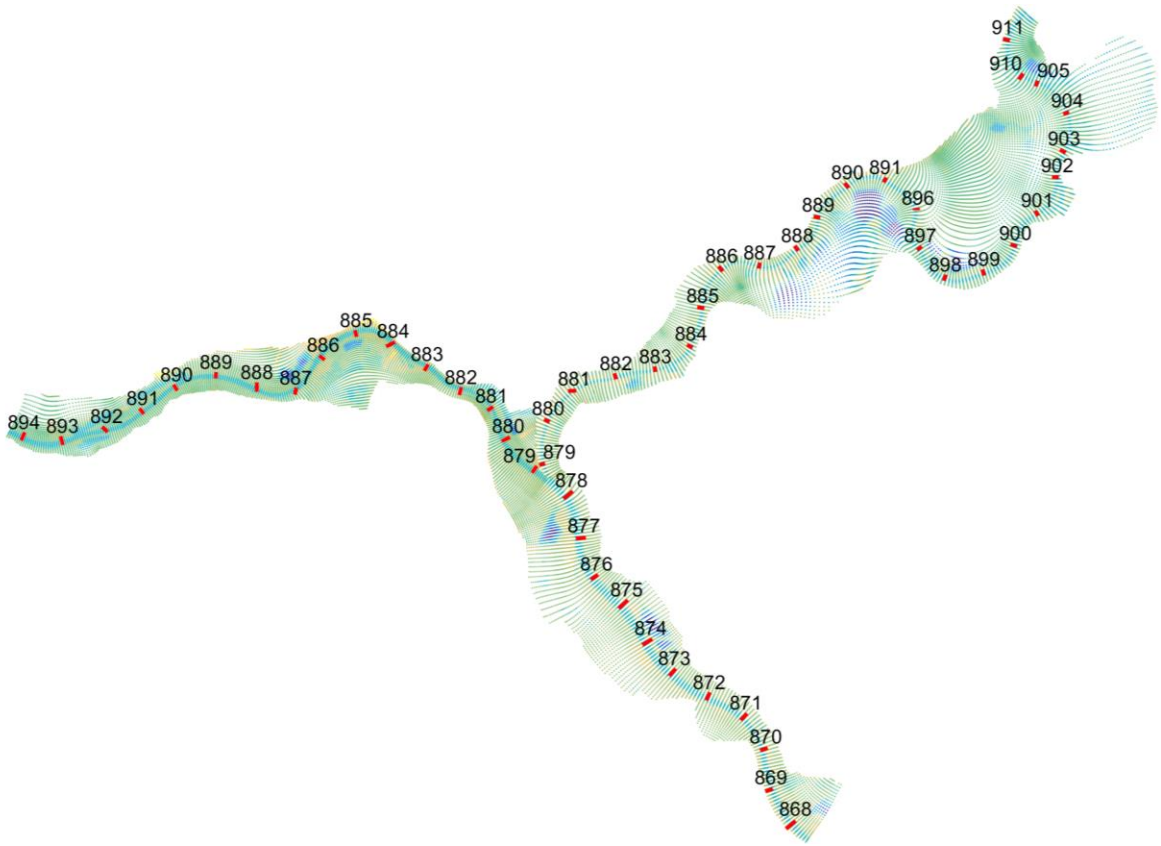

Figure 6-1: Domain and kilometre markers for which model output is stored

6.2 Scenario 1 – hydrodynamics only

This computation is used as reference scenario, which implies the hydrodynamic evolution only. The bed composition and bathymetry remains constant for the entire computation.

Water levels

One of the expectations is the presence of a lower water level in the IJssel compared to the water level at the Lower Rhine, which is showed in the previous chapters. The corresponding water levels of 4 different discharge regimes are presented in Figure 6-2. The development of the water levels show an increase in water level difference between the IJssel and Lower Rhine at increasing discharge. The maximum water level difference, at about 0.5 km from the IJsselkop[12], is approximately 16 cm and may cause strong lateral velocities.

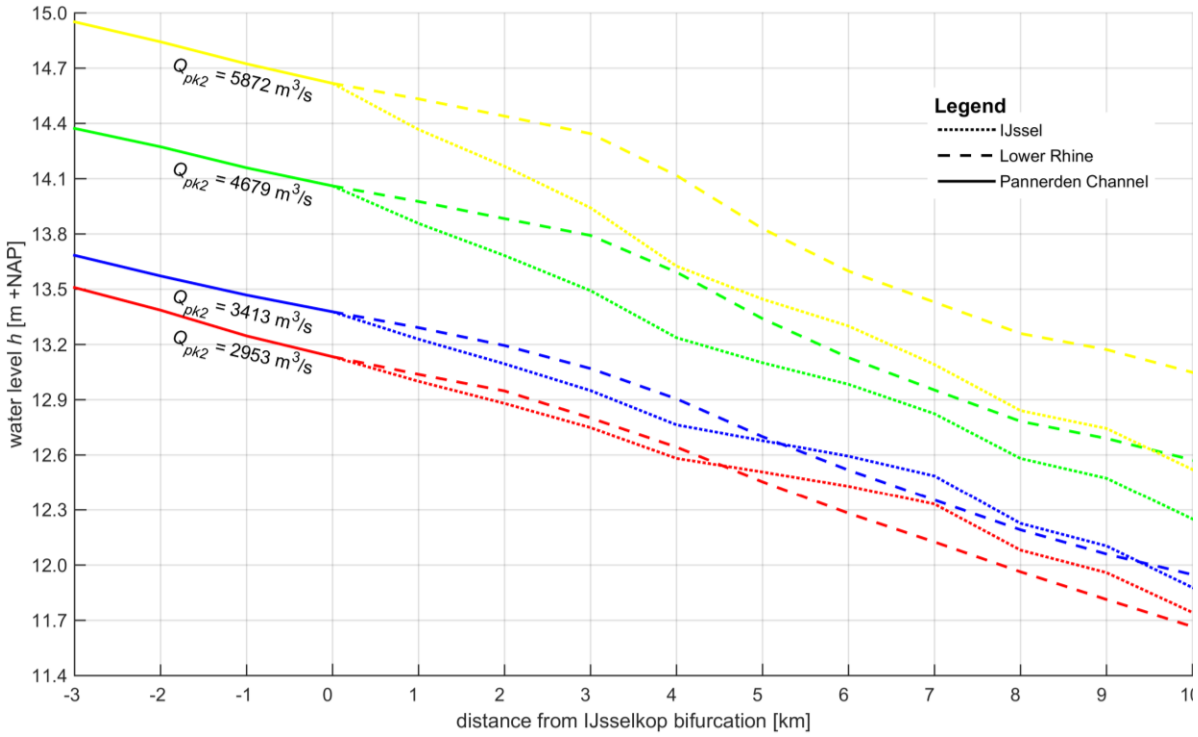

Figure 6-2: Computed water levels along the river axis for fixed moments in time, with the minimum (red) and maximum (yellow) discharge included

The water level slope of the Lower Rhine (dashed line) remains more or less constant in the first 3 km downstream of the bifurcation, while the water level slope of the IJssel (dotted line) increases for increasing discharge. This indicates that a backwater curve in the Lower Rhine influences the water level at the bifurcation and thus in the IJssel. The water level difference extends to more than 10 km downstream of the bifurcation, which causes the IJssel to attract a larger part of the discharge.

Discharge

The desired discharge regarding water management is 2/3 of the Pannerden Canal discharge into the Lower Rhine and 1/3 into the IJssel, which is not provided during the simulated flood wave (Figure 6-3). A numerical error is observed during the first day of the output is observed. This is caused by the difference between the file that is used as input in the model and the imposed initial boundary conditions and dissolves after the first day.

[12] This is the location where still interaction takes place between both branches (at the flood plain)

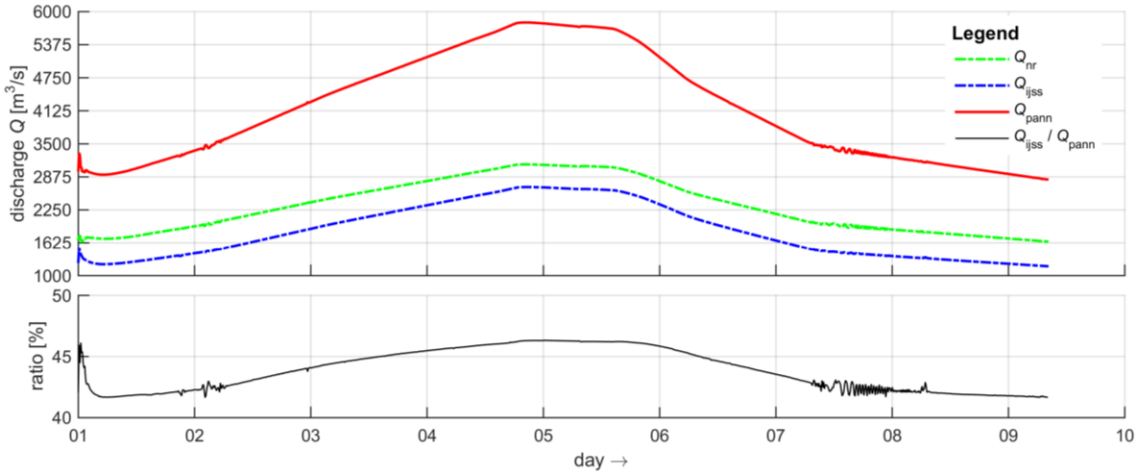

Figure 6-3: Computed discharge at the Pannerden Canal (km868) and the IJssel (km879) with corresponding distribution ratio

The relative IJssel discharge is at its maximum right after the peak discharge of the Pannerden Canal. The IJssel discharges 47% of the Pannerden Canal discharge during these circumstances, which is more or less equivalent as the *Q-f* relation derived by Rijkswaterstaat[13]. The maximum discharge that is distributed into the IJssel is approximately 2700 m^3/s and occurs when the Pannerden Canal peak discharge occurs too. It is observed that the discharged water into the IJssel and Lower Rhine during the peak discharge (between day 5 and 6), is decreasing less than the discharge in the Pannerden Canal. The Pannerden Canal discharge decreases for about 200 m^3/s during that day and both downstream branches decreases with 100 m^3/s during this period. The discharge ratio remains more or less equal.

Velocities

A 2D velocity profile is presented in Figure 6-4 for the three branches. Areas with high flow velocities are highlighted. The figure presents the moment that the highest flow velocities occur, which is during peak discharge. The areas with high flow velocities are located in the river bends. In the IJssel branch, the higher velocities are relative close to the bifurcation, with one peak located just downstream the bifurcation. This peak is expected, because of the attraction of the water into the IJssel. The velocity at this point reaches about 2.54 m/s. These areas with the highest flow velocities are expected to be the areas with the largest erosion, which will become clear when the results of scenario 2 are treated. The velocities over time, at 879kmp, for both downstream branches are plotted in Figure 6-5. Significant higher velocities in the IJssel branch are observed, which is likely to be caused by the smaller cross-sectional area of the IJssel and the larger bed gradient compared to the Lower Rhine. Another aspect that can be noticed is that an increase in discharge causes an increase of the flow velocity in the IJssel, while the velocity in the Lower Rhine decreases. A flow velocity reduction in the main channel of the Lower Rhine indicates that more water is discharged over the wide floodplain. The width of the main channel in the Lower Rhine is small compared to the total width, which makes it likely that the flood plain of the Lower Rhine discharges more water during extreme conditions.

[13] From 5,000 m^3/s at Lobith is the IJssel discharge 43% of the total discharge

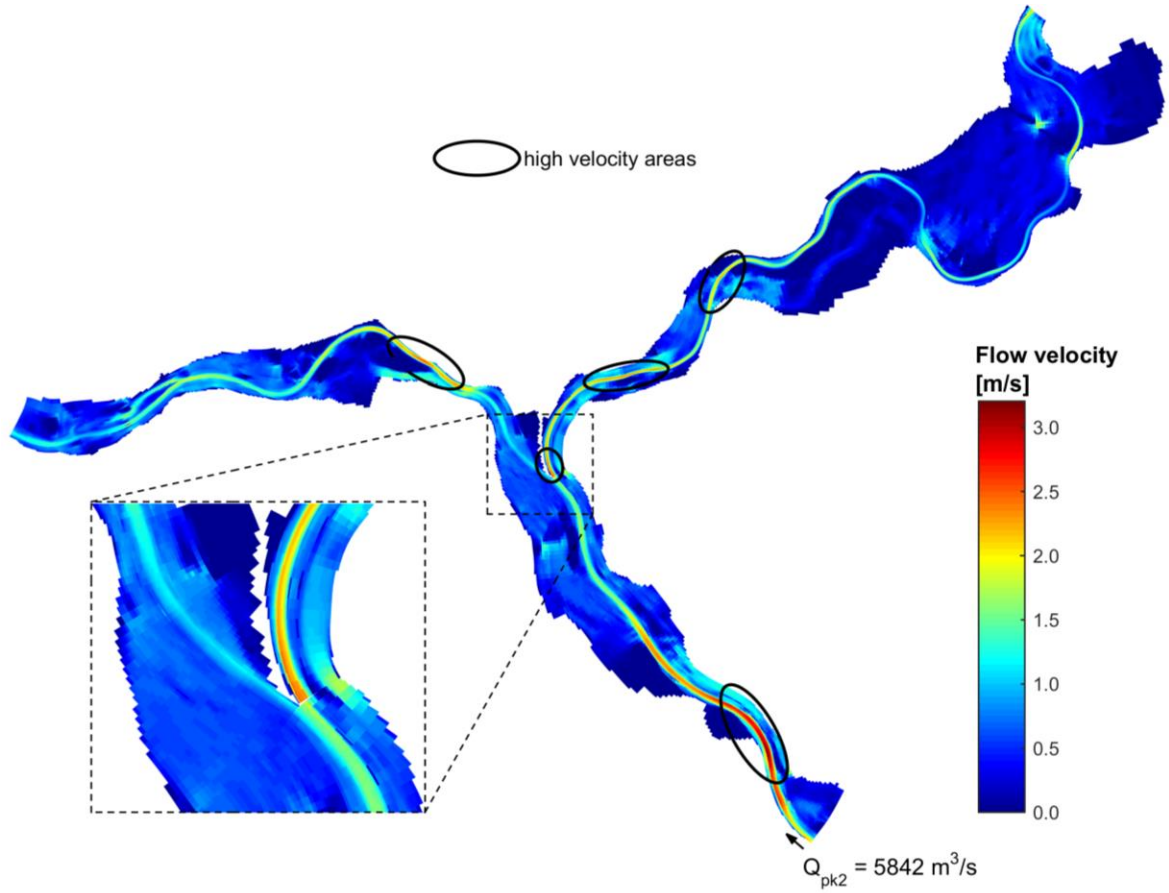

Figure 6-4: Computed velocity profile for the discharge peak with highlighted areas with high flow velocities

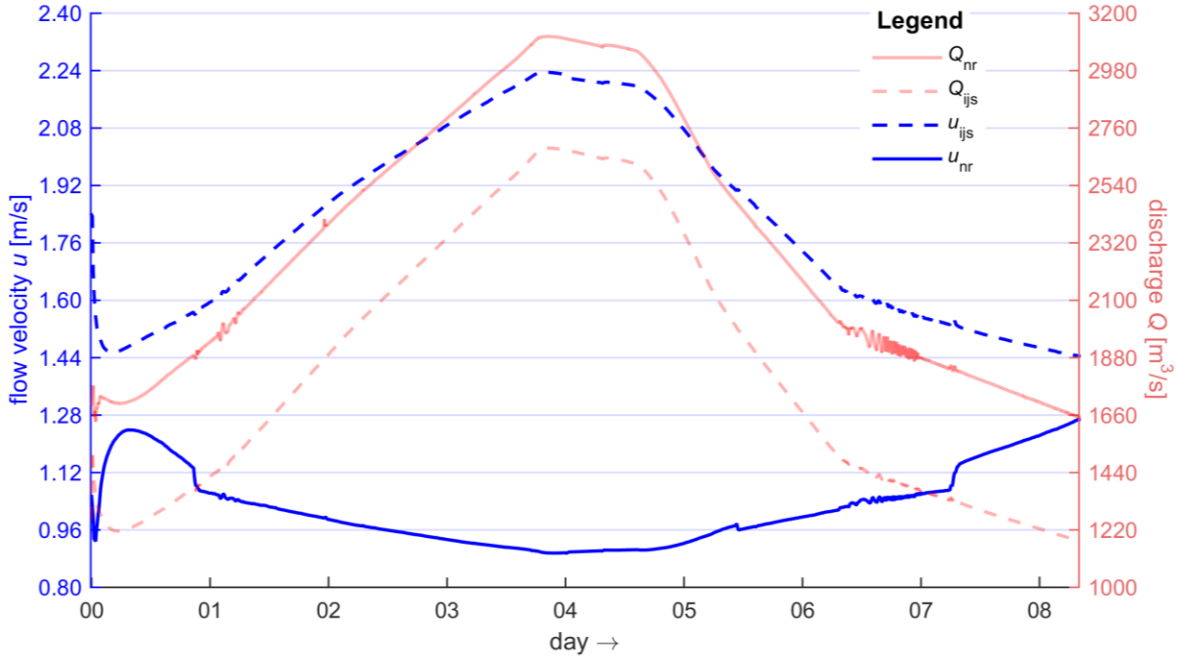

Figure 6-5: Computed flow velocity and discharge over time at 879kmp for the Lower Rhine and IJssel branch

6.3 Scenario 2 – Morphodynamic update applied

For Scenario 2 a morphodynamic update is applied to the model to find out how the bed reacts to the hydrodynamics. Bed levels and bed composition are updated at each computational time step. The changes in bed level are treated first, where after differences with Scenario 1 regarding water level, velocities and discharges are discussed. For the background of the morphodynamical input is referred to Chapter 5

Bed levels

The amount of sedimentation/erosion at the end of the flood wave with respect to the initial bed level, is presented in Figure 6-6 for the area around the bifurcation. Erosion occurs along the outer bends and sedimentation at the inner bends, because of secondary flow and lateral sediment sorting. Some locations have parts with slight sedimentation at the floodplain, mostly in inner bends, which is shown in Figure 6-7 by the orange areas next to the main channel.

An area with a large change in bed level is observed just downstream the bifurcation, where the scour hole (see Section 2.4) was present. Further downstream of the IJssel branch, relatively large erosion and sedimentation peaks are present in the bends (of about 1.5m). The locations of the erosion peaks at the end of the flood wave (Figure 6-7) corresponds with the high velocity areas from the hydrodynamic simulation (Figure 6-4). The IJssel shows an overall lowering of the bed level after the flood wave (Figure 6-8) with an erosion rate that varies between 5 – 30 cm. The highest rate is present at 4 km downstream of the bifurcation. The armour layer is approximately 1 m thick (Section 2.3) so that break-up of this layer is not likely to occur. The Lower Rhine shows no changes in the first 3 km downstream of the bifurcation, while more downstream both sedimentation and erosion occurs.

Water level

The water level data between the hydrodynamic run (scenario 1) and the morphodynamic run (scenario 2) shows a decrease of about 1 – 2 cm in the IJssel branch during the peak discharge. For other moments there is a slight increase of the water level, but no value exceeds the water level during the peak discharge. No large changes occur regarding the water level when the morphodynamic update is applied.

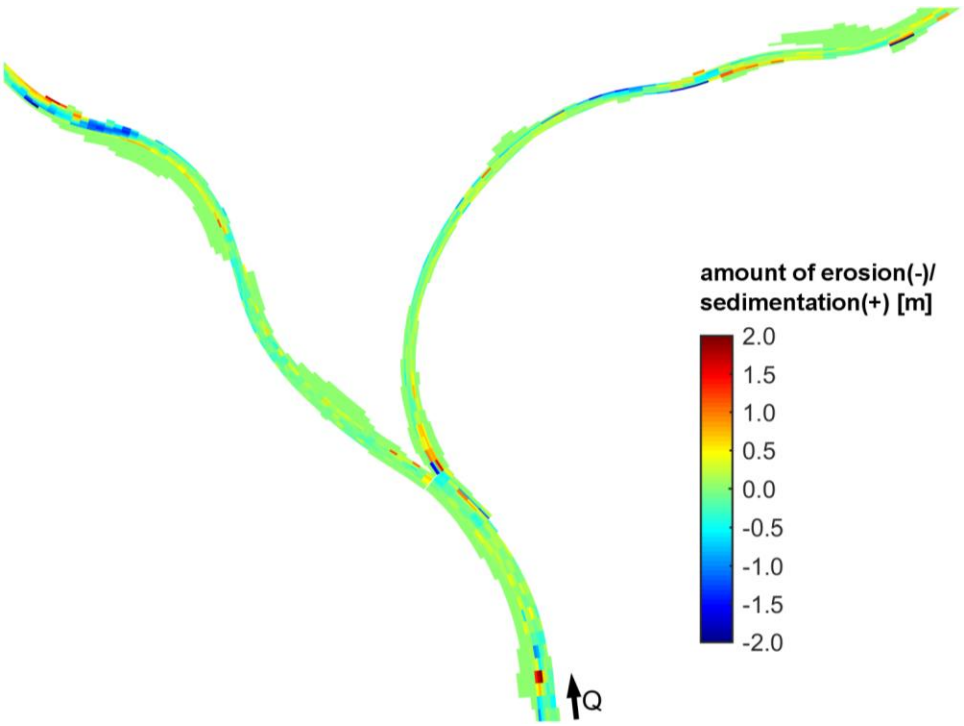

Figure 6-6: Computed actual amount of erosion and sedimentation at the rivers (locations without changes, mostly at the floodplains, are left out of the picture)

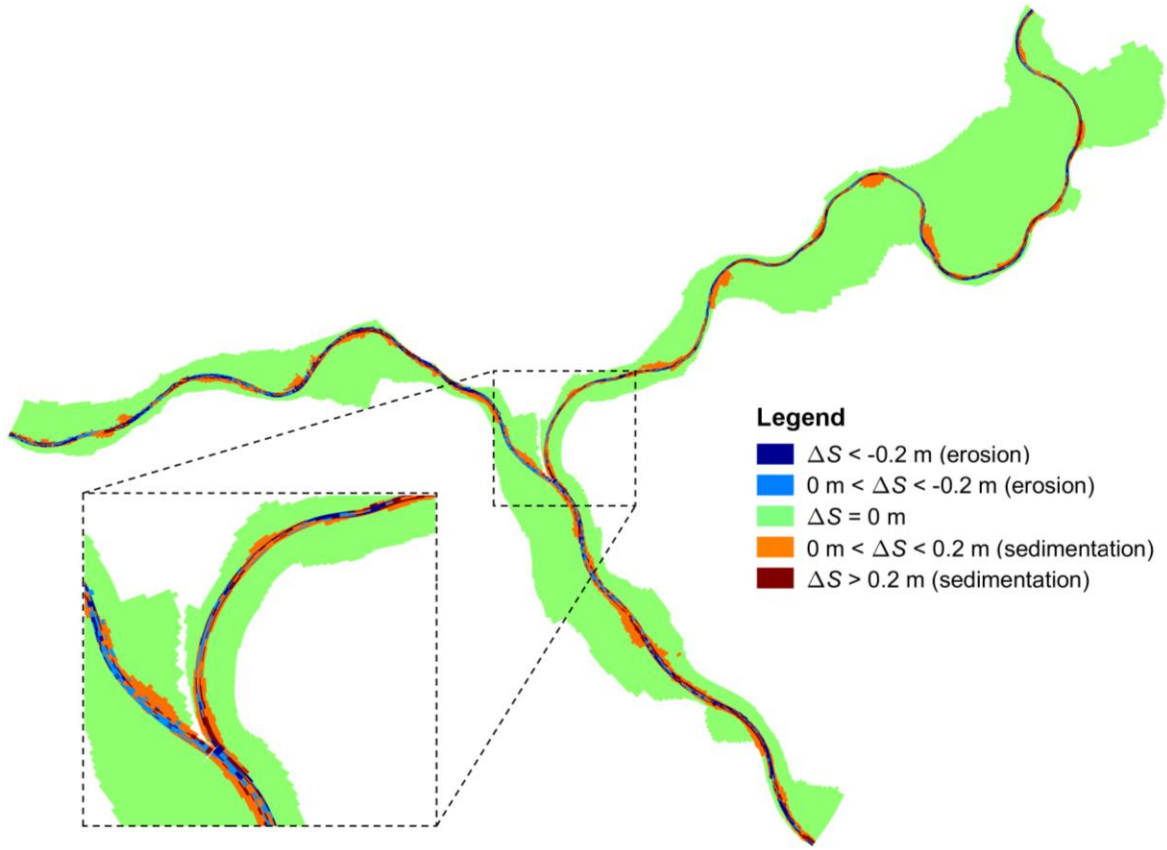

Figure 6-7: 2D-profile of locations with sedimentation(+) or erosion(-) for scenario 2

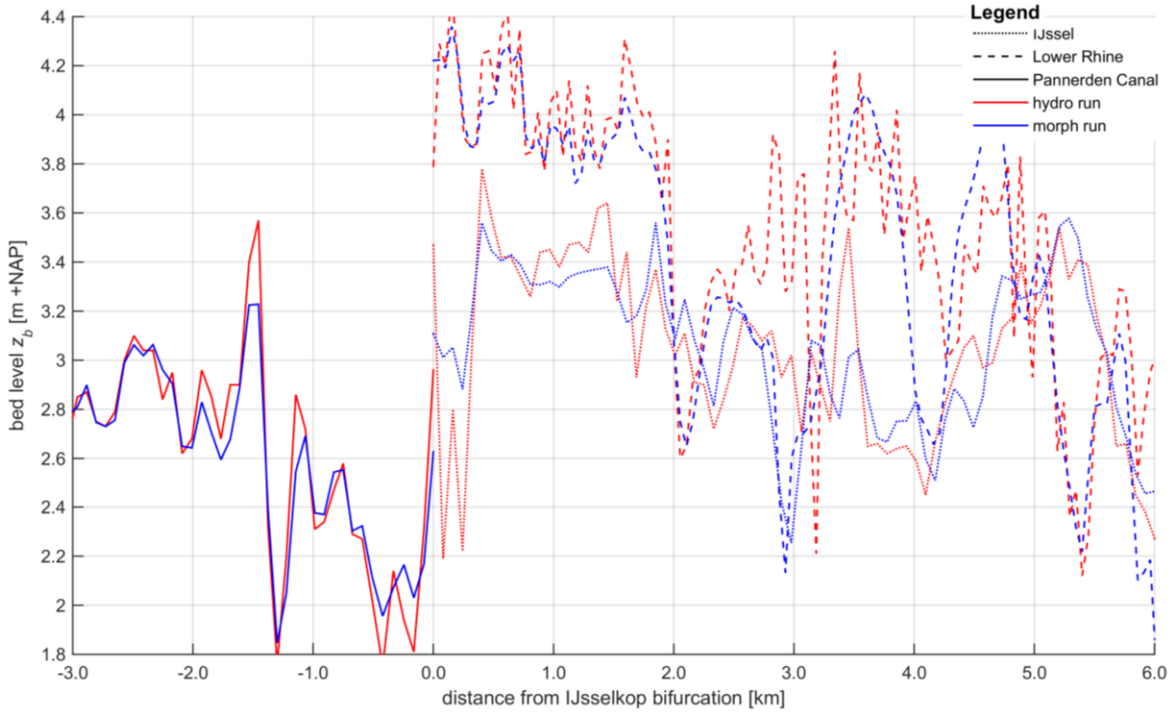

Figure 6-8: Computed bed levels along the river axis. The bed level jump at km0.0a is caused by the fact that the (grid cell) data points at the bifurcation are not connected to each other. The values strongly depends on the exact location of the cell.

Flow velocity

The velocity profile for the morphodynamic computation shows a limited difference in velocity at peak discharge between Scenario 1 and 2, see Figure 6-9. In the main channel a deceleration is present at most locations, while the opposite is true for the downstream regions of the IJssel. The order of magnitudes of the acceleration or deceleration have a maximum difference of 0.19 m/s acceleration (upstream region of the Pannerden Canal) and a 0.33 m/s deceleration (at the Lower Rhine), see Figure 6-9. The areas with the largest acceleration in the IJssel are just downstream the bifurcation and just downstream of the first bend, with velocity changes up to 0.1 m/s. All the areas with a relatively large velocity difference are correlated to the erosion/sedimentation pattern, which are the locations that are likely to erode.

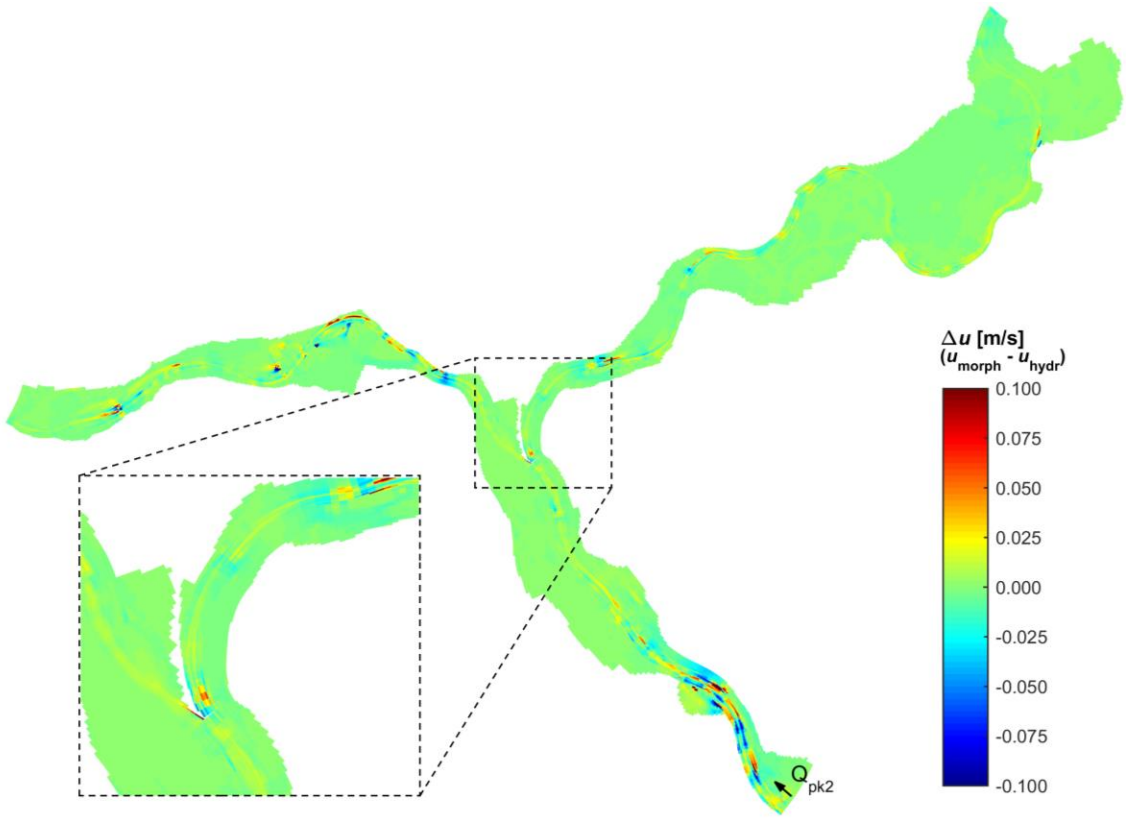

Figure 6-9: Computed velocity differences between reference run and scenario 2 (morphodynamics added) at peak discharge. The minimum and maximum values of the colourbar are less than the actual extreme values, which makes the smaller differences better visible

Discharge

The change in discharge distribution is limited and in the order of 0.1% compared to the hydrodynamic computation (scenario 1). It can be concluded that the discharge distribution is not influenced by erosion caused by the design flood wave.

6.4 Scenario 3 – artificial deepening

This scenario is identical to scenario 2 except that a local artificial deepening of the IJssel river bed is applied for an area of 35 x 450m, with runs of a depth of 1 m, 2 m and 3 m. This deepening simulates a hypothetical situation, where suddenly a large amount of sediment is eroded if the armour layer fails. The changes in bed level are compared with scenario 2.

The location in Figure 6-10 is selected to be deepened since there is a lot of bed erosion and high velocities. It is expected that the deepening causes a lowering of the water level and that the resulting backwater curve initially causes a lowering in water level at the bifurcation. Sedimentation occurs at the upstream boundary of the deepening and erosion occurs at the downstream boundary of the deepening. The deepening is eventually filled up to its depth without the artificial deepening. Theoretical background about this process is described in Appendix E.

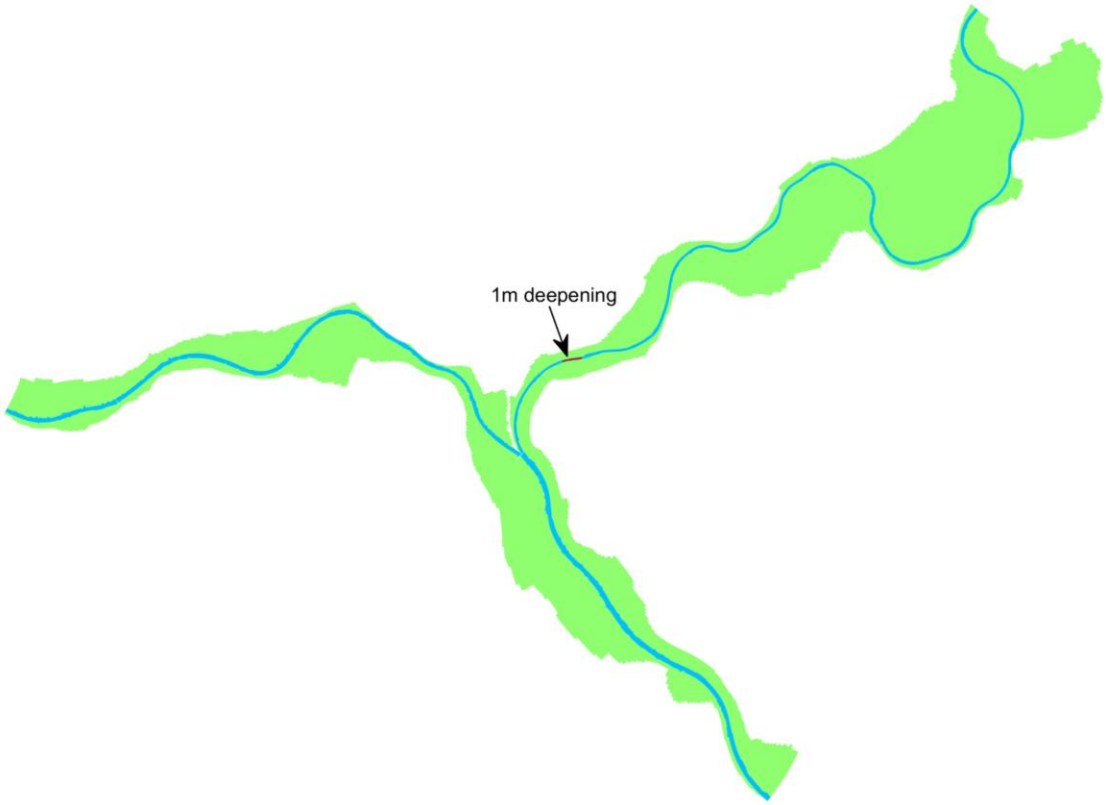

Figure 6-10: Location of the artificial deepening

Water levels

The deepening does not have a large influence on the water level. It causes a small increase (≤ 0.8 cm), in water level downstream of the modification and a small decrease upstream of this area.

Velocity

Overall, the velocity does not show significant differences when the deepening is imposed. Around the deepening itself there is a relatively large decrease and increase as is expected. The flow is decelerated (up to 0.1 m/s) at the deepened part and an accelerated (up to 0.15 m/s) at the end of the deepened part.

Bed level

At the end of the flood wave there is slightly more sedimentation in the Lower Rhine, while the Pannerden Canal and the IJssel are exposed to slightly more erosion compared to the scenario without

artificial deepening. The deepened part itself is filled with approximately 0.5 m of sediment at the end of the flood wave.

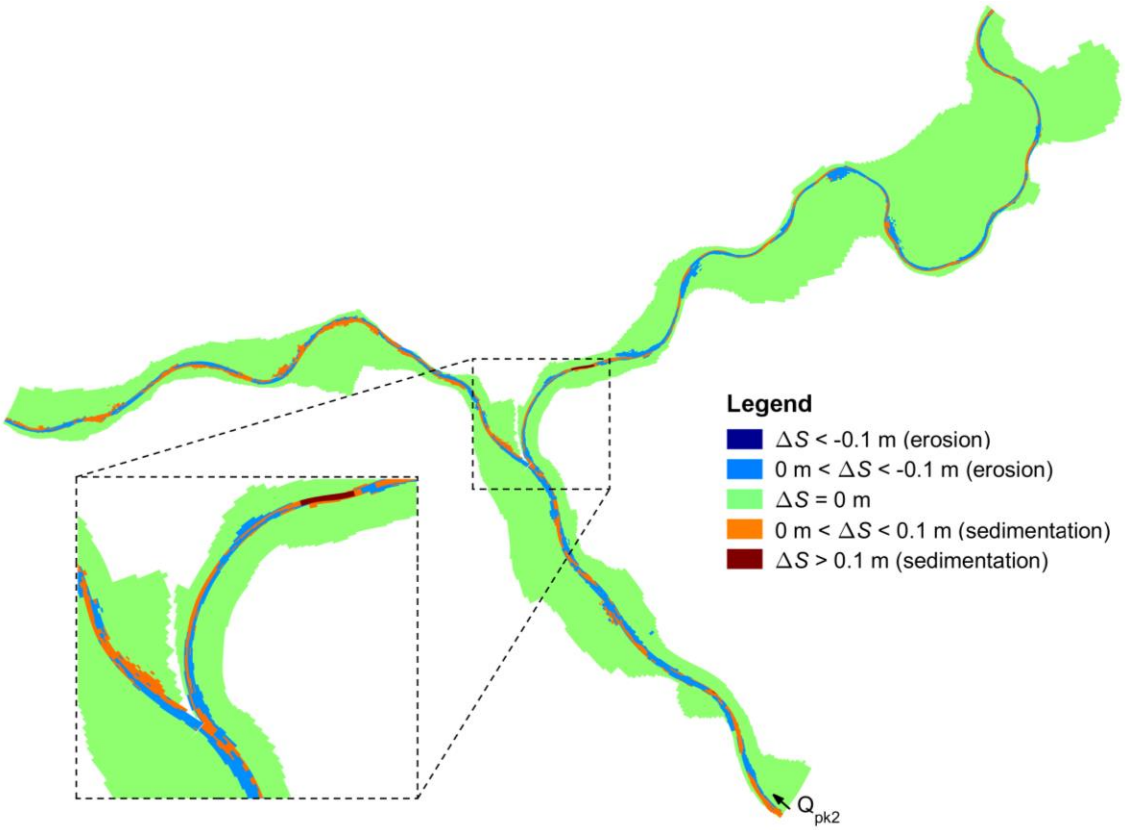

Figure 6-11: Computed locations with sedimentation(+) or erosion(-) with respect to the first morphodynamic computation

Discharge

The artificial deepening has a small influence on the discharge distribution (Figure 6-12). There is less water discharged into the IJssel with an amount of 0.35% and is negligible small. The moment in the flood wave when the IJssel discharge has its peak (between day 5 and 6), there is slightly more water discharged into the IJssel (about 0.05%) compared to the scenario without the deepening. A 2 m or 3 m deepening at the same location gives results with the same order of magnitude (~ 0.50%) and are therefore not significant for the discharge redistribution.

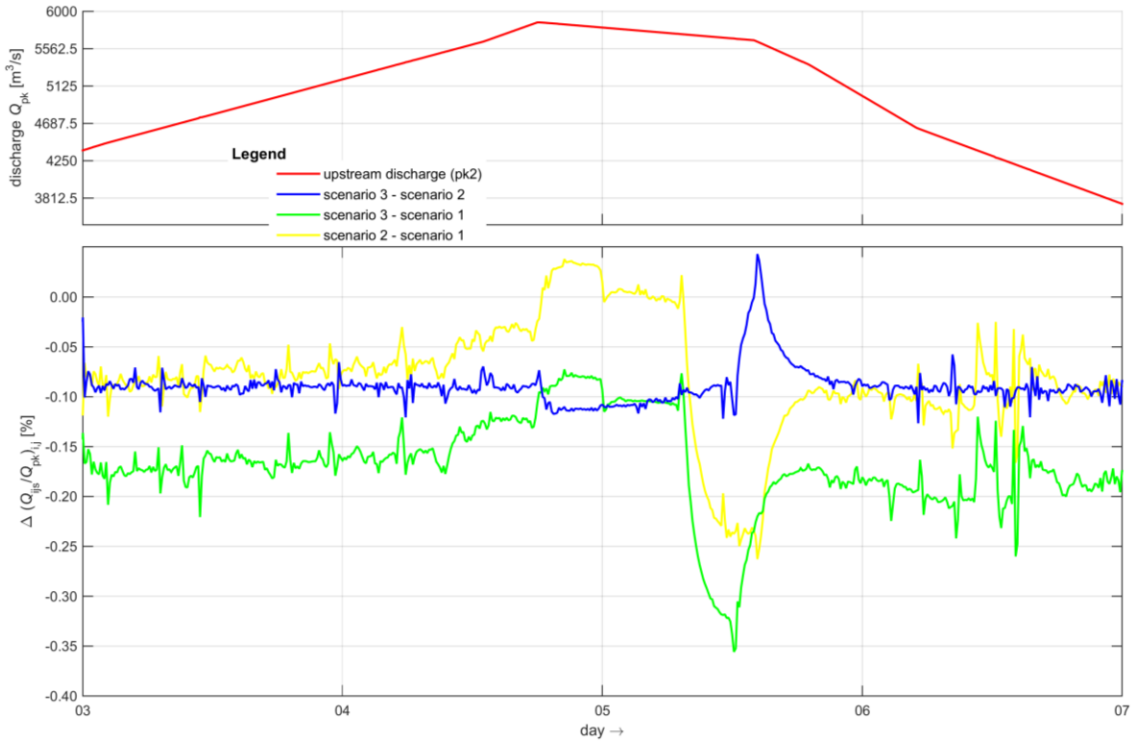

Figure 6-12: Calculated discharge distribution differences between the scenario's (lower figure) and the computed total discharge in the Pannerden Canal (upper figure). The figure show the difference of the IJssel discharge (in terms of percentage of the total discharge) between the scenarios

6.5 Conclusions

This provides an answer to the question: *What are the consequences of erosion of the bed layer of the IJssel for the discharge distribution?*

The morphodynamic model show that a large scale break-up of the armour layer during the design flood wave is not likely to occur. When the break-up of the armour layer is imposed with an artificial deepening, of 1, 2 or 3 m over an area of 35 m x 400 m, at a location where high flow velocities occur, no significant changes occur regarding the discharge distribution at the IJsselkop bifurcation and water levels in the IJssel branch.

A hydrodynamic computation, with a fixed bed (scenario 1), showed that there is a water level difference between the Lower Rhine and the IJssel at the flood plain that separated both branches just downstream the bifurcation, with a maximum water level difference of 16 cm at peak discharge. This difference is a result of the steeper bed slope in the IJssel. The water level development also showed that a hydrodynamic conditions in the Lower Rhine (probably by a backwater curve) determines the water level at the bifurcation, which also determines the upstream water level in the IJssel. The IJssel water level slope increases when the discharges increases.

The maximum flow velocities occur during peak discharge and are located mostly in river bends. When the discharge increases, the velocity in the IJssel increases as well, while the velocity in the Lower Rhine decreases. The latter is a result of more water that is discharged over the Lower Rhine floodplain area when the discharge increases, i.e. the flow velocity increases at the floodplain. The discharge percentage that enters the IJssel differs during the flood wave, from 42% at the start and end of the flood wave to 47% at the peak discharge, which differs slightly from the percentage as derived from the Rijkswaterstaat guidelines (42% during the 16,000 m^3/s discharge).

When the morphodynamic update is applied (scenario 2) the bed level changes with an order of 10 cm and a few small scale areas with a rate up to 2.5 m. The sedimentation and erosion areas are located at the inner bend and outer bend respectively and correspond to the locations with high flow velocities. The morphodynamic update shows also flow velocity differences (compared to scenario 1) of about 0.05 m/s, with accelerations up to 0.19 m/s in the Lower Rhine and decelerations up to 0.33 m/s in the Pannerden Canal. Also a small decrease in water level, of about 1 – 2 cm, is observed when the river bed is erodible. These small changes in hydrodynamics do not cause a large change in discharge distribution at the IJsselkop. According to this computation it is not likely that the design flood wave has a large influence on the stability of the IJsselkop bifurcation.

When simulating a break-up of the armour layer on the river bed, by artificially decreasing the bed level for 1 m, 2 m and 3 m at a location with high velocities, no large changes in water level, bed level and flow velocity are observed. The discharge distribution between both branches has changed with about 0.10% for the 1 m deepening and 0.30% for 3 m deepening, which is not significant. It can be concluded that the artificial deepening does not cause a significant change in discharge distribution at the bifurcation. Moreover, erosion already occurs during discharges lower than the peak discharge. A sudden break-up of the top layer in the river bed is therefore not expected.

Chapter 7 Discussion

The conclusions of this research is partly based on assumptions. These assumptions are discussed in this chapter. This clarifies the limitations of this research and provides the foundations for further research.

7.1 IJssel bed stability

Erosion of the sub layers

The research focussed on the upper 20 cm of the obtained drilling data, which is also the coarsest part of the bed. It is assumed that if this part erodes, the part below erodes as well. A more thorough analysis of the stability of each of the 20 cm thick layers (i.e. when the upper 20 cm is eroded, the part below is exposed to the flow) would give a more accurate result regarding the instability of the bed at each location.

Mobility parameter

The applied Shields mobility parameter is based on the assumption of 'continuous movement of grains'. This indicates that the grains are transported out of the domain, which definitely result in bed instability. A state of 'occasionally movement of the grains' may already result in an unstable bed. This condition leads to a more safe approach regarding the uncertainties of the analysis. The same area becomes unstable but it may indicate more erosion or even a break-up of the layer.

Area of analysed data

The area for which the data have been analysed could be increased. Potential instable locations can be compared with the outcomes of the numerical model, which may lead to a more secure assumption of an unstable location.

Artificial deepening

Erosion at the locations (just downstream the bifurcation) where the analytical calculation has been performed is likely to occur. Therefore it may be interesting to see what the consequences on the discharge distribution are if an artificial deepening is imposed at this location.

7.2 Flood plain stability

Quality of grass cover

A site visit gave information about the flood plain surface and the grass properties. Still little is known about the exact conditions and characteristics of the grass cover at the flood plain. Field research gives more information regarding the quality of the grass cover and subsoil, so the accuracy of the stability analysis could be increased.

Discontinuities

The exact influence on the presence of objects and/or damages at the flood plain is unknown, but definitely unfavourable for the stability of the flood plain. Transitions between the grass/subsoil and the bank protection/dams could be critical. This should be assessed in more detail. Especially at the IJssel bank, where high flow velocities occur.

7.3 Numerical model

Input accuracy

The better part of the input files from the existing Rhine branch model have been used for the Delft3D-model in this research. To reduce the computational time, the computed domain has been reduced. The imposed boundary conditions are defined with the available data. An error in these values is likely, which may result in discrepancies close to the bifurcation. Increasing the computational domain reduces the influence of boundary discrepancies at the bifurcation. A downstream boundary can for example be imposed at the IJsselmeer, for which the water levels can be determined more accurately. A relation between the increase in accuracy and the computational time need to be considered.

Implementing soil investigations

The bed composition in the model has also been obtained from the existing Rhine branch model. It is a sediment mixture that varies for each grid cell and it consists of one transport layer with a uniform sediment distribution over depth. A more accurate representation of the river bed can be modelled if the obtained drilling data is implemented in the model, because the coarse material is present at the top layer and the material below is less coarse.

Implementing areas to the model

The model did not include the presence of the flood channel (Hondsbroeksche Pley) and the interaction between the Lower Rhine and the IJssel at the flood plain. Implementing these aspects increases the accuracy of the results for the present situation

Chapter 8 Conclusions

This research shows the behaviour of the river system around the IJsselkop bifurcation. It shows the background of the area and the behaviour of the river system during a design discharge of 16,000 m^3/s at Lobith. A stability analysis of both the grass cover on the flood plain and the IJssel river bed is performed. Based on this analysis it is concluded that the IJsselkop bifurcation remains stable during design discharge conditions. No significant changes are likely to occur to the discharge distribution at this bifurcation and the water levels at the IJssel branch. The conclusion is presented as the answer to the four research questions as presented below.

What are the characteristics of the IJsselkop area?

An analysis of the characteristics of the IJsselkop area showed that coarse material is present at the IJssel river bed with an average bed level and water level decrease of 1- 2 cm/yr. A coarse sediment layer is present just below surface and at the top of the river bed around the IJsselkop area. Drillings show that the first metre below bed level consists of coarse material, up to a grain size (d_{50}) of 8 mm, on top of a less coarse sediment layer with a grain size up to 2 mm. The flood plain has a top layer of sandy/clayey sediment, which is covered with vegetation. Bed level data show a decrease in bed level of 1-2 cm/year in the IJssel branch, which is the same order of magnitude as the average water level decrease per year over the last 50 years at the IJsselkop. This decrease may be caused by a deficit in sediment supply and the fact that bend cut-offs have been constructed. Turbulent processes are present around the bifurcation as indicated by a scour hole development close to the bifurcation.

Is the bed layer of the IJssel likely to fail during design conditions?

The bed just downstream the bifurcation is likely to erode during the design discharge. A stability analysis is performed by calculating the ratio between acting and critical velocities. The first stability analysis is performed based on uniform sediment (d_{50}). When accounting for mixed sediment, by adding the hiding and exposure principle, the areas with large grain sizes become less stable and fines become more stable compared the scenario based on uniform sediment. This is the result of a decrease in critical shear stress because of the exposure of the larger grains when it is surrounded by finer grains. It is expected that the presence of dunes cause locally higher velocities, because of the turbulent region downstream of the dunes. Adding the dune influence in the stability analysis shows that the armour layer becomes more unstable. It can be concluded that a large area just downstream of the bifurcation may erode during the peak flow velocity and is most likely caused by sediment mixture and the presence of dunes.

Is the grass cover likely to erode during the design discharge and what are the consequences for the discharge distribution?

The flood plain is able to withstand the design discharge if the subsoil is not exposed and no discontinuities are present. If the grass cover is in good condition it should be able to withstand the flow velocities during the design conditions (1.89 m/s). The grass layer is in good condition if it has a good coverage (> 70%), it is well maintained and the subsoil is good resistant against erosion, which may be assumed for the grass cover at the IJsselkop flood plain. Imperfections in the grass cover may cause large scale scour. Turbulence due to local disturbances may cause instantaneous forces on the grass cover, which can initiate erosion. For the present situation it is concluded that the presence of disturbances cause undesirable scour during a 1/1,250 year flood event. Removing discontinuities reduces the possibility of large scale scour. If large scale erosion of the flood plain occurs it will have a large influence on the lateral discharge (flow from the Lower Rhine to the IJssel). Flood plain erosion

of 1 m increases the lateral discharge with 50% and the total IJssel discharge increases with 9%, based on a conservative estimation.

What are the consequences for the hydrodynamic conditions and bed scour when the armour layer breaks up?

The analysis shows no significant changes for the discharge distribution at the IJsselkop bifurcation as a consequence of the armour layer break-up. The hydrodynamic computation (scenario 1) showed that during the flood wave the percentage of the discharge that flows in the IJssel branch increases slightly from 42% at the start of the flood wave to 47% at the peak discharge, which slightly differ from the Rijkswaterstaat guidelines (42% during a 16,000 m^3/s discharge). The flow velocity increases as the flood wave reaches its peak discharge. The opposite is true for the Lower Rhine; the flow velocity decreases as the discharge increases. This is the result of the diversion of the discharge over the entire flow width for increasing discharge. This leads to an increase in discharge and flow velocity over the flood plain and a decrease of flow velocity in the main channel. In the IJssel the flow velocity is significantly larger, which is caused by the smaller flow width and the steep bed slope. Immediately downstream of the bifurcation there is a water level difference between the Lower Rhine and the IJssel, with a maximum of 16 cm at peak discharge. The morphodynamic run (scenario 2) shows that bed level changes of 10 cm, with local peaks of 2.5 m, do not cause significant changes in the overall discharge distribution, water level or flow velocity. The model shows that a large scale break-up of the armour layer during the design flood wave of 16,000 m^3/s is unlikely to occur. Erosion already occurs during less extreme conditions. When the break-up is imposed (scenario 3) no significant changes of the discharge distribution at the IJsselkop bifurcation are visible. A sudden break-up of the top layer in the river bed is not expected since erosion already occur during discharges lower than the peak discharge. If the break-up occurs, which has been simulated by imposing an artificial deepening, no significant changes are visible regarding the discharge distribution and water levels.

Chapter 9 Recommendations

This research has been performed with the use of available data and assumptions, which formed the base for this thesis. Some of these assumptions have been discussed and this gives possibilities for further research. This chapter describes topics that could be assessed in more detail, which provides a more detailed assessment of the stability of the IJsselkop bifurcation.

Improving the input files in the Delft3D model would result in more accurate outcomes. If the domain of the model is increased, in both downstream direction and upstream direction, the errors at the bifurcation (e.g. the discharge distribution) are reduced to a minimum. Moreover, the Rijkswaterstaat guidelines regarding the discharge distribution of the Rhine branches could be analysed and improved if necessarily.

The present input of the bed layer consist of a fully mixed bed composition of one transport layer. If a more detailed model run is performed, it is recommended that the detailed bed composition data is implemented in the model as well by introducing more than one vertical bed layer. By doing so, the bed can be schematized by a coarse layer on top of a less coarse layer, according to the detailed bed sediment data. This reduces the error of the behaviour of the river bed during a model run.

The analysis regarding the consequences of erosion of the IJsselkop flood plain is assessed with a rough and conservative approach. In order to connect this process with the overall hydrodynamic and morphodynamic development of the IJssel river, it is recommended to add this area to the Delft3D model with the use of a flexible mesh. Both the local consequences (e.g. discharge flow over the flood plain) as the global consequences (e.g. consequences for the water level at the IJssel branch) . This connection gives a more realistic behaviour of the IJsselkop bifurcation during these discharges. Also an analysis of the consequences of an artificial deepening just downstream the bifurcation, which is likely according to the analytical calculations, provides an insight in the influence of the break-up location on the discharge distribution.

The analysis of the IJsselkop characteristics showed a decrease in bed level of the IJssel branch, which is probably caused by the decrease in sediment supply. Former cut-offs in the river branches, the construction of dams in the German Rhine and the works regarding the 'Room for the river programme' have impact on the hydrodynamic and morphodynamic conditions. A more detailed analysis of the long term development of these works might be considered in order to get more knowledge about the extent of influence on the Rhine branches.

References

ANKUM, P. 2002. *Design of open-channels and hydraulic structures,* Delft, TU Delft - Faculteit CITG.

ASHIDA, K. & MICHIUE, M. 1972. Study on hydraulic resistance and bedload transport rate in alluvial streams. *Transactions.* Japan Society of Civil Engineering.

BLOM, A., RIBBERINK, J. S. & DE VRIEND, H. J. 2003. Vertical sorting in bed forms: Flume experiments with a natural and a trimodal sediment mixture. *Water resources research,* 39.

CENTRE NATIONAL OCEANOGRAPHY. 2014. Echo-sounders. Available: http://noc.ac.uk/research-at-sea/ships/onboard-equipment/echo-sounders.

COHEN, K. M. & STOUTHAMER, E. 2012. Opleveringsrapport Basisbestand Paleogeografie RMMDelta. Utrecht: Dept. Fysical Geography, University of Utrecht.

COHEN, K. M., STOUTHAMER, E., HOEK, W. Z., BERENDSEN, H. J. A. & KEMPEN, H. F. J. 2009. Zand in banen. Zanddieptekaarten van het Rivierengebied en het IJsseldal in de provincies Gelderland en Overijssel.

DELTARES 2014. Delft3D - FLOW user manual. Delft: Deltares.

EGIAZAROFF, I. V. 1965. Calculation of nonuniform sediment concentrations. *Journal of the Hydraulics Division.* Proceedings of the American Society of Civil Engineers.

FRINGS, R. M. 2008. Downstream fining in large sand-bed rivers. *Earth-Science Reviews,* 87**,** 39-60.

GOOGLE 2013. Google Earth.

HEWLETT, H. W. M., BOORMAN, L. & BRAMLEY, I. 1987. Design of reinforced grass waterways. London: Construction Industry Research and Information Association.

JANSEN, P. P., BENDEGOM, J., DE VRIES, M. & ZANEN, A. 1979. *Principles of river engineering; the non-tidal alluvial river,* Delft, Delftse Uitgever Maatschappij.

KLEINHANS, M., VAN DEN BERG, J., WILBERS, A. & DE KRAMER, J. 2000. De Allier als morfologisch voorbeeld voor de grensmaas, deel III: sedimenttransport en afpleistering. *Natuurhistorisch maandblad,* 89**,** 202-207.

MINISTERIE VERKEER EN WATERSTAAT 2007. Voorschrift Toetsen op Veiligheid Primaire Waterkeringen. Utrecht: Rijkswaterstaat.

PARKER, G. 2004. *Relations for 1D Bedload Transport* [Online]. Available: http://hydrolab.illinois.edu/people/parkerg/.

RIJKSWATERSTAAT 2011. Waterhuishouding en waterverdeling in Nederland. Utrecht: Rijkswaterstaat.

RIJKSWATERSTAAT. 2014a. *Mapviewer - ecotopen systeem* [Online]. Available: http://www.rijkswaterstaat.nl/apps/geoservices/mapviewer2i/ 2014].

RIJKSWATERSTAAT 2014b. Watermanagement en het stuwensemble Nederrijn en Lek. Den Haag/Utrecht: Rijkswaterstaat.

RIJKSWATERSTAAT OOST-NEDERLAND. 2014a. *Daily discharge and water levels 1901-2013* [Online]. Arnhem: Rijkswaterstaat Oost-Nederland CIV.

RIJKSWATERSTAAT OOST-NEDERLAND 2014b. Yearl multibeam altimetry measurements 2002-2013. Arnhem: Rijkswaterstaat Oost-Nederland CIV.

SCHIERECK, G. J. 2000. *Introduction to bed, bank and shore protection,* Delft, VSSD.

SHIELDS, A. 1936. *Anwendung der Aehnlichkeitsmechanik und der Turbulenz-forschung auf die Geschiebewgung,* Berlin, Mitt Preuss. Versuchsanstalt für Wasserbau und Schiffbau.

STOWA 2009. Handboek debietmetingen in open waterlopen. Utrecht: STOWA.

SURYADI, F. X. & MOSSELMAN, E. 2005. Morfologische verschijnselen ten gevolge van het project Hondsbroeksche Pleij. Delft: WL | Delft Hydraulics.

TAW 1985. Leidraad voor het ontwerpen van rivierdijken. Deel 1 – bovenrivierengebied. 's-Gravenhage.

TAW 1996. Technisch rapport: Klei voor dijken. Delft.
TNO 2003. Kartering ondergrond IJsselkop. Fase 3: eindrapport. Utrecht: TNO-NITG.
TNO 2011. GeoTOP data of the dutch subsoil up to 50 m below surface. *In:* TNO (ed.). Utrecht.
VAN DE VEN, G. P. 1976. *Aan de wieg van Rijkswaterstaat: wordingsgeschiedenis van het Pannerdens kanaal,* Zutphen, De Walburg Pers.
VAN HEEZIK, A. A. S. 2007. Strijd om de rivieren - 200 jaar rivierenbeleid in Nederland of de opkomst en ondergang van het streven naar de normale rivier. Den Haag/Haarlem: HNT Historische producties.
VAN KEULEN, C. 2014. Geschiedenis van Westervoort. Available: http://www.chrisvankeulen.nl/westervoort.htm.
YUE, W., LIN, C.-L. & PATEL, V. C. 2006. Large-Eddy Simulation of Turbulent Flow over a Fixed. *JOURNAL OF HYDRAULIC ENGINEERING,* 132**,** 643-651.

Appendix A. Data measurements

A.1 Data measurements - bathymetry

Echo-sounders are used for the measurement of the bathymetry, performed by Rijkswaterstaat. The sonar instrument uses a transducer that is mounted on the bottom of a ship. The transducer sends sound pulses straight down. When the pulse reaches the river bottom, it reflects and returns to the transducer. The time between sending and receiving of the sound pulse is an indication for the depth of the river bed with respect to the transducer. The distance between the transducer and the river bed can be calculated by multiplying the travelled time by the speed of sound in water (≈ 1500 m/s) and divide this by 2. This principle is sketched in Figure A-1. The sound pulses are sent regularly as the ship moves along the river. For a *single beam echo sounding*, the ship has to zig zag along the river in order to gather data of both the longitudinal as the lateral direction of the river. By sending several beams at the same time, the *multi beam echo sounding*, a wide range is measured at. Here multi-beam data have been considered.

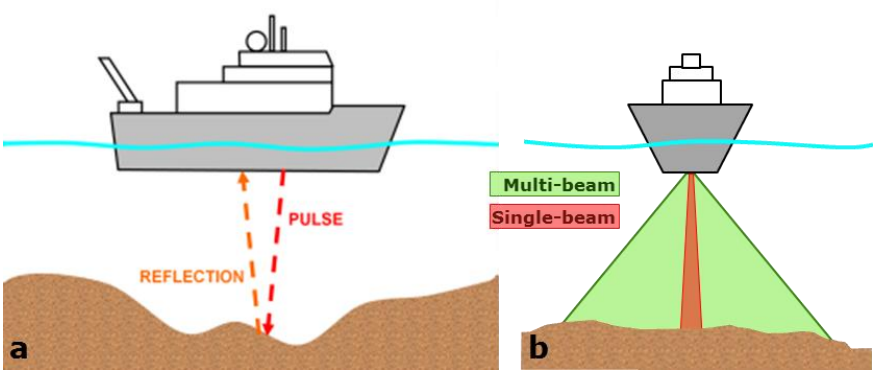

Figure A-1: Schematization of measuring the bed level by using echo-sounding. In (a) the principle of the echo-sounding is shown and (b) the difference between single- and multi-beam measurements (Centre National Oceanography, 2014)

The measured data has been converted into a format in which the location (X- and Y coordinates) and the bed level (z_b, m +NAP) are included, in which the depth values representing one square meter. This xyz-format makes it applicable for the data processing. The conditions of the yearly measurements, summarized in Table A-1 with the measured discharge, differ from year to year. The average discharge at Lobith is approximately 2200 m^3/s, while this value for the IJssel amounts to approximately 340 m^3/s. The IJssel discharge is not $1/9^{th}$ of the Lobith discharge for low discharges (as imposed and executed by the design of the Pannerden kop and IJsselkop), since the Rhine is weir-controlled for a discharge up to 2400m^3/s (Table 2-2).

Table A-1: Discharge values with corresponding dates of measurements in both the IJssel and Lower Rhine

	IJssel			Lower Rhine		
year	Date of measurement	Q_{Lob} [m^3/s]	Q_{IJssel} [m^3/s]	Date of measurement	Q_{Lob} [m^3/s]	Q_{IJssel} [m^3/s]
2002	02-09-2002	1844	294	10-06-2002	2190	329
2003	09-12-2003	1140	201	x	x	x
2004	31-08-2004	2088	310	19-05-2004	1965	303
2005	13-09-2005	1733	302	11-05-2005	3145	450
2006	12-10-2006	2526	363	02-08-2006	1203	212
2007	31-10-2007	1274	223	24-07-2007	2179	316
2008	x	x	x	05-08-2008	1778	300
2009	25-08-2009	1394	248	29-06-2009	2076	309
2010	02-09-2010	3045	427	16-06-2010	2205	315
2011	09-09-2011	1450	245	24-06-2011	1581	267
2012	23-07-2012	1941	297	23-03-2012	1598	279
2013	06-11-2013	2970	404	25-09-2013	2212	313

First, it must be noted that the measurements of the IJssel in 2008 and the Lower Rhine in 2003 are left out of this study, because of errors in the measurements. Secondly, the measurements are performed at the average discharge conditions. The measurement dates, and the discharge conditions around those dates, are represented in Figure A-2. The discharge conditions just before the measurements date were mostly between 1000 and 3000 m^3/s, which indicates that the measured bed profile is formed under average conditions.

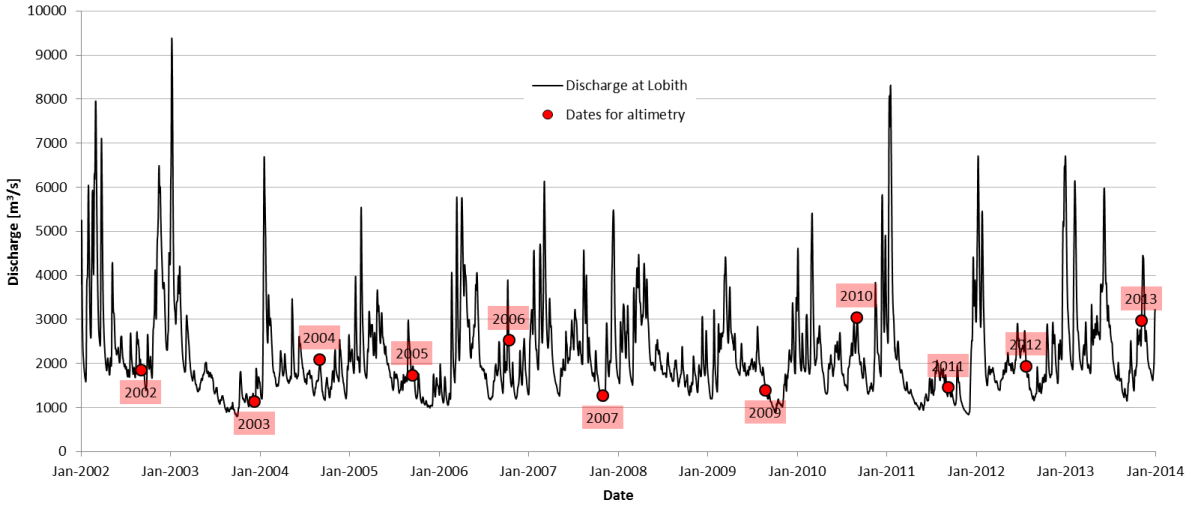

Figure A-2: Dates of yearly altimetry measurements at the time-series of the discharge at Lobith

A.1 Data measurements – hydrodynamics

The water level data has been gathered by measuring the actual water level at a monitoring station. Figure A-3 shows the present water level monitoring station at the IJsselkop.

The measuring methods have changed over the last century. In the early years of the 20th century the water level was read from a gauge. From the mid-thirties to the end of the eighties a float level meter was used and the values were read from a paper. Since the nineties a digital level meter is used, in which every 10 minutes the data is saved. Until 1993 this value was the average of the last ten minutes. Since then, the saved value is the average of the last five minutes and the next five minutes. The accuracy, and therefore the reliability, of the values increased during the years. A summary of the measuring methods through the years is given in Table A-2.

Figure A-3: The water level monitoring station for the IJsselkop. In the lower-right corner a cross-section of the measuring method with a monitoring well

Table A-2: Water level measurement methods through the years

	Measuring device		Data evaluation	
Date	**Lobith**	**IJsselkop**	**Lobith**	**IJsselkop**
Nov-1824 t/m Dec-1934	Gauge	x	Read from gauge	x
Jan-1935 t/m Sept-1962	Float level meter	x	Read from plot by eye	x
Oct-1962 t/m Apr-1979	Float level meter	Float level meter (type TNO1926)	Read from plot by eye	
May-1979 t/m Jun-1987	Float level meter	Float level meter (type TNO1975)	Read from plot by eye	
Jul-1987 t/m Sept-1993	Float level meter (type DNM)		Average water level of the last 10 minutes	
Oct-1993 t/m Dec-2013	Float level meter (type DNM)		Average water level of the last 5 minutes and the next 5 minutes	

Relation between discharge and water level

Discharge measurements are performed periodically to determine a relation between the discharge and the water level. Subsequently, this relation is used for the conversion of all the other daily water levels to a discharge. Two relations are described shortly in this section: the *Q-h* relation (the stage-discharge curve) and the *Q-f* relation. More information and the relations behind these methods is found in the guidebook for discharge measurements (STOWA, 2009).

Stage-discharge curve

The relation between the discharge *Q* and the water level *h* is empirical and is derived from the Chézy equation, which is applicable at uniform flow conditions. The velocity, *u* (m/s), depends on the water level *h* the bed slope i_b and the bed roughness *C*.

$$u = C\sqrt{hi_b} \tag{A.1}$$

From this equation it can be stated that $Q \sim h^{3/2}$. The *Q-h* relation is often used for the determination of the water level at extreme discharge conditions. Since these conditions do not occur that often, it

is almost impossible to monitor these values. Therefore, the extreme value has to be assessed by extrapolation of existing data. For an accurate relation it is important to choose a measurement location where the water level remains more or less constant. Another possible inequality is caused by a phenomenon called hysteresis: a discharge occurs twice during a flood wave, with a lower w ater level for a given discharge before the peak discharge than the same discharge after the peak discharge. For an accurate relation, it is therefore important to choose a measure location where this water level difference is minimal. In The Netherlands there are almost no locations where this hysteresis does not occur, although it can be created by creating subcritical flow.

When a *Q-h* relation is determined, a *Qh*-curve can be constructed by a polynomial function. This curve visualizes the relation between the discharge and the water level. The curvature originates from the presence of a flood plain. The extra flowing area causes the water level to increase less than before and therefore causing a decrease in the gradient of the curve, which is shown in Figure A-1.

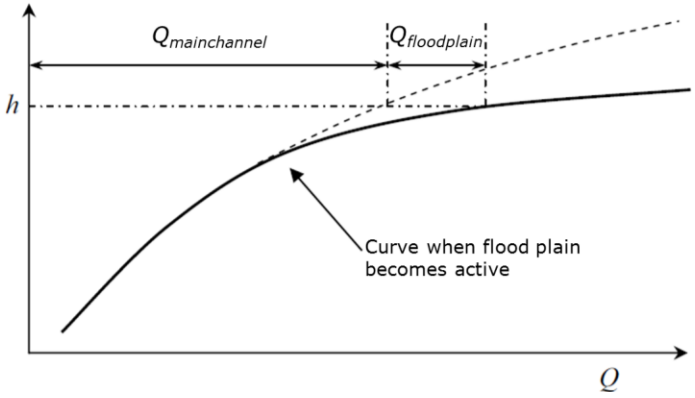

Figure A-1: Influence of the flood plain to the *Qh*-curve

When a *Q-h* relation is determined, it is not necessarily representative for a long period. Changes in the relation can be caused by large fluctuating water levels, a change of cross-sectional flowing area by erosion or sedimentation, a change of vegetation, backwater curves or subsidence. These factors can cause an under- or overestimation by using the existing relation.

Q-f relation

A *Q-h* relation is sufficient for most studies, but for using the data in more detail there are a few disadvantages. Possible inaccuracies of this method, as mentioned above, may cause crucial under- or overestimations. Because of these errors, a new method is set up with a relation between the water level on one side and the hysteresis and subsidence of the soil on the other side. The last two are combined in a function *f*. The relation is derived by analyzing the historical data. This method causes a decrease of the inaccuracy by 50% (STOWA, 2009).

Appendix B. Governing equations

B.1 Governing equations

The Navier-Stokes equations for incompressible fluid $\left(\nabla \cdot \vec{u} = 0\right)$ are solved by the Delft3D-FLOW module, with the shallow water and Boussinesq assumptions taken into account. Together with the initial and boundary conditions, these equations are solved on a finite difference grid.

Continuity equation

The continuity equation is a result of the volume conservation within a grid cell, which states that the total volume of water remains constant in the cell. This implies that each water volume that enters the grid cell (q_{in}) minus the amount that remains in the cell (Q), equals the amount that leaves the cell (q_{out}). The depth-averaged continuity equation, as used in Delft3D, is given by:

$$\frac{\delta\zeta}{\delta t} + \frac{1}{\sqrt{G_{\xi\xi}}\sqrt{G_{\eta\eta}}}\frac{\delta\left[\left(d+\zeta\right)U\sqrt{G_{\eta\eta}}\right]}{\delta\xi} + \frac{1}{\sqrt{G_{\xi\xi}}\sqrt{G_{\eta\eta}}}\frac{\delta\left[\left(d+\zeta\right)V\sqrt{G_{\xi\xi}}\right]}{\delta\eta} = Q \qquad \text{(A.2)}$$

with

ζ	=	Water level above a reference plane [m]
t	=	Time [sec/min/hours]
d	=	Depth below a reference plane [m]
U	=	Depth-averaged flow velocity in main direction [m/s]
V	=	Depth-averaged flow velocity perpendicular main direction [m/s]
Q	=	Global source or sink per unit area per second [$m^3/s\ m^{-2}$]

Momentum equation

The momentum balance, which originates from Newton's second law ($F = ma$) includes the influence of the shear stresses and the turbulent processes within the volume unit (i.e. the grid cell). The momentum equation in general can be shown as. The momentum equations in Delft3D are defined in both ξ-direction (velocity U) and η-direction (velocity V) in the Cartesian co-ordinate system. The momentum equation in the ξ-direction is given by:

$$\underbrace{\frac{\delta U}{\delta t}}_{1} + \underbrace{\frac{U}{\sqrt{G_{\xi\xi}}}\frac{\delta U}{\delta\xi} + \frac{V}{\sqrt{G_{\eta\eta}}}\frac{\delta U}{\delta\eta}}_{2} - \underbrace{\frac{V^2}{\sqrt{G_{\xi\xi}}\sqrt{G_{\eta\eta}}}\frac{\delta\sqrt{G_{\eta\eta}}}{\delta\xi} + \frac{UV}{\sqrt{G_{\xi\xi}}\sqrt{G_{\eta\eta}}}\frac{\delta\sqrt{G_{\xi\xi}}}{\delta\eta}}_{4}$$
$$+ \underbrace{\frac{1}{\rho_0\sqrt{G_{\xi\xi}}}P_\xi}_{3} + \underbrace{\frac{gU\sqrt{U^2+V^2}}{C^2\left(d+\zeta\right)}}_{5} = \underbrace{fV + F_\xi + F_{s\xi} + M_\xi}_{6} \qquad \text{(A.3)}$$

The momentum equation in the η-direction is given by:

$$\underset{1}{\frac{\delta V}{\delta t}} + \underbrace{\frac{U}{\sqrt{G_{\xi\xi}}}\frac{\delta V}{\delta \xi} + \frac{V}{\sqrt{G_{\eta\eta}}}\frac{\delta V}{\delta \eta}}_{2} - \underbrace{\frac{U^2}{\sqrt{G_{\xi\xi}}\sqrt{G_{\eta\eta}}}\frac{\delta \sqrt{G_{\xi\xi}}}{\delta \eta} + \frac{UV}{\sqrt{G_{\xi\xi}}\sqrt{G_{\eta\eta}}}\frac{\delta \sqrt{G_{\eta\eta}}}{\delta \xi}}_{4}$$
$$+ \underbrace{\frac{1}{\rho_0 \sqrt{G_{\eta\eta}}} P_\eta}_{3} + \underbrace{\frac{gV\sqrt{U^2+V^2}}{C^2(d+\zeta)}}_{5} = \underbrace{fU + F_\eta + F_{s\eta} + M_\eta}_{6} \qquad \text{(A.4)}$$

With

f	=	Coriolis force
P_i	=	Pressure in *i*-direction [N/m^2]
F_i	=	Resultant of the Reynold stresses in *i*-direction [m/s^2]
F_{si}	=	Resultant of the forces due to spiral motion in *i*-direction [m/s^2]
M_i	=	Contributions of momentum due to external sources or sinks in *i*-direction [m/s^2]
C	=	Chézy coefficient [m$^{1/2}$/s]
ρ_0	=	Reference density of water

The subscript *i* is the direction parameter (ξ or η). The equations are categorized in the local inertia (1), convective inertia (2), pressure gradient (3), Reynold stresses (4), viscous shear stresses (5) and additional terms (6). For the background of these equations and the derivation of the parameters will be referred to (Deltares, 2014).

Appendix C. Background model input

C.1 Defining hydrograph discretization

The input discharge of the delft3d model is a representation of a flood wave with a peak of 16000 m^3/s. A representative hydrograph is gathered from '*Hydraulische Randvoorwaarden primaire waterkeringen*', which is a handbook with design criteria regarding hydraulic boundary conditions of the primary water retaining structures (Table C-1).

Table C-1: Discharge data of a flood wave with 16,000 m^3/s at Lobith

Time [hours]	Discharge [m^3/s]
-200	4,362
-150	5,676
-125	6,616
-100	7,794
-75	9,421
-50	11,812
-25	14,561
-15	15,433
-10	15,749
-5	15,936
0	16,000
5	15,946
10	15,781
15	15,508
25	14,704
50	12,457
75	10,480
100	9,052
125	8,077
150	7,342
200	6,046

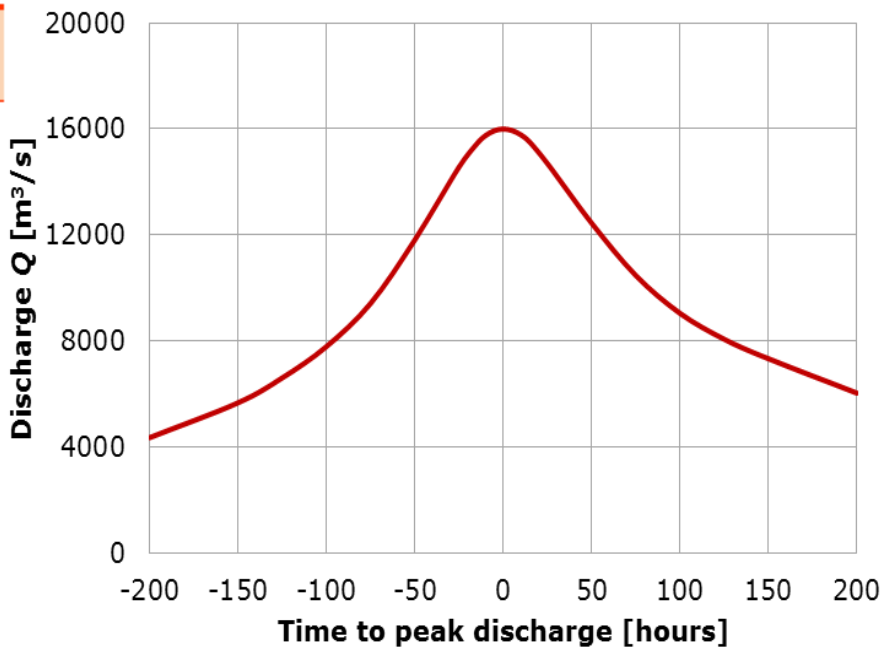

The flood wave is schematized with a discharge time-series. These time-series implies that there are several time blocks of static discharges computed after each other, which should represent the total hydrograph as shown above. At an infinite small duration of each discharge step, the hydrograph will be approached very accurately. With increasing time steps the error with respect to the hydrograph at a moment of time will increase, but on the other hand will the computation time decrease as well. Next to that, there is also some computation time to win by starting at a higher discharge. The base model that is applied (e.g. the grid and roughness files), is already used for computations with less extreme conditions. The discharge input for that computation is mentioned below in Table C-2.

Table C-2: Discharge input as used in existing Delft3D-model

Duration [min]	Discharge [m³/s]
28	2250
84	3053
120	3824
84	4717
36	6151
36	8592
36	6151
84	4717
132	3824
126	3053
182	2250
182	1635
76	1203
28	1635

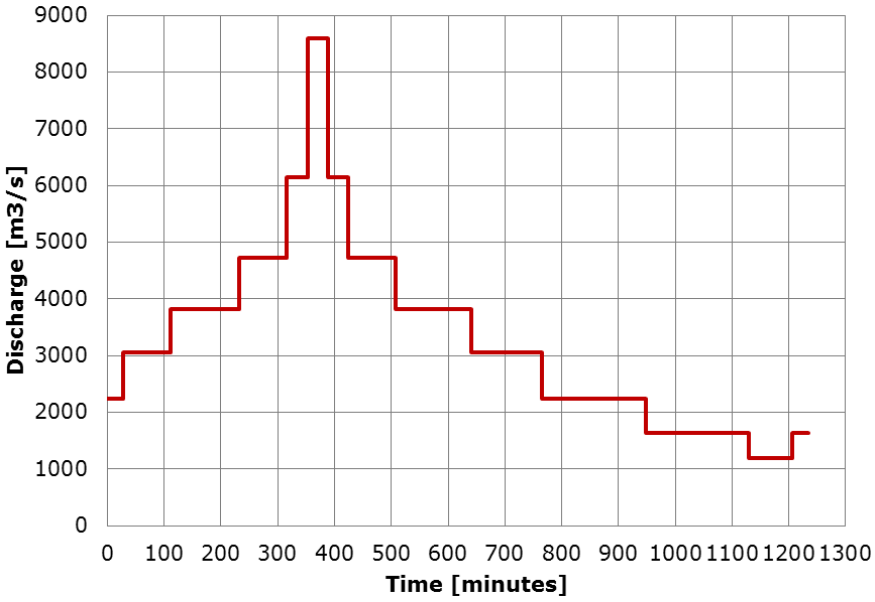

These time-series shows that the computations already have been performed for conditions with low discharges. This implies that the hydrodynamic conditions for a maximum discharge of 8592 m^3/s are known, so that the outcomes of these computations can be used as input in the model for this research. This also means that an initial discharge of 8592 m^3/s can be applied and thus the focus can lie on the peak discharge.

Calculations are performed by averaging several time steps in the hydrograph (Table C-1). By trial-and-error, nine discharge time steps have been applied with such a duration and magnitude that the total amount of water that passes during that period equals to that of the original hydrograph. The discharge discretization is shown in Table C-3. These values are used as upstream boundary of the model.

Table C-3: Derived time-series discharge input at the upstream boundary

Duration [hours]	Lobith [m³/s]
25	8592
25	10617
25	13187
10	14997
5	15591
20	16000
5	15645
10	15106
25	13581
50	10617
25	8592

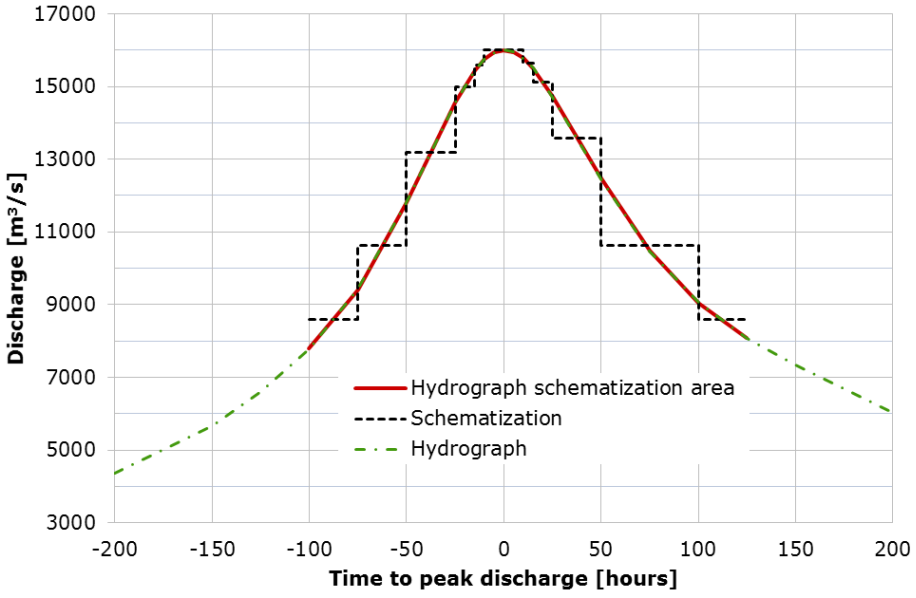

C.2 Defining total discharge Pannerden Canal

Rijkswaterstaat set-up a discharge distribution of the Waal, Lower Rhine and IJssel branches by using a *Q-f* relation, shown in Figure C-5. The discharge in the Waal and Pannerden Canal together equals the Lobith discharge, and the discharge in the Lower Rhine and IJssel together equals the Pannerden Canal discharge.

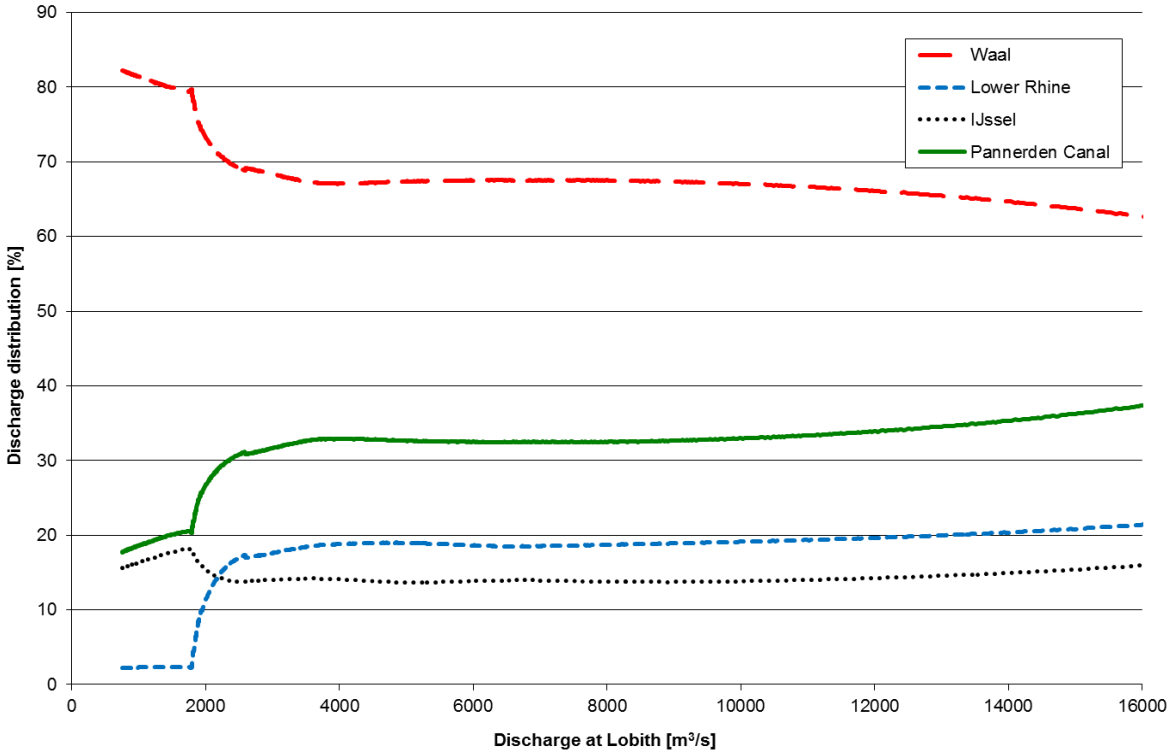

Figure C-5: Discharge distribution over the Rhine branches as determined by (Ministerie van Verkeer en Waterstaat, 2007)

The influence of the weirs in the Lower Rhine are visible during low discharge conditions. Up to a discharge of +- 1800 m^3/s at Lobith, the distribution is completely forced by the weirs so that the IJssel receives a relatively high percentage of the total discharge. For higher discharges, the weirs are of less influence, by opening them, and the distribution eventually becomes natural for discharges higher than +- 2300 m^3/s (i.e. the weirs are completely open). Since the computations are performed for discharges above 6000 m^3/s, this process is not of relevance. The discharge that is needed as input in the Pannerden Canal is gathered from the data above. Table C-4 shows the equivalent Pannerden Canal discharge.

Table C-4: Derived discharges for the Pannerden Canal

Lobith [m^3/s]	Pannerden [m^3/s]
8592	2754
10617	3455
13187	4482
13581	4661
14997	5360
15106	5429
15591	5709
15645	5723
16000	5942

C.3 Defining discharge per cell

Since WAQUA computations are performed for these extreme conditions, there is some information available about the discharge distribution along the upstream boundary. It has to be converted from the WAQUA cells to the Delft3D cells though. It is therefore important to find out what errors may be present by this transformation. The distribution with the maximum computed discharge in Delft3D (Q = 8592 m^3/s) is compared with the outcomes from WAQUA (Q=8650 m^3/s), which is shown in Figure C-6. Globally, the lines follow the same pattern (a large amount of the discharge goes to the main channel, the first ten cells, and a low amount goes to the flood plain). In the main channel itself, however, a large difference is present. Where the WAQUA data show two peaks, has the distribution in Delft3D one peak. Since the two peaks in the main channels are not likely to occur (i.e. the most discharge is transported through the middle of the main channel and less discharge towards the river banks), the WAQUA data will be corrected in this part so that the distribution along the cells is according to the Delft3D distribution. By determining the correction factors for each of the cells (#1-10), it is kept in mind that the total discharge (100%) may not change. These correction factors are applied for all discharges. The difference of the WAQUA and Delft3D is assumed to be negligible at the other cells (no. 10-37). The WAQUA data is for the calculation of the discharge distribution for several severe discharges. The WAQUA outcomes are not stored every hour. Therefore linear interpolation is applied between two data points were the input discharge (Table C-4) is in between. The discharge distributions per cellare visualized in Figure C-7 below.

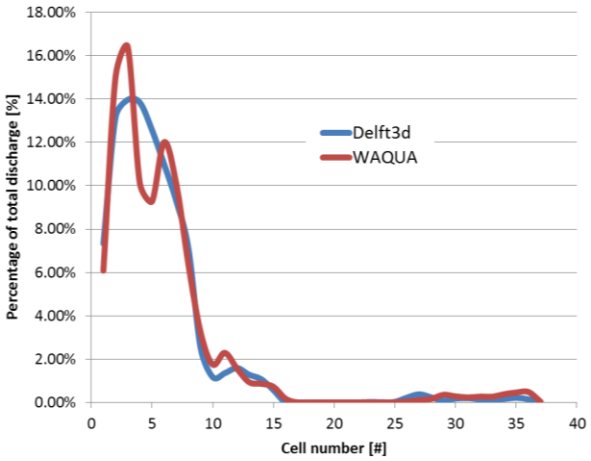

Figure C-6: Discharge distribution along the upstream boundary of pk2, for Q = 8650 m3/s

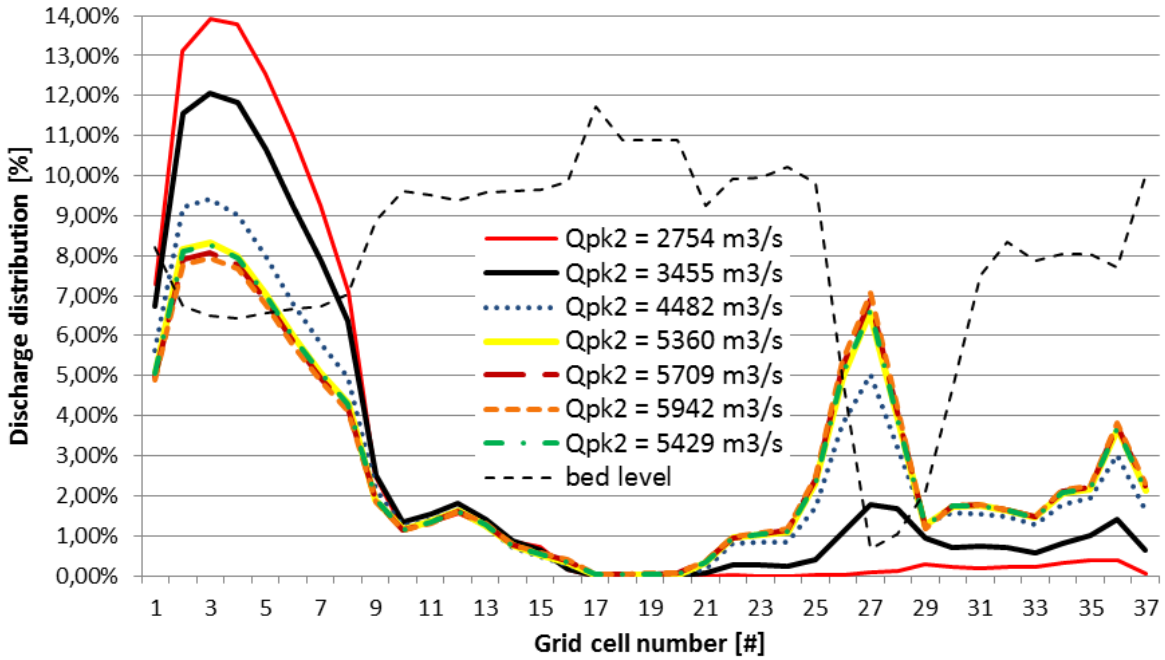

Figure C-7: Discharge distribution for the input discharges at the upstream boundary in the Pannerden Canal. The bed level contours shows the main channel on the left side of the graph and a basin at the deeper part on the right

C.4 Sediment input – distribution along the river

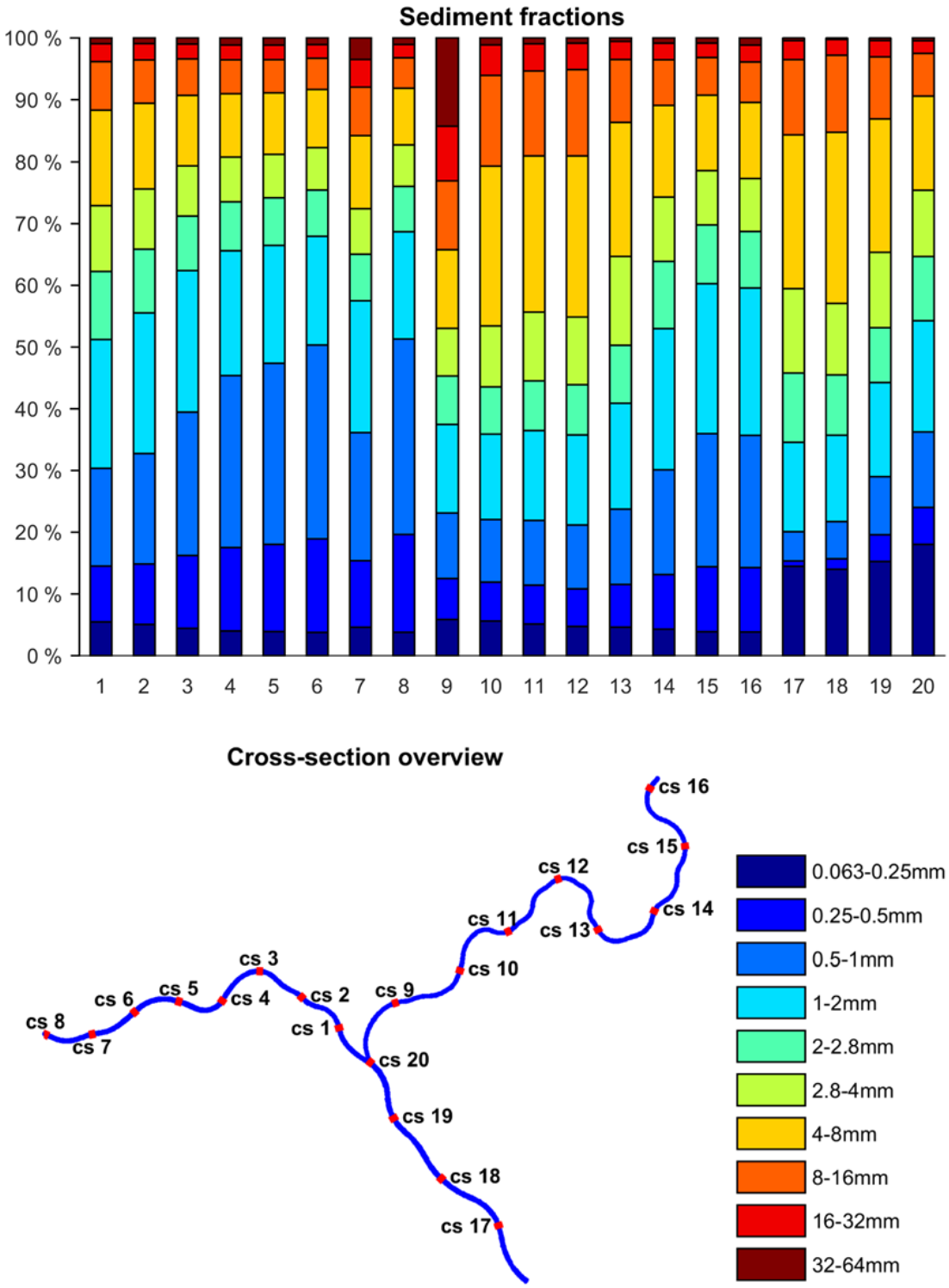

Figure C-8: Sediment input - distribution of the sediment

Appendix D. Delft3D input values

D.1 Input data Pannerden Canal (pk2)

Menu	tab	parameter	value	unit
Domain	grid	grid	pk2.grd	
		grid enclosure	pk2.enc	
		co-ordinate system	Cartesian	
		grid points M-direction	81	[-]
		grid points M-direction	139	[-]
		latitude	0	[deg]
		orientation	0	[deg]
		number of layers	1	[-]
	bathymetry	file	pk2.dep	
		values specified at	grid cell centres	
	thin dams	thin dams	pk2.thd	
Time frame		reference date	01 01 2014	[dd mm yyyy]
		simulation start time	01 01 2014 00 00 00	[dd mm yyyy hh mm ss]
		simulation stop time	09 01 2014 08 00 00	[dd mm yyyy hh mm ss]
		time step	0.2	[min]
		local time zone	0	[+GMT]
Processes		physical	secondary flow	
Initial conditions		restart file	tri-rst.pk2_Q8592	
Boundaries	Boundaries	boundary definitions	pk2.bnd	
		time-series flow conditions	pk2.bct	
Physical parameters	Constants	gravity	9.81	[m/s^2]
		water density	1000	[kg/m^3]
		beta_c	0.5	[-]
	Roughness	bottom roughness	White-Colebrook	
		U	0.255	
		V	0.255	
		wall roughness	free	
	Viscosity	background horizontal viscosity/diffusivity	uniform	
		horizontal eddy viscosity	0.5	[m^2/s]
		horizontal eddy diffusivity	0.5	[m^2/s]
Numerical parameters		drying and flooding check at	grid cell centres and faces	
		depth at grid cell faces	min	
		threshold depth	0.1	[m]
		marginal depth	-999	[m]

Menu	tab	parameter	value	unit
		smoothing time	0	[min]
		advection scheme for momentum	cyclic	
Monitoring	observations		pk2.obs	
	cross-sections		pk2.crs	
Additional parameters		TraFrm	graded.tra	
		Fil2dw	pk2.wr	
		Thetaw	0.0	
		Trtrou	Y	
		Trtdef	rough_karak.MvdR	
		Trtu	pk2.aru	
		Trtv	pk2.arv	
		TrtDt	1.2	
Output	Storage	Store map results		
		start time	01 01 2014 00 00 00	[dd mm yyyy hh mm ss]
		stop time	31 05 2014 00 00 00	[dd mm yyyy hh mm ss]
		interval	60	[min]
		history interval	10	[min]

D.2 Input data Lower Rhine (nr1a)

Menu	tab	parameter	value	unit
Domain	grid	grid	nr1a.grd	
		grid enclosure	nr1a.enc	
		co-ordinate system	Cartesian	
		grid points M-direction	71	[-]
		grid points M-direction	302	[-]
		latitude	0	[deg]
		orientation	0	[deg]
		number of layers	1	[-]
	bathymetry	file	nr1a.dep	
		values specified at	grid cell centres	
	thin dams	thin dams	nr1a.thd	
Time frame		reference date	01 01 2014	[dd mm yyyy]
		simulation start time	01 01 2014 00 00 00	[dd mm yyyy hh mm ss]
		simulation stop time	09 01 2014 08 00 00	[dd mm yyyy hh mm ss]
		time step	0.2	[min]
		local time zone	0	[+GMT]
Processes		physical	secondary flow	
Initial conditions		restart file	tri-rst.nr1a_Q8592	
Boundaries	Boundaries	boundary definitions	nr1a.bnd	

Menu	tab	parameter	value	unit
		time-series flow conditions	nr1a.bct	
Physical parameters	Constants	gravity	9.81	[m/s^2]
		water density	1000	[kg/m^3]
		beta_c	0.5	[-]
	Roughness	bottom roughness	White-Colebrook	
		U	0.255	
		V	0.255	
		wall roughness	free	
	Viscosity	background horizontal viscosity/diffusivity	uniform	
		horizontal eddy viscosity	0.5	[m^2/s]
		horizontal eddy diffusivity	0.5	[m^2/s]
Numerical parameters		drying and flooding check at	grid cell centres and faces	
		depth at grid cell faces	min	
		threshold depth	0.1	[m]
		marginal depth	-999	[m]
		smoothing time	0	[min]
		advection scheme for momentum	cyclic	
Monitoring	observations		nr1a.obs	
	cross-sections		nr1a.crs	
Additional parameters		TraFrm	graded.tra	
		Fil2dw	nr1a.wr	
		Thetaw	0.0	
		Trtrou	Y	
		Trtdef	rough_karak.MvdR	
		Trtu	nr1a.aru	
		Trtv	nr1a.arv	
		TrtDt	1.2	
Output	Storage	Store map results		
		start time	01 01 2014 00 00 00	[dd mm yyyy hh mm ss]
		stop time	31 05 2014 00 00 00	[dd mm yyyy hh mm ss]
		interval	60	[min]
		history interval	10	[min]

D.3 Input data IJssel (yac1)

Menu	tab	parameter	value	unit
Domain	grid	grid	yac1.grd	
		grid enclosure	yac1.enc	
		co-ordinate system	Cartesian	
		grid points M-direction	124	[-]
		grid points M-direction	303	[-]
		latitude	0	[deg]
		orientation	0	[deg]
		number of layers	1	[-]
	bathymetry	file	yac1.dep	
		values specified at	grid cell centres	
	thin dams	thin dams	yac1.thd	
Time frame		reference date	01 01 2014	[dd mm yyyy]
		simulation start time	01 01 2014 00 00 00	[dd mm yyyy hh mm ss]
		simulation stop time	09 01 2014 08 00 00	[dd mm yyyy hh mm ss]
		time step	0.2	[min]
		local time zone	0	[+GMT]
Processes		physical	secondary flow	
Initial conditions		restart file	tri-rst.yac1_Q8592	
Boundaries	Boundaries	boundary definitions	yac1.bnd	
		time-series flow conditions	yac1.bct	
Physical parameters	Constants	gravity	9.81	[m/s^2]
		water density	1000	[kg/m^3]
		beta_c	0.5	[-]
	Roughness	bottom roughness	White-Colebrook	
		U	0.255	
		V	0.255	
		wall roughness	free	
	Viscosity	background horizontal viscosity/diffusivity	uniform	
		horizontal eddy viscosity	0.5	[m^2/s]
		horizontal eddy diffusivity	0.5	[m^2/s]
Numerical parameters		drying and flooding check at	grid cell centres and faces	
		depth at grid cell faces	min	
		threshold depth	0.1	[m]
		marginal depth	-999	[m]
		smoothing time	0	[min]
		advection scheme for momentum	cyclic	

Menu	tab	parameter	value	unit
Operations	Discharges	discharge definitions	yac1.src	
		discharge data	yac1Q8592.dis	
Monitoring	observations		yac1.obs	
	cross-sections		yac1.crs	
Additional parameters		TraFrm	graded.tra	
		Fil2dw	yac1.wr	
		Thetaw	0.0	
		Trtrou	Y	
		Trtdef	rough_karak.MvdR	
		Trtu	yac1.aru	
		Trtv	yac1.arv	
		TrtDt	1.2	
Output	Storage	Store map results		
		start time	01 01 2014 00 00 00	[dd mm yyyy hh mm ss]
		stop time	31 05 2014 00 00 00	[dd mm yyyy hh mm ss]
		interval	60	[min]
		history interval	10	[min]

Appendix E. Theoretical background – deepening

The sudden local deepening of the bed level has consequences for the hydrodynamics and morphodynamics around the deepening. At each point the river tends to reach its equilibrium state for its bed level, bed slope and water level, which is unlikely to be reached for a varying discharge. Figure 9-1a shows the schematization of the situation before a deepening assuming an equilibrium state. Figure 9-1b shows the bed level situation right after the deepening in area II, which now has a new equilibrium water level h_e where it tends to go to. Backwater curves occurs because of the varying equilibrium water level. Depending on the length of area II, the water level reaches its equilibrium level at the upstream boundary of this area. Further upstream, area I, the water level increases to its local equilibrium water level. Whether or not the water level has reached its equilibrium at the upstream boundary of area I, depends on the length of the area. The IJsselkop bifurcation is located somewhere in area I of Figure 9-1b, which indicates that the deepening is likely to cause a backwater curve that lowers the water level at the IJssel side of the bifurcation. The following water level difference between the Lower Rhine and the IJssel at the bifurcation is equalized since the IJssel receives more water, and the Lower Rhine receives less (i.e. the water levels of the Lower Rhine and the IJssel have to be the same at the bifurcation).

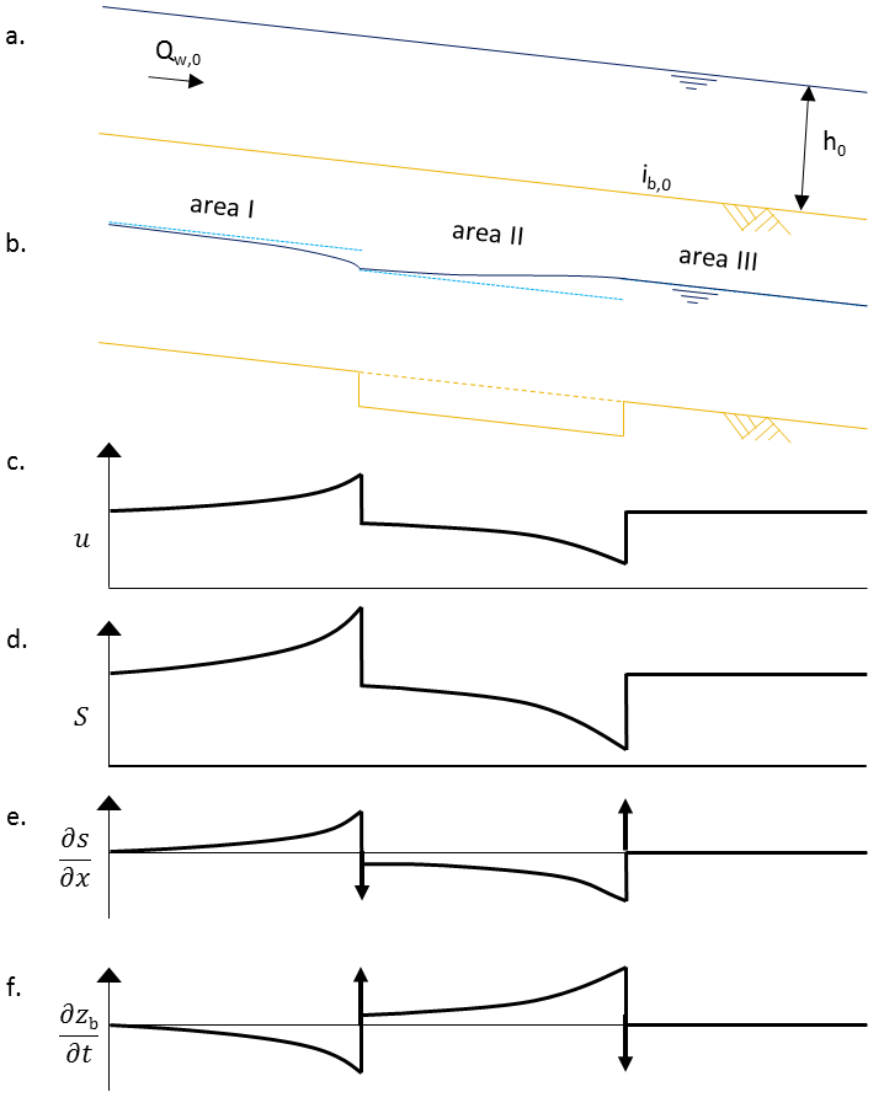

Figure 9-1: Upstream morphodynamic and hydrodynamic consequences of the artificial deepening

The behaviour of the bed level is explained with the equation of motion for water and sediment. Assuming an unchanged discharge over the areas, the velocity profile can be determined by the continuity equation for water:

$$q = uh \tag{1.5}$$

The actual velocity decreases compared to its equilibrium value when the water level is higher than its equilibrium ($h > h_e$), and the other way around, which is presented in Figure 9-1c. The sediment transport (Figure 9-1d) depends non-linearly on the flow velocity, according to the sediment transport formula:

$$s = mu^n \tag{1.6}$$

The initial change of sedimentation/erosion in space (Figure 9-1e) is obtained by integrating the sediment transport (Equation (1.6)). The sedimentation/erosion rate is obtained by using the sediment balance:

$$\frac{\partial z_b}{\partial t} + \frac{\partial s}{\partial x} = 0 \tag{1.7}$$

Figure 9-1f shows that an shock (sedimentation) wave propagates from the upstream boundary of area II in downstream direction, while a expansion (erosion) wave propagates from the downstream boundary of area II in downstream direction, which eventually leads to a closure of the de epening and the return of the situation as in Figure 9-1a. Total recovering of the hole is, however, not expected to happen during the flood wave since the duration is too short.